Topographic Effects on Seismic Ground Motion

GEO Report No. 303

T.K.C. Wong

Geotechnical Engineering Office
Civil Engineering and Development Department
The Government of the Hong Kong
Special Administrative Region

Topographic Effects on Seismic Ground Motion

GEO Report No. 303

T.K.C. Wong

This report was originally produced in September 2011 as GEO Technical Note No. TN 4/2011

First published, November 2014

Prepared by:

Geotechnical Engineering Office,
Civil Engineering and Development Department,
Civil Engineering and Development Building,
101 Princess Margaret Road,
Homantin, Kowloon,
Hong Kong.

Preface

In keeping with our policy of releasing information which may be of general interest to the geotechnical profession and the public, we make available selected internal reports in a series of publications termed the GEO Report series. The GEO Reports can be downloaded from the website of the Civil Engineering and Development Department (http://www.cedd.gov.hk) on the Internet. Printed copies are also available for some GEO Reports. For printed copies, a charge is made to cover the cost of printing.

The Geotechnical Engineering Office also produces documents specifically for publication in print. These include guidance documents and results of comprehensive reviews. They can also be downloaded from the above website.

These publications and the printed GEO Reports may be obtained from the Government's Information Services Department. Information on how to purchase these documents is given on the second last page of this report.

H.N. Wong
Head, Geotechnical Engineering Office
November 2014

Foreword

This Technical Note reviews the key factors that influence topographic effects on seismic ground motions. It presents the results of a parametric study conducted to investigate the influence of different parameters on the topographic effects of a soil slope overlying bedrock and the interaction between topographic effects and soil layer effects.

This Technical Note was prepared by Mr Thomas K.C. Wong. The work was based largely on Mr Wong's dissertation completed during his MSc course at Imperial College London in the academic year of 2009-2010, together with further work done during his subsequent debriefing in the Standards & Testing Division. Mr Lawrence K.W. Shum assisted to review a draft of this report. Ove Arup & Partners Hong Kong Limited also gave useful comments on the draft report. All contributions are gratefully acknowledged.

Ken K.S. Ho
Chief Geotechnical Engineer/Standards & Testing

Abstract

It is well known that surface topography can substantially affect the amplitude of seismic ground motions during earthquakes. Observations from destructive earthquakes, instrumental evidence and numerical studies have shown that seismic ground motion can be amplified over convex topographies such as hills, ridges and crest of slopes. Various numerical studies have been conducted in the past to analyse and predict the effects of topographic irregularities on seismic ground motions, the majority of which consider topographic irregularity as an isolated feature in a homogeneous half-space. Despite the qualitative agreement between theory and observations on topographic effects, these past studies usually obtained amplification factors that are smaller than those from instrumental studies.

This Technical Note presents the results of a parametric study conducted to investigate the effects of different parameters on the topographic effects on seismic ground motions for a soil slope overlying bedrock. This study revealed that the presence of a soil/rock interface would result in another type of site amplification effect, namely soil layer effect. The findings of this study also indicated that as compared to the simple model in which slopes in a homogeneous half-space are considered, the presence of a soil/rock interface would result in larger topographic amplification factors and complicate the topographic effects. Given the complex interaction between topographic effects and soil layer effects, these effects should not be handled separately for the prediction of the overall site amplification factors. The study findings have implications to seismic site response analysis.

Contents

List of Tables

List of Figures

1 Introduction

It is well known that surface topography can substantially affect the amplitude of seismic ground motion. Observations of earthquake damage, instrumental records and numerical studies have shown that seismic ground motion is amplified over convex topographies such as hills, ridges and crest of slopes. A considerable amount of research has been done to analyse and predict the effects of topographic irregularities on seismic ground motion.

However, the majority of these numerical studies focused on two-dimensional simulations in which the topographic features are treated as isolated ridges or depressions on the surface of a homogeneous half-space. Furthermore, seismic input is usually modelled as single-frequency, vertically propagating incident waves that cannot describe the broad-band nature of real earthquake motion. Despite the qualitative agreement between theory and observations on topographic effects, these studies usually obtain amplification factors smaller than those from instrumental studies. Some more complicated models which considered presence of soil layering were able to obtain higher amplification factors, and therefore, some researchers suggested that soil layering is a possible reason for the discrepancy between observed and predicted topographic amplification factors. The presence of a soil/rock interface results in another type of site amplification effects, namely soil layer effects. Researchers have different views on whether the topographic effects and soil layer effects can be uncoupled and considered separately for prediction of the overall site amplification factors.

This Technical Note presents the methodology and findings of a parametric study conducted to study the influence of different parameters on topographic effects on seismic ground motion for a soil slope overlying rigid bedrock and the interaction between topographic effects and soil layer effects. The objectives of the study were:

(a) to investigate the topographic effects on seismic ground motion for a soil slope overlying rigid bedrock subjected to seismic input motions of different predominant periods, for different bedrock depths and slope inclinations;

(b) to study how the topographic effects for a soil slope overlying rigid bedrock are affected by the presence of the soil/rock interface underneath the slope toe; and

(c) to investigate whether the topographic effects and soil layer effects can be uncoupled and handled separately to predict the overall site amplification factors.

2 Literature Review

2.1 Seismic Waves

When an earthquake occurs, two types of seismic waves, namely body waves and surface waves, are produced.

Body waves travel through the interior of the earth and consist of two types: P waves and S waves (Figure 2.1).

P waves, also known as primary, compressional, or longitudinal waves, involve successive compression and rarefaction of the materials through which they pass. They are analogous to sound waves. The motion of an individual particle that a P wave travels through is parallel to the direction of travel.

S waves, also known as secondary shear or transverse waves, cause shearing deformations as they travel through a material. The motion of an individual particle is perpendicular to the direction of S wave travel. The direction of particle movement can be used to divide S waves into two components, SV (vertical plane movement) and SH (horizontal plan movement).

The velocity of body waves depends on the stiffness of the materials they travel through. Since geologic materials are stiffer in compression, P waves travel faster than other seismic waves.

$$\text{Velocity of P wave:} \quad v_p = \sqrt{\frac{M}{\rho}} \quad \text{..... (2.1)}$$

$$\text{Velocity of S wave:} \quad v_s = \sqrt{\frac{G}{\rho}} \quad \text{..... (2.2)}$$

where ρ = Density of the material through which the wave propagates

M = Constrained modulus $= \left\{ \frac{(1-\nu)}{[(1+\nu)(1-2\nu)]} \right\} E$

G = Shear modulus $= \left\{ \frac{1}{[2(1+\nu)]} \right\} E$

E = Young's modulus

ν = Poisson's ratio

Surface waves are generated by the interaction between body waves and the surface and surficial layers of the earth. They travel along the earth surface with amplitudes that decrease roughly exponentially with depth. The most important surface waves, for engineering purposes, are Rayleigh waves and Love waves (Figure 2.2).

Rayleigh waves, produced by interaction of P and SV waves with the earth's surface, involve both vertical and horizontal particle motion. Love waves are generated by the interaction of SH waves with a soft surficial layer and have no vertical component of particle motion.

It is noted that the interference between S waves and Rayleigh waves is important for generation of topographic effects on seismic ground motion (see Section 2.3).

2.2 Difference between Soil Layer Effects and Topographic Effects

2.2.1 General

The destructiveness of seismic ground motion can be significantly affected by local

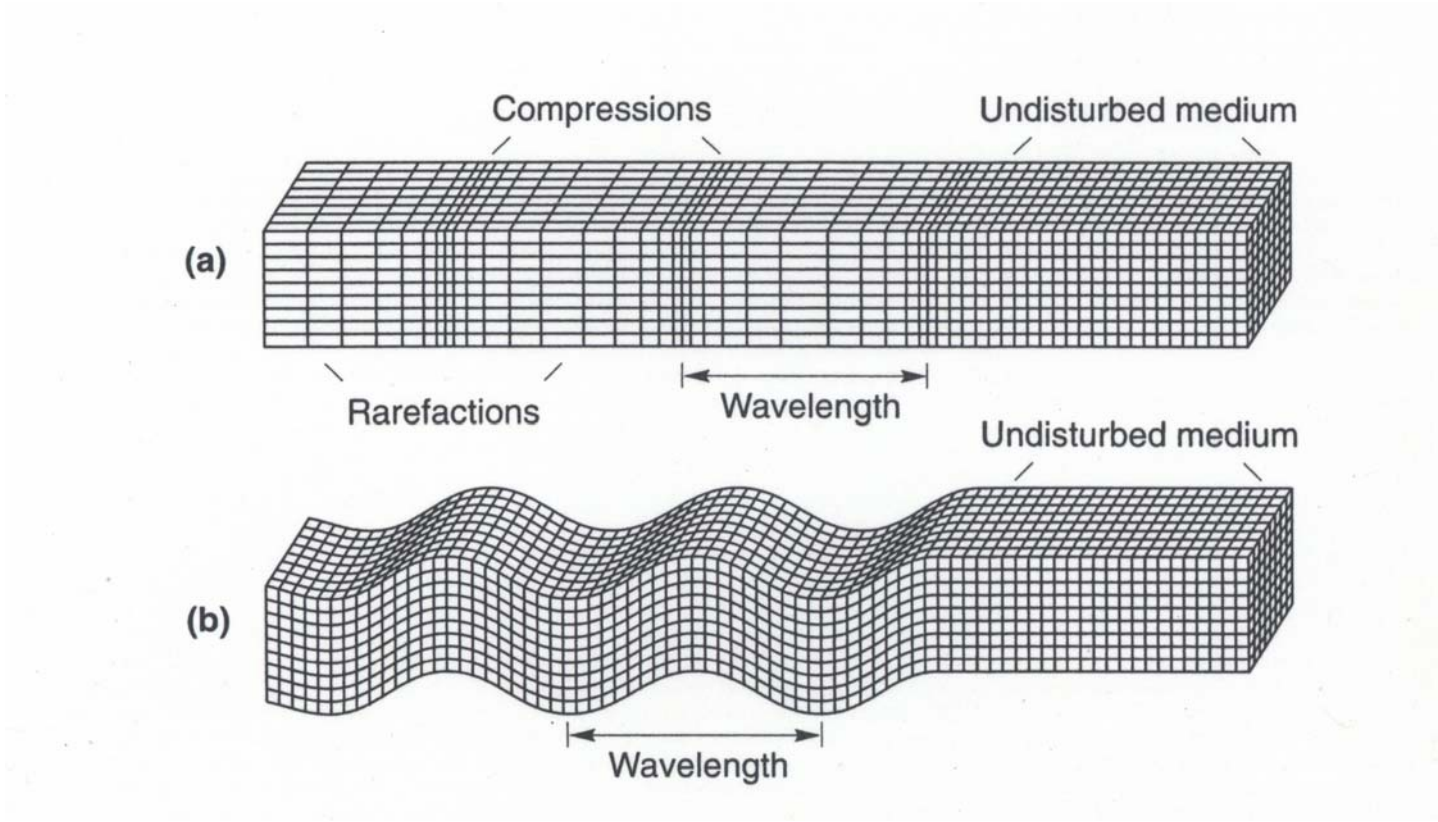

Figure 2.1 Body Waves: (a) P Wave and (b) S Wave (from Kramer, 1996)

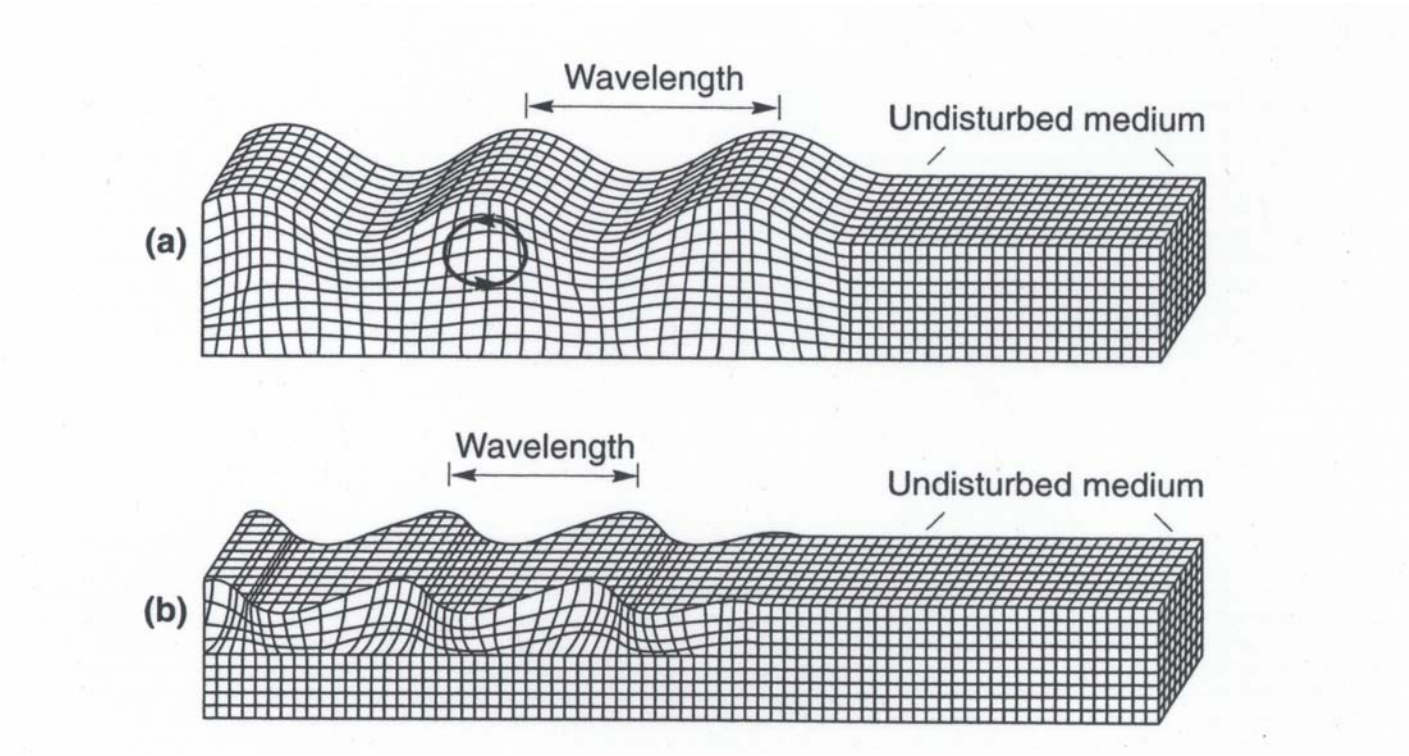

Figure 2.2 Surface Waves: (a) Rayleigh Wave and (b) Love Wave (from Kramer, 1996)

site conditions, a term which refers to amplification effects that relate to the geometry (topography) of the earth surface and the mechanical properties and thickness of surficial geological formations (soil layering). These conditions may result in large amplification and significant variation of seismic ground motion, and thus are of a particular significance in the assessment of seismic risk, microzonation studies, and planning and seismic design of important facilities.

The most common approach to quantify site effects including topographic effects and soil layer effects is to compare recordings of ground motion at nearby sites (where only local site conditions are believed to be different) through either (i) frequency-domain spectral ratios of Fourier amplitude spectra to give amplification factors at different frequencies, or (ii) time-domain ratios of peak ground motion parameters such as acceleration or displacement.

It should be emphasised that topographic effects and soil layer effects are two different phenomena – the former related to geometry of the earth surface and the latter to mechanical properties and thickness of surficial geologic materials. In some cases, they can occur alone without presence of the other. For example, topographic effects alone can occur at a homogeneous site with surface topographic irregularities while soil layer effects alone can occur at a flat site with a thick layer of soft soil deposits underneath. In many cases, both phenomena can occur at the same site simultaneously during an earthquake event. Many previous studies have investigated whether topographic effects and soil layer effects can interact with each other or they work independently; however, apparently, there is no consistent conclusion on this issue.

2.2.2 Soil Layer Effects

Soil layer effects relate to the thickness and stiffness of soil layers from ground surface down to bedrock at a particular site.

The influence of soft soil layers on the intensity of ground shaking and earthquake damage has been known for many years. Numerous observations after destructive earthquakes around the world have illustrated the effects of local soil conditions resulting in non-uniform distribution of damage. In recent years, the availability of strong-motion records has also shown the soil layer effects on amplitude, frequency composition, and duration of ground motions and has allowed soil layer effects to be measured quantitatively. Examples of earthquakes showing significant soil layer effects include the 1985 Mexico City earthquake and the 1989 Loma Prieta (California) earthquake (Kramer, 1996).

The fundamental phenomenon responsible for amplification of seismic ground motion due to soil layer effects is the trapping of seismic energy due to the impedance contrast between bedrock and overlying soil. The interference between these trapped waves leads to resonant patterns, the shape and frequency of which are related to the thickness and the geometrical and mechanical characteristics of the soil. The amplitude of amplification is related to the impedance contrast between the surface layers and the underlying bedrock, as well as to the soil material damping.

One-dimensional ground response analysis shows that for a uniform layer of isotropic, linear elastic soil overlying rigid bedrock, the magnitude of the transfer function, $|F_1(\omega)|$,

which describes the ratio of displacement amplitudes at the top and bottom of the soil layer, is given by the following equation.

$$|F_1(\omega)| = \frac{1}{|cos(\omega H / v_s)|} \quad \text{..... (2.3)}$$

where ω = angular frequency of the seismic excitation
H = thickness of soil layer
v_s = shear-wave velocity of soil

When the angular frequency of the seismic excitation, ω, is equal to multiples of $\left[\left(\frac{\pi}{2}\right)\times\left(\frac{v_S}{H}\right)\right]$, the magnitude of the transfer function, $|F_1(\omega)|$, will become infinity (Figure 2.3). In other words, infinite amplification will occur.

For a more realistic case of uniform, damped soil on rigid bedrock, one-dimensional ground response analysis shows that the magnitude of the transfer function will reach a local maximum whenever the angular frequency of the seismic excitation, ω, is very close to multiples of $\left[\left(\frac{\pi}{2}\right)\times\left(\frac{v_S}{H}\right)\right]$, but will never reach a value of infinity (Figure 2.4). The frequencies that correspond to the local maxima are the natural frequency of the soil deposit.

The n^{th} natural frequency of the soil deposit is given by:

$$\omega_n = \left[\frac{(2n+1)\pi}{2}\right]\times\frac{v_S}{H} \qquad , n = 0, 1, 2, \ldots\infty \quad \text{..... (2.4)}$$

Since the peak amplification factor decreases with increasing natural frequency, the greatest amplification factor will occur approximately at the lowest natural frequency, also known as the fundamental frequency, $\omega_0 = \frac{\pi v_S}{2H}$.

The period of vibration corresponding to the fundamental frequency is called the fundamental site period:

$$T_s \left(\text{or } T_0\right) = \frac{4H}{v_s} \quad \text{..... (2.5)}$$

The fundamental site period, which depends only on the thickness and shear wave velocity of the soil, provides a very useful indication of the period of vibration at which the most significant amplification can be expected.

Similarly, the n^{th} natural site period of the soil deposit is given by:

$$T_n = \frac{4H}{(2n+1)v_S} \qquad , n = 0, 1, 2, \ldots\infty \quad \text{..... (2.6)}$$

When the bedrock is rigid, any downward-travelling waves in the soil will be

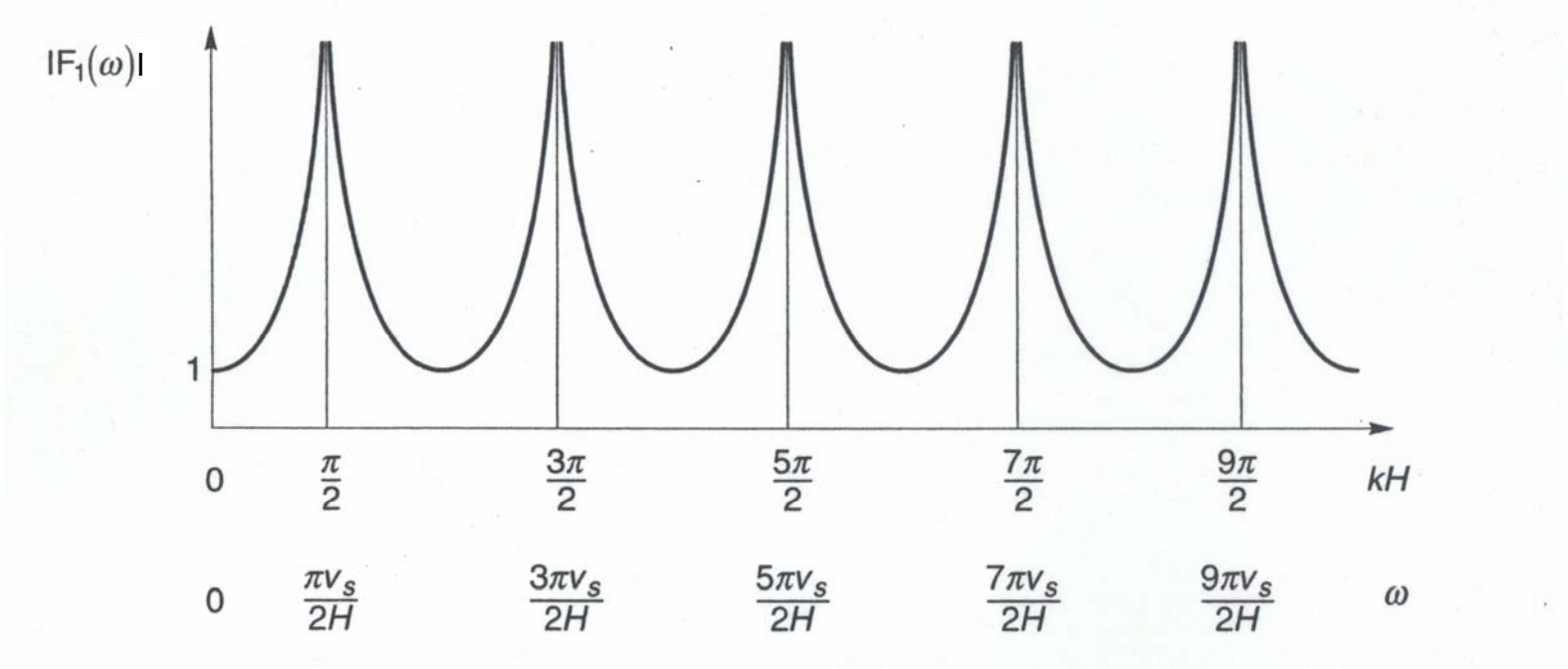

Figure 2.3 Influence of Frequency on Steady-state Response of Undamped Linear Elastic Layer (from Kramer, 1996)

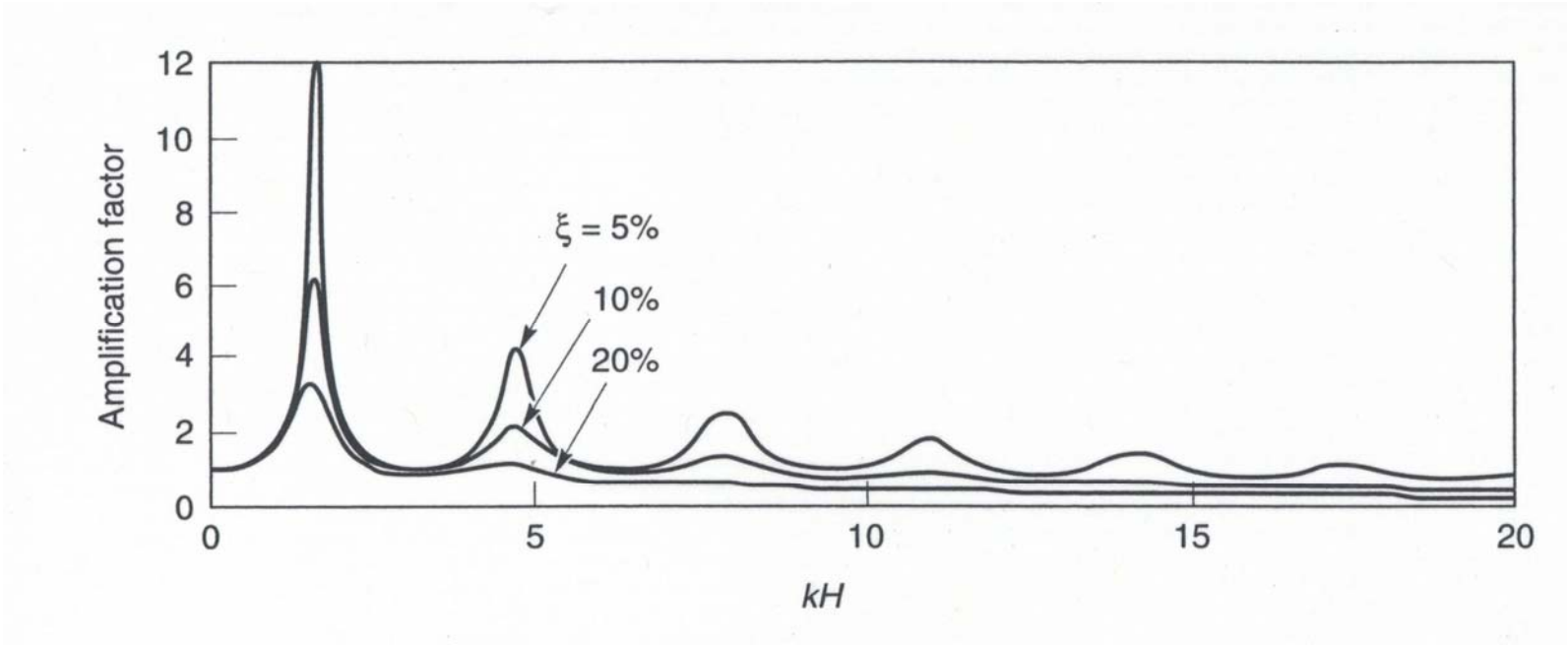

Figure 2.4 Influence of Frequency on Steady-state Response of Damped, Linear Elastic Layer (from Kramer 1996)

completely reflected back toward the ground surface by the rigid layer, thereby trapping all of the elastic energy within the soil layer. However, if the bedrock is elastic, downward-travelling waves that reach the soil-rock boundary will be only partially reflected; part of their energy will be transmitted through the boundary to continue travelling downward through the rock, and the elastic energy of these waves will effectively be removed from the soil layer. The free surface motion amplitudes will become smaller than those for the case of rigid bedrock. Therefore, the amplification ratio depends on the bedrock stiffness (or the impedance ratio). A stiffer bedrock (a higher impedance ratio) will result in a greater amplification.

2.2.3 Topographic Effects

Topographic effects are associated with the presence of surface topographic irregularities, such as hills, ridges, canyons, cliffs and slopes, which can have effects on the intensity, frequency composition and duration of ground motions during earthquakes.

It is obvious that topographic effects are more complicated than soil layer effects, due to their truly two- or three-dimensional nature. Although the effects of topographic irregularities have been studied by many researches, only few seismic codes (e.g. Eurocode 8) contain provisions for surface topography effects, despite their significance in engineering practice. This is primarily due to the complexity of the problem that involves a large number of governing parameters, the quantitative discrepancies between theoretical and instrumental studies, and the lack of adequate instrumental data to justify rigorous regression analysis. The physical phenomena explaining occurrence of topographic effects on seismic ground motion are described in Section 2.3.

2.3 Physical Phenomena Leading to Occurrence of Topographic Effects

The topographic effects due to surface topography such as hills, ridges and slopes can be recognised by observations of structural damage after destructive earthquakes. Instrumental data as well as analytical and numerical studies also allow identification and understanding of the topographic effects from a quantitative perspective.

From field observations, instrumental data and theoretical studies, the following general pattern of topographic effects on seismic ground motion can be observed:

(a) amplification of seismic motion on convex topographies, e.g. ridge crests and cliffs;

(b) de-amplification over concave topographic features, e.g. canyons and hill toes; and

(c) complex amplification and de-amplification patterns on hill slopes that result in significant differential motions.

In theory, these topographic effects are primarily a result of scattering or diffraction of the incident seismic waves by topographic irregularities. According to Bard & Riepl-Thomas (2000), these effects are related mainly to the following three physical phenomena:

(a) Body and surface waves are diffracted at and propagated outward from the topographic feature and this leads to interference patterns between the direct and diffracted waves. However, these diffracted waves generally have smaller amplitudes on the surface than the direct body waves.

(b) Surface motion is sensitive to the incidence angle and this sensitivity is especially large for SV waves near the critical angle of incidence (defined as that which produces a refracted wave that travels parallel to the ground surface). Therefore, the slope angle can produce significant variations in surface motions (Figure 2.5). Kawase & Aki (1990) suggested that this effect was a contributing cause to the peculiar damage distribution observed on a mild slope during the 1987 Whittier Narrows (California) earthquake.

(c) Reflections of seismic waves can result in focusing or defocusing of energy along the topographic surface. Sanchez-Sesma (1990) provided insights into this effect by means of a wedge-shaped medium. If this wedge has an angle of 360°/n and is subjected to plane SH waves (Figure 2.6), then the response can be computed by considering the multiple wave reflections within the wedge. All these waves interfere positively at the vertex and the resulting amplitude of motion at the vertex is n times greater than the incident wave. However, instrumental proof of such focusing/defocusing effects in strong seismic shaking has not been adequate because the lack of dense strong-motion arrays on or near topographic features.

The phenomenon of wave diffraction had been observed by Ohtsuki & Harumi (1983) in their numerical study on the effect of cliff topography on seismic SV waves. The results of their numerical study (Figure 2.7) showed that when the incident SV wave travelling vertically in the elastic half medium encounters the lower ground surface, it produces a reflected SV wave (SV1), which returns into the half-space. Later when the incident SV wave encounters the upper ground surface, it produces another reflected SV wave (SV2), which also returns into the half-space. While the incident SV wave reaches the lower corner of the slope, a Rayleigh wave (R1) is produced from the lower corner of the slope, and it propagates along the slope and upper surface to the right. Later when the upcoming incident SV wave reaches the upper corner of the slope, another Rayleigh wave (R2) is also produced at the upper corner of the slope, and it propagates along the upper surface ahead of the R1 wave. Figure 2.7 clearly shows that Rayleigh waves, which consist of both horizontal and vertical displacements, are produced in the vicinity of the slope of the cliff. The incident SV waves and Rayleigh waves combine near the slope crest resulting in a zone of amplification.

Similarly, Bouckovalas & Papadimitriou (2005), in their numerical analyses for the seismic response of steep slopes under vertically propagating SV waves, mentioned that the topographical effects could be attributed to the reflection of the incoming SV waves on the

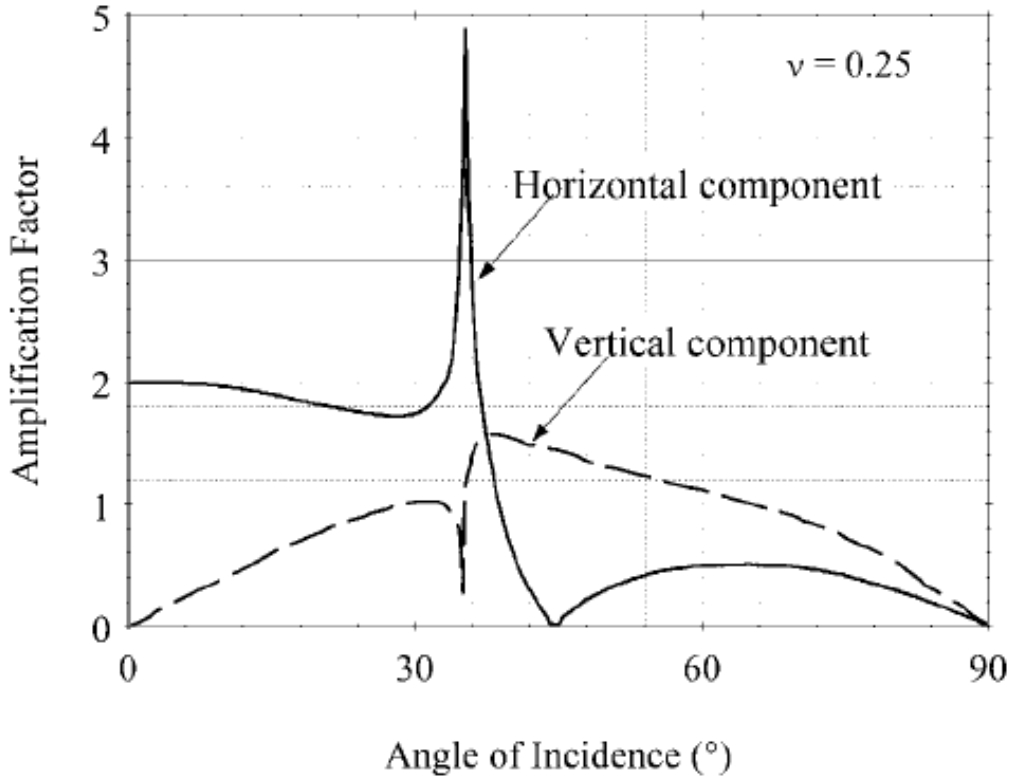

Figure 2.5 Sensitivity of Surface Motion to Incidence Angle for Obliquely Incident SV Waves (from Bard & Riepl-Thomas, 2000)

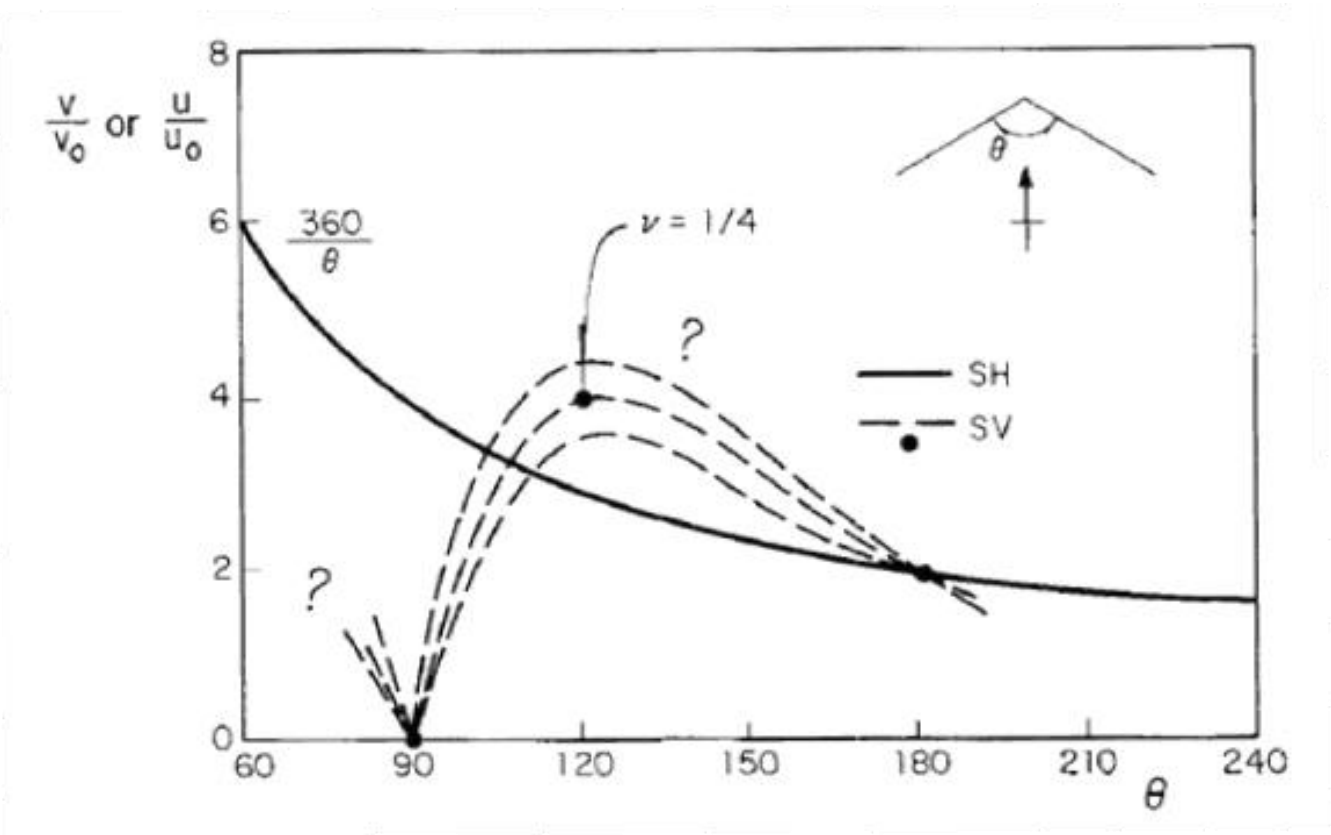

Figure 2.6 Top Amplifications Versus Wedge Internal Angle for Incidence of Plane SH and SV Waves (from Sanchez-Sesma, 1990)

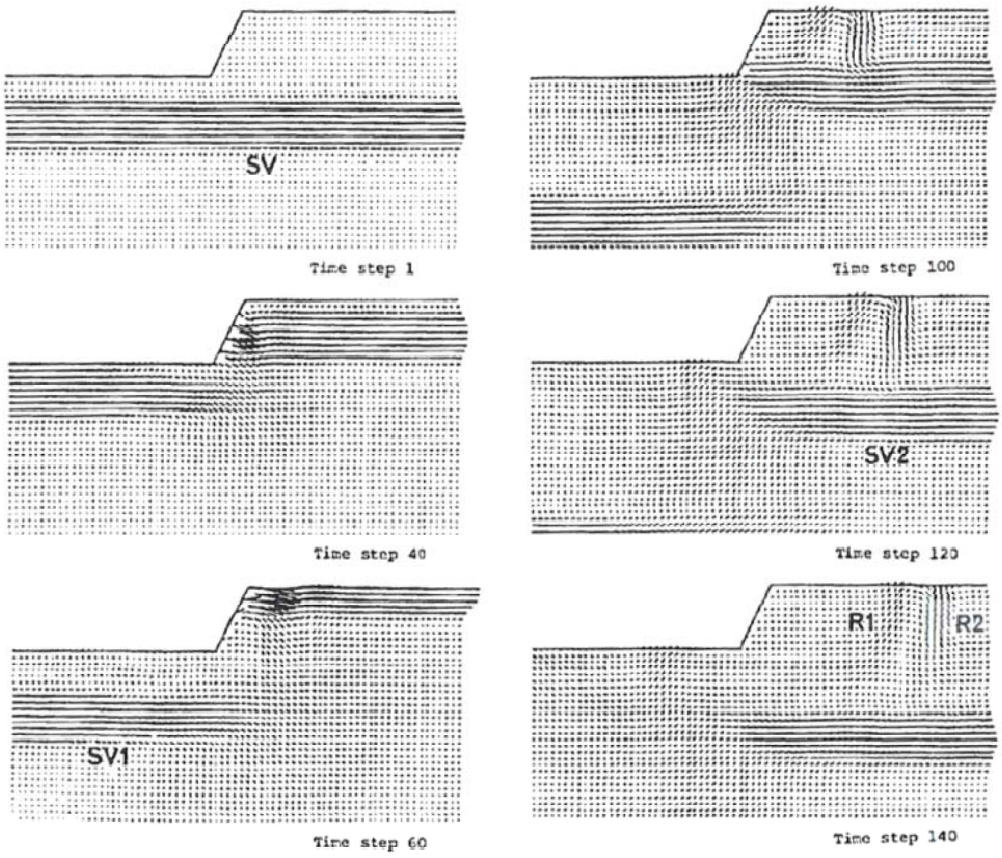

Figure 2.7 Wave Propagation in Cliff Induced by an SV Wave (from Ohtsuki & Harumi, 1983)

inclined free surface of the slope (Figure 2.8), which leads to reflected P and SV waves impinging obliquely at the free ground surface behind the crest, as well as Rayleigh waves. All these induced waves arrive with a time lag and a phase difference at the different points of the ground surface so that their superposition to the incoming SV waves may lead either to amplification or to de-amplification of the horizontal seismic motion.

From the above, it can be seen that topographic effects on seismic ground motion are complicated. They are not caused by one single physical phenomenon and they are also two- or three dimensional in nature.

2.4 Evidence of Topographic Effects

2.4.1 Documented Observations of Earthquake Damage

Many documented observations from destructive earthquakes have repeatedly show concentration of heavy damage near the crest of cliffs and slopes, or near the tops of hills and ridges. Examples of such observations can be found in the 1985 Chile earthquake (Celebi, 1987 & 1991), 1987 Whittier Narrows (California) earthquake (Kawase & Aki, 1990), 1994 Northridge (California) earthquake (Sitar et al, 1997), 1995 Aegion (Greece) earthquake (Bouckovalas et al, 1999), 1999 Parnitha (Athens) earthquake (Gazetas et al, 2002), and 1999 'Eje Cafetero' (Colombia) earthquake (Restrepo & Cowan, 2000).

A summary of the documented observations that have been identified and reviewed as part of this study is presented in Table 2.1.

These documented observations clearly show that buildings located at the top of hills and at the crest of slopes suffer much more intensive damage than those located at the base. However, it should be noted that these observations cannot provide any quantitative information concerning the amplitude of the topographic effects on seismic ground motion.

2.4.2 Instrumental Evidence

Apart from observations of earthquake damage, there is very strong instrumental evidence showing that surface topography affects considerably the amplitude and frequency contents of seismic ground motion. These instrumental evidence usually come from strong motion records of major earthquakes and also data obtained from instrumented arrays during aftershocks, small-magnitude earthquakes and mining blasting.

A summary of the instrumental studies that have been identified and reviewed as part of this study is presented in Table 2.2.

Many of the instrumented arrays were installed after major destructive earthquakes and therefore, these instrumental studies were generally limited to low amplitude recordings of aftershock events. In some cases, instruments were installed in seismically active regions or areas with mining or quarry blasting operations for a sufficiently long period of time so that abundant instrumental data can been obtained for small-magnitude earthquakes and blastings. As a result, instrumental evidence of topographic amplification of seismic ground motion is

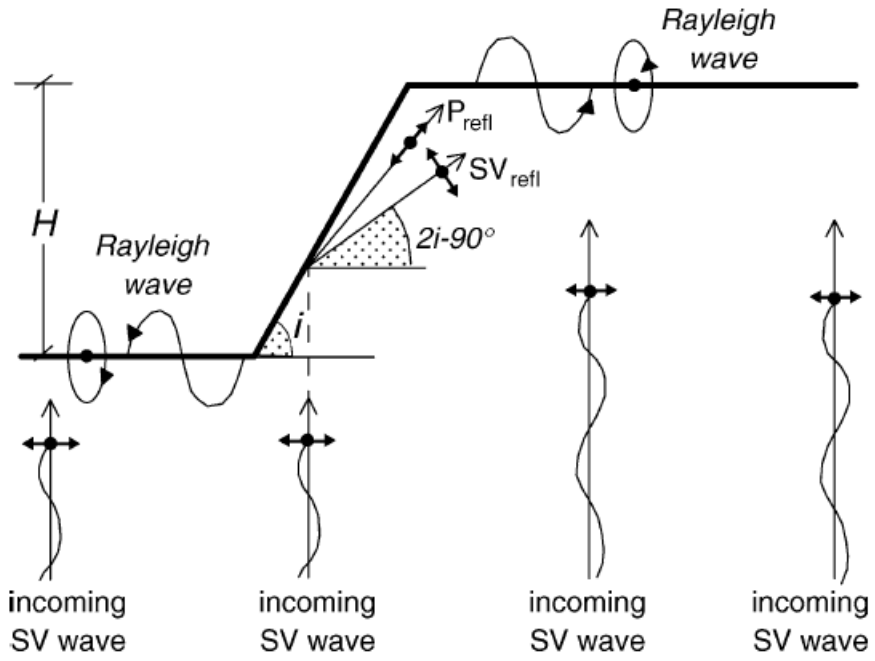

Figure 2.8 Schematic Illustration of Incoming SV Waves and Induced Reflected P Wave, Reflected SV Wave and Rayleigh Wave (from Bouckovalas & Papadimitriou, 2005)

Table 2.1 Evidence of Topographic Effects: Documented Observations of Earthquake Damage (Sheet 1 of 3)

Cases	Reference	Types of topography	Seismic source	Observations
Lambesc, Provence, France, 1909	Levret et al (1986)	Hillocks, steep ridges and slopes	1909 Lambesc (Provence) earthquake (Ms=6.0)	• More serious damage was observed in places situated either at the top of a hill, at the end of a steep ridge, or on the slopes of escarpments.
Pacoima Dam, California, 1971	Boore (1972)	Ridge	1971 San Fernando (California) earthquake (M=6.6)	• Churned ground and overturned boulders were observed following earthquakes. These observations, indicating accelerations greater than 1.0 g, were noted only on ridge crests or other topographically high features.
Canal Beagle, Chile, 1985	Celebi (1987 & 1991)	Ridges, canyons and hilltops	1985 Chile earthquake (Ms=7.8)	• The 4-storey buildings in the canyon did not suffer any damage. • All of the 4- and 5-storey buildings on the ridges were extensively damaged, some beyond repair.

Table 2.1 Evidence of Topographic Effects: Documented Observations of Earthquake Damage (Sheet 2 of 3)

Cases	Reference	Types of topography	Seismic source	Observations
Puente Hills, Whitter Narrows, California, 1987	Kawase & Aki (1990)	Hill (300m high, 2400m wide)	1987 Whittier Narrows (California) earthquake (M_L=5.9)	• The most heavily damaged area was the northern part of the city of Whittier. • Damage was concentrated along the slope of the hill rather than at the hilltop, which was not expected. • The incident angle for the heavily damaged area roughly corresponds to the critical angle for the realistic Poisson's ratio and the reported focal depth. • A combination of the topographic irregularity with a critically incident SV-wave source may cause a sharply localized amplification.
Pacific Palisades, California, 1994	Sitar et al (1997)	Costal bluffs (40 m to 60 m high; 45° to 60° steep)	1994 Northridge (California) earthquake (Mw=6.7)	• The most severely damaged zone occurred within about 50 m of the slope crest, a dimension approximately equal to the height of the bluffs. • Most of the remaining damage occurred within about 100 m of the slope crest. • Most severe damage occurred nearest the steepest slope.

Table 2.1 Evidence of Topographic Effects: Documented Observations of Earthquake Damage (Sheet 3 of 3)

Cases	Reference	Types of topography	Seismic source	Observations
Aegion, Greece, 1995	Bouckovalas et al (1999)	A vertical drop of about 90 m formed by a normal fault	1995 Aegion earthquake, Greece (Ms=6.2)	• Structural damage was concentrated in the central part of the city situated behind the fault escarpment. • Little damage was observed in the harbour located below the fault escarpment.
Adames, Kifisos Canyon, Greece, 1999	Gazetas et al (2002)	Slope (30° steep, 40 m high)	1999 Parnitha (Athens) earthquake (Ms=5.9)	• Structural damage was concentrated in two regions: one located 10 to 50 m from the slope crest, and the other at a distance of about 200 to 300 m from it. • The observed concentration of damage could be attributed to combined effects of topography and soil heterogeneity.
Armenia, Colombia, 1999	Restrepo & Cowan (2000)	• Southern part - Deep gullies with urban development on ridge • Northern part - Broad ridges and fewer stream gullies	1999 'Eje cafetero' earthquake, Colombia (Mw=6.2)	• A development of mainly 2-storey houses and 4-storey buildings in the southeast part of the city suffered partial or total collapse of 90% of the dwelling. • The northern part of the city had relatively light damage. • Despite being in the northern part of the city, some buildings built on the crest of steep roadside cut slopes still suffered appreciable damage. • Lateral spreading was observed around the crest of some ridges in rural areas.

Table 2.2 Instrumental Evidence of Topographic Effects (Sheet 1 of 6)

Cases	Reference	Types of topography	Source of data	Seismic source	Measure of amplification	Observations
Pacoima Dam, California, 1971	Boore (1972)	Ridge	Strong motion record	1971 San Fernando (California) earthquake (M=6.6)	N/A	• High acceleration up to 1.25 g was recorded. • The wavelengths of the recorded seismic energy were comparable to the dimensions of the mountain (Kagel Mountain) directly above the station.
Kagel Mountain and Josephine Peak, California, 1971	Davis & West (1973)	Mountain (Kagel Mountain - 1400 ft high) (Josephine Peak - 3500 ft high)	Instrumental data (A total of 4 stations on the top and the base of the two mountains)	Aftershocks (M=2.6-3.2) from the 1971 San Fernando (California) earthquake	Spectral ratios (crest to base) of pseudo-relative velocity response spectrum	• Frequency-dependent amplification of the motion at the crest relative to the base was observed at both mountains. • At Kagel Mountain, amplification factors in frequency domain were typically more than 10 and up to 30. • At Josephine Peak, amplification factors in frequency domain were about 3 to 5. • Amplifications in time domain were smaller than those in frequency domain. The peak amplitude ratios (crest-to-base) were smaller than the peak spectral ratios. • The wavelengths corresponding to largest amplification were comparable to mountain half-width. • The amplifications were larger than the values predicted by theoretical models.

Table 2.2 Instrumental Evidence of Topographic Effects (Sheet 2 of 6)

Cases	Reference	Types of topography	Source of data	Seismic source	Measure of amplification	Observations
NASA Mountain, Nevada	Rogers et al (1974)	Mountain (6 km long, 2 km wide)	Instrumental data	Underground nuclear explosion	Time-domain crest/base ratios of peak ground velocities	• Observed amplifications were about 25% which was in good agreement with theoretical predictions.
Tien Shan mountains, Garm Region, USSR, 1976-1978	Tucker et al (1984)	Ridges and tunnels	Instrumental data from seismometers	25 earthquakes (M_L=1.6-4.2)	Spectral ratios (crest to tunnel)	• Rock outcrop sites on ridges had spectral amplification ratios with respect to a nearby tunnel (not with respect to the ridge base) as high as 8. • Amplification was higher for horizontal than for vertical motions, and was frequency-dependent.
Coalinga anticline, California, 1983	Celebi (1991)	Ridges and gulleys	Instrumental data from a temporary closely spaced accelerographs	Aftershocks from the 1983 Coalinga (California) earthquake	Spectral ratios (ridge to gulley)	• Amplification of motions was up to 10. • The effects were frequency-dependent.
Canal Beagle, Chile, 1985	Celebi (1987 & 1991)	Ridges, canyons & hilltops	Instrumental data from a temporary dense array	Several aftershocks from the 1985 Chile earthquake	Spectral ratios (ridge to valley)	• Horizontal amplification was frequency-dependant and occurred at frequency range of 2 to 4 Hz. • Amplification typically was up to 10, few even reached 20. • The frequency range of 2 to 4 Hz correlated well with the fundamental frequencies of the heavily damaged 4- and 5-storey buildings.

Table 2.2 Instrumental Evidence of Topographic Effects (Sheet 3 of 6)

Cases	Reference	Types of topography	Source of data	Seismic source	Measure of amplification	Observations
Superstition Mountain, California, 1987	Celebi (1991)	Mountain (top and flanks)	Instrumental data from three temporary digital recording stations	11 aftershocks from the 1987 Superstition Hills (California) earthquake	Spectral ratios (top to flank)	• Horizontal motions were amplified by as much as a factor of 20. • The effects were frequency-dependent.
Robinwood Ridge, California, 1989	Hartzell et al (1994)	Ridge (110 m high)	Instrumental data from seven seismograph stations	1989 Loma Prieta earthquake (Ms=7.1)	Spectral ratios (crest to base)	• Topographic effect with amplification from 1.5 to 4.5 in the frequency range from 1.0 to 3.0 Hz was seen, part of which may be caused by local site effects. These wavelengths were comparable to the base width of the ridge. • Amplifications of up to a factor of 5 were seen at higher frequencies and are attributed to local site effects.
Epire, Northern Greece, 1989	Chavez-Garcia et al (1996)	An elongated hill (200 m high, 1000 m wide)	Instrumental data from 10 seismometers	68 small seismic events (M=1.7-4.5)	Horizontal-to-vertical spectral ratios (HVSR)	• Maximum amplification at mountain top computed from HVSR was moderate. • Observed and theoretical amplifications were similar and were below a factor of 5.
Tarzana, California, 1987	Celebi (1995)	Small hill (20 m high, 500 m long, 200 m wide)	Strong motion record	1987 Whittier Narrows (California) earthquake (Ms=6.1)	N/A	• High horizontal peak acceleration (0.61 g) was recorded, much larger than the expected values for an earthquake of that magnitude.

Table 2.2 Instrumental Evidence of Topographic Effects (Sheet 4 of 6)

Cases	Reference	Types of topography	Source of data	Seismic source	Measure of amplification	Observations
Tarzana, California, 1994	Celebi (1995)	Small hill (20 m high, 500 m long, 200 m wide)	Strong motion record	1994 Northridge (California) earthquake	N/A	• Unusually high horizontal peak acceleration (1.82 g) was recorded, much larger than those estimated by attenuation relationships.
			Instrumental data from a temporary dense array	Aftershocks from the 1994 Northridge (California) earthquake	Spectral ratios (crest to base)	• Amplitude of motions and spectral ratios decreased from the hilltop towards the more level part of the hill.
Tarzana, California, 1994	Spudich et al (1996)	Small hill (15 m high, 500 m long, 130 m wide)	Strong motion record	1994 Northridge (California) earthquake (Mw=6.7)	N/A	• Unusually high horizontal peak acceleration (1.78 g) was recorded, while two other stations located within 2 km of the station at Tarzana recorded considerably smaller accelerations.
			Instrumental data from a dense array	Aftershocks from the 1994 Northridge (California) earthquake (M=1.7-2.9)	Spectral ratios (crest to base)	• Amplifications of about 4.5 and 2 were observed for horizontal components oriented perpendicular and parallel to the long axis of the hill respectively. • The numerical study by Bouchon & Barker (1996) obtained an amplification of about 1.6.

Table 2.2 Instrumental Evidence of Topographic Effects (Sheet 5 of 6)

Cases	Reference	Types of topography	Source of data	Seismic source	Measure of amplification	Observations
Sourpi, Greece, 1992	Pederson et al (1994b)	Ridge (300 m high, 5 km long, 2.5 km wide)	Instrumental data from seven seismometers	14 local and regional shallow earthquakes	Spectral ratios (crest to base)	• The average spectral ratios showed amplifications of 1.5 to 3. • The horizontal components were more amplified than the vertical component. • The observed spectral ratios were modest and within the range predicted by numerical simulations.
Mont Saint Eynard, France, 1993	Pederson et al (1994b)	Ridge (25° steep, 400 m high, 7-8 km long, 2-3 km wide)	Instrumental data from two seismometers	7 teleseismic events and 5 local/regional (M_b=1.4-2.0) events	Spectral ratios (crest to flank)	• The average spectral ratio was up to 4. • The observed amplifications were modest and within the range predicted by numerical simulations.
Kitheron Mountain, Corinth, Greece, 1993	LeBrun et al (1999)	Hill (700 m high, 6 km long, 3 km wide)	Instrumental data from seven seismometers across the ridge	51 earthquakes (M_L=0.5-3.6)	Spectral ratios	• The E-W elongation of the hill produced a larger amplification in the N-S component than in the E-W one. • Spectral ratios were smaller than 5 for all stations, except one which showed a larger (almost 10) amplification on both horizontal components. • The vertical component showed much smaller effect than the horizontal one.

Table 2.2 Instrumental Evidence of Topographic Effects (Sheet 6 of 6)

Cases	Reference	Types of topography	Source of data	Seismic source	Measure of amplification	Observations
Nice, France,1994 (Locations: Castillon & Piene)	Nechtschein et al (1995)	Two ridges (about 200 m and 400 m high) with steep slopes on both sides	Instrumental data from 11 seismic stations along the slopes	Micro-earthquakes and mining explosions (total 46 events)	Spectral ratios	• Amplification and attenuations were mainly observed on the horizontal components. The vertical component did not exhibit any strong effect. • Significant amplifications for ground motions was observed at the ridge crest, with a peak value around 10. • Attenuation was observed near the base. • Ground motion showed a strong variability along the slopes. • Amplification at ridge top was largest along the horizontal direction perpendicular to the ridge axis.

not much for strong and destructive seismic shaking, and therefore it seems not possible to derive reliable conclusions of a general nature.

Nevertheless, unlike documented observations, these instrumental studies can quantify the amplitudes of topographical amplification of seismic ground motion. Typically, the amplitudes of topographical amplification are calculated directly by either the time-domain ratios of peak ground motion parameters (usually acceleration or displacement), or the frequency-domain spectral ratios of Fourier amplitude spectra, of a particular location on topography to a selected reference site which is assumed as the free-field condition. It is noted that in these studies, the base of ridges or hills, or the slope toe, is usually selected as the reference site.

The following general observations are obtained from the instrumental studies reviewed in this study:

(a) Some strong ground motion records show unusually high horizontal peak accelerations which are much higher than those estimated by attenuation relationships for an earthquake of that magnitude. Many researchers believe that these unusually high horizontal accelerations are related to the surface topography of the sites. Examples are the recorded PGA values of 1.25 g at Pacoima Dam in the 1971 San Fernando (California) earthquake (Boore, 1972) and of 1.82 g on a small and relatively flat hill in Tanzana during the 1994 Northridge (California) earthquake (Celebi, 1995; Spudich et al, 1996).

(b) The crest-to-base spectral ratios (see Section 2.2.1) consistently show a frequency-dependent amplification of the horizontal components of ground motion. In general, the wavelengths corresponding to amplification frequencies are comparable to the dimensions of the topography (e.g. ridge width). There are cases where modest amplifications are observed (e.g. Pederson et al, 1994b; LeBrun et al, 1999). There also exist many observations of amplification factors up to 10 (e.g. Celebi, 1991; Nechtschein et al, 1995). In some cases, the observed amplification factors even reach the order of 20 to 30 (e.g. Davis & West, 1973; Celebi, 1987 & 1991).

(c) The time-domain crest-to-base ratios show relatively smaller amplification factors than frequency-domain spectral ratio.

(d) The amplification of the vertical motion is much smaller than the horizontal motion.

As instrumental studies have provided valuable quantitative information on the amplitudes of the topographic amplification on seismic ground motion, a comparison between

these instrumental (experimental) results and theoretical (numerical) results has been made. The findings of such comparison will be presented in Section 2.5.

2.5 Previous Numerical Studies on Topographic Effects

2.5.1 General

Prompted by observational and instrumental evidence, a large number of numerical studies have been conducted using different numerical methods in an attempt to model, quantify and predict the topographic effects on seismic ground motions, and to compare the theoretical amplifications with observations. In addition, some numerical parametric studies have been performed to identify the parameters that affect topographic effects on seismic ground motion and to investigate their influence. Typically these numerical studies show:

(a) systematic amplification of seismic motion over convex topographies such as hills and ridges,

(b) de-amplification over concave topographic features such as canyons and hill toes,

(c) complex amplification and de-amplification patterns on hill slopes that result in significant differential motions,

(d) amplification being frequency dependent, and

(e) higher amplification on the horizontal components than vertical.

In general, there is a qualitative agreement between theoretical and observed topographic amplifications. However, from a quantitative viewpoint, there exist clear discrepancies between theory and observations.

2.5.2 Numerical Studies on Ridges and Hills

The majority of numerical studies on ridges and hills focus on two-dimensional simulations in which the topographical features are treated as isolated ridges on the surface of homogeneous half-spaces, usually under further simplified assumptions of vertically propagating incident waves and harmonic steady-state excitation.

Geli et al (1988) presented a comprehensive review of previous numerical studies on ridges and hills, and they found that most of them gave consistent results:

(a) The time-domain crest-to-base acceleration amplification ratios remain below two.

(b) The frequency-domain crest-to-base amplification ratios are up to three and the peaks occur when wavelength is about

equal to the ridge width.

(c) Varying amounts of amplification and attenuation occur along the surface of the slope from the crest to the base.

(d) The amplification is lower for incident P waves than for incident S waves.

(e) The amplification is slightly larger for in-plane horizontal motion (SV waves) than for anti-plane motion (SH waves).

Geli et al (1988) also noted that most of the numerical studies reviewed considerably underestimate amplifications observed in the field, which mostly range from 2 to 10, and up to as much as 30. In the same paper, they carried out a detailed examination of several cases and they considered that the discrepancy between observations and theory may be due to subsurface soil layering and/or neighbouring ridges, and suggested that a more complex numerical model incorporating subsurface soil layering and neighbouring ridges could reduce the discrepancy.

In this connection, Geli et al (1988) analysed a more complex configuration to evaluate the effects of subsurface layering and/or nearby ridges to incident SH waves and they arrived at conclusions similar to those of the previous researchers. In particular, their results showed that:

(a) The topographic effect itself is difficult to isolate from other effects, like subsurface soil layering, and therefore the topographical amplification cannot be predicted by a priori estimations based solely on topography.

(b) The high crest-to-base amplification ratios observed in the field usually cannot be matched even with complex two-dimensional structures with incident plane SH waves, which suggests that more complex models are needed to incorporate more complex wave fields (e.g. SV, surface) and three-dimensional geologic configurations.

There are also other numerical studies which involve relatively more complex models. Bard & Tucker (1985) investigated the SH response of a set of ridges with irregular subsurface layering. Bouchon & Barker (1996) and Bouchon et al (1996) investigated the response of three-dimensional homogeneous hills. In general, these three-dimensional models lead to slightly higher crest-to-base amplification ratios than two-dimensional models and they show a higher amplification on the horizontal component along the direction of motion perpendicular to the ridge axis.

In summary, based on the comparison of instrumental and theoretical results, the following observations can be made:

(a) A qualitative agreement exists between theory and observations about the existence of seismic motion

amplification at ridges and mountain tops, and de-amplification at the base of hills. The amplification is generally larger for horizontal components than for the vertical component.

(b) This amplification (or de-amplification) phenomenon is frequency-dependent. There is a rather good qualitative agreement between instrumental observations and theoretical results for the relationship between mountain width and the approximate frequency range where amplification is significant.

(c) However, from a quantitative viewpoint, clear discrepancies exist between theory and observations. Cases have been reported in which field measurements exhibit only weak to modest amplifications at ridge crests or hilltops and fit fairly well with the numerical results (e.g. Rogers et al, 1974; Pedersen et al, 1994b; LeBrun et al 1999). On the other hand, numerous cases also exist in which the observed amplifications are significantly larger than the theoretical predictions obtained from sophisticated, two- or three-dimensional models (e.g. Bouchon & Barker, 1996; Bouchon et al, 1996). Numerous observations have been made of spectral amplifications around 10, and up to the range of 20 to 30 for some cases (e.g. Davis & West, 1973; Celebi, 1987 & 1991; Nechtschein et al, 1995), but such amplitudes are rarely predicted by numerical models.

The confusing results from quantitative comparison between observed and theoretical amplifications could be attributed to the following:

(a) Internal structure (e.g. subsurface layering, lateral variations of geology) of the topography features is not adequately accounted for in numerical models.

(b) Three-dimensional shape of the topography features and neighbouring ridges are not adequately taken into account in numerical models.

(c) It is important to note that the crest-to-base spectral ratios are not measurements of absolute amplifications with respect to a half-space. Motions at stations at the base of a hill or ridge can be de-amplified while those at the slope or flank can be amplified or de-amplified as a function of frequency. This means in practice that amplification on mountain tops estimated by comparison with a reference station at the base or flank can be severely biased and very large observed amplifications can be obtained.

2.5.3 Numerical Studies on Slopes

While some of the procedures and concepts developed for the analysis of ridges and hills may be extended to steep slopes, there are significant differences between the response of steep slopes and the response of rock ridges simulated as homogeneous half-spaces. The most important differences are the semi-infinite nature of material in the horizontal direction behind the slope crest and the potential for soil amplification of the motions in the one-dimensional (i.e. vertical) sense.

Ashford et al (1997) presented a comprehensive review of previous numerical studies that specifically considered seismic response of soil slopes. Many researchers (Idriss & Seed, 1967; Idriss, 1968; Kovacs et al, 1971; Sitar & Clough, 1983) suggested that if the motions were amplified in the vicinity of the slope crest, the natural period of the one-dimensional soil column behind the crest is responsible for larger amplification of the input motion than the amplification due to slope geometry. Therefore, when a soil layer over bedrock is considered, the amplitudes of the amplification of seismic ground motions near the crest of slopes will be different from the case of slopes with a homogenous half-space.

Among the published studies specific to topographical effects on seismic response of steep slopes, the recent ones performed by Ashford et al (1997), Ashford & Sitar (1997), and Bouckovalas & Papadimitriou (2005) are the most extensive and most relevant to the scope of the present study.

Ashford et al (1997) conducted a frequency-domain parametric study to evaluate the significance of topographic effects on the seismic response of steep slopes in a homogeneous half-space (i.e. with no impedance contrasts). Both vertically propagating SH and SV waves were considered. The key findings of their study are summarised below:

(a) The topographical effects of a steep slope on the seismic response of that slope can be normalised as a function of the ratio of the slope height (H) and wavelength of the motion (λ).

(b) For both SH and SV waves, the magnitude of the response at slope crest is significantly reduced by increased damping, particularly at higher frequencies. However, the amplification of the motion at the crest over that in the free field behind the crest is relatively unaffected by damping.

(c) The peak topographical effect occurs at $H/\lambda = 0.2$ (defined as 'topographic frequency' by the authors) for both vertically propagating SH and SV waves. The amplification at slope crest (relative to the free-field behind the crest) at the topographic frequency is in the order of 25% for SH waves, and 55% for SV waves (Figures 2.9a and 2.9b). The topographical amplification on the vertical component has a monotonic increase with normalised frequency and peaks at $H/\lambda = 1.0$ for SV waves (Figure 2.9c).

(d) The topographical effects, as reflected by the initial peak amplifications of horizontal response at the topographic frequency, tend to increase with slope angle (Figures 2.9a and 2.9b).

In an attempt to investigate the influence of soil amplification on topographic effects, Ashford et al (1997) also carried out a parametric study on the response of a slope in a soil layer overlying a homogeneous half-space, with an impedance ratio of three. They concluded that the natural frequency of the site behind the crest dominates the response, which agrees with the findings of Sitar & Clough (1983). They also established that if the natural frequency of the site is approximately equal to the topographic frequency, then the response at slope crest would be amplified by over 50% relative to the free-field motion, and this amount of amplification is similar to the amount they observed at the topography frequency of the stepped half-space. Based on these results, Ashford et al (1997) suggested that the effects of natural frequency and those of topography may work independently and hence the effects of topography can be handled separately from amplification due to the natural frequency of the soil layer behind the slope crest.

Bouckovalas & Papadimitriou (2005) also conducted a similar parametric study to evaluate the topographical effects of step-like slopes in homogeneous material on seismic response. The numerical analyses were performed with the Finite Difference method and only vertically propagating SV waves and homogeneous half-space were considered. Despite the use of distinctly different methodologies of analyses (i.e. Finite Difference method versus generalised consistent boundary method), Bouckovalas & Papadimitriou (2005) obtained very similar results to that from Ashford et al (1997) (see Figure 2.10), and their key findings are as follows:

(a) Even a purely horizontal excitation, such as vertically propagating SV waves, can result in considerable parasitic vertical motion at the ground surface near the slope. The results of the parametric analyses show that the vertical parasitic component of seismic motion may become comparable to the horizontal free-field motion.

(b) The topography aggravation of the horizontal ground motion fluctuates intensely with distance away from the crest of the slope, alternating between amplification and de-amplification within very short horizontal lengths. Similarly, the topographic apparition of parasitic vertical motion is also intensely variable with distance. The authors highlighted that actual ground motion recordings near slopes must therefore be obtained via very dense seismic arrays.

(c) The horizontal ground motion is de-amplified at the toe of the slope and amplified near the crest. As a result, topography aggravation may be seriously overestimated, when calculated as the peak seismic ground motion at the crest over that at the toe of the slope. The authors believed

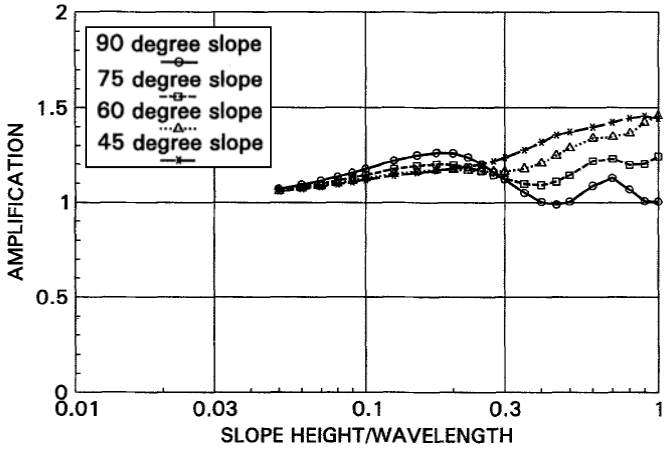

(a) Horizontal amplification for a vertically incident SH wave

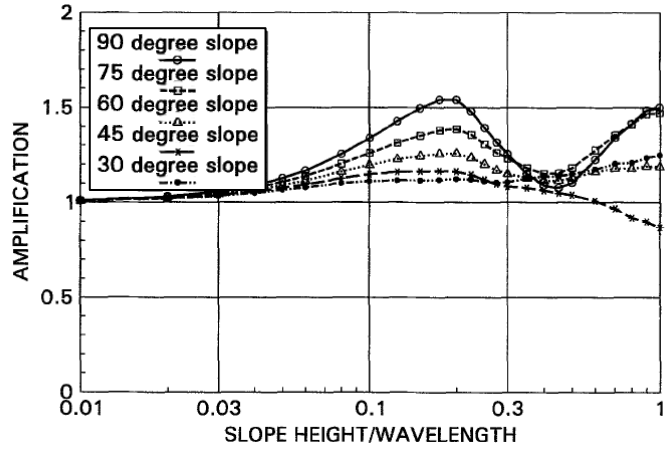

(b) Horizontal amplification for a vertically incident SV wave

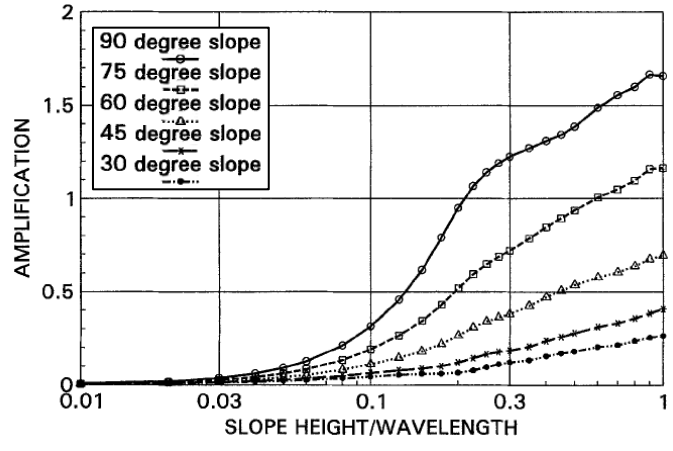

(c) Vertical amplification for a vertically incident SV wave

Figure 2.9 Amplification at the Crest of an Inclined Slope in a Homogeneous Half-space (β = 1%) (from Ashford et al, 1997)

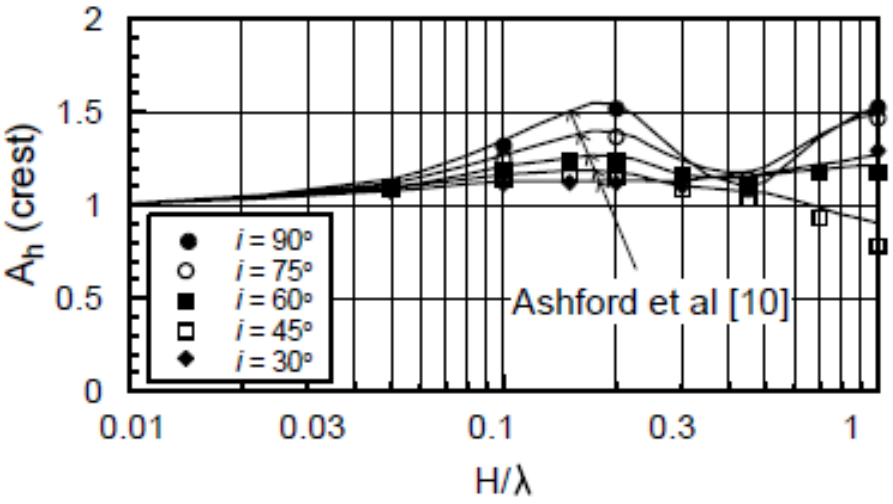

(a) Horizontal amplification

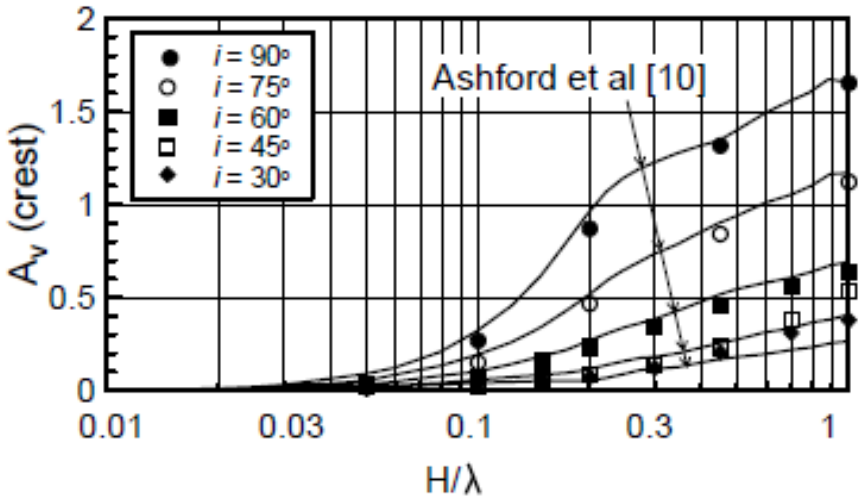

(b) Vertical amplification

Figure 2.10 Amplification at the Crest of an Inclined Slope in a Homogeneous Half-space for a Vertical Harmonic SV Wave (β = 5%) (from Bouckovalas & Papadimitriou, 2005)

that this overestimation may explain, at least in part, why field measurements (without appropriate free field selection) of topography aggravation are usually significantly higher than analytical predictions.

Bouckovalas & Papadimitriou (2005) also studied the effects of different parameters (including slope angle i, dimensionless frequency of excitation H/λ, hysteretic damping ratio of soil ξ, and number of significant excitation cycles, N) on the topographical effects on seismic ground motion. More details will be given in Section 2.6.

It should be emphasised that the amplitudes of topographical amplification of steep slopes given in both on Ashford et al (1997) and Bouckovalas & Papadimitriou (2005) were obtained from the analyses of step-like slopes in homogenous half-space, without an impedance contrast (i.e. bedrock).

Tripe (2009) carried out a parametric study to investigate topographic amplification in the presence of soil layer effects using the Imperial College Finite Element Program (ICFEP) (Potts & Zdravkovic, 1999). His analysis considered a soil slope in a homogeneous layer overlying bedrock. Tripe (2009) made the following conclusions in his study:

(a) With presence of bedrock, the amplification of ground motion relative to the input motion at bedrock has two components, one directly related to the amplification due to soil layer effects and the other to the interaction of the topographic effects with the soil layer effects. The second component increases with reducing bedrock depth.

(b) Similar trends in the behaviour of topographic effects were observed compared with Ashford et al (1997) and Bouckovalas & Papadimitriou (2005), but the magnitude of amplification was considerably larger due to the interaction with soil layer effects.

As only one bedrock depth was analysed in his parametric study, Tripe (2009) could not make any general quantitative assessment of the effects of bedrock depth on the magnitude of amplification.

From literature review, it remains uncertain whether for steep slopes, the geometry of topographic irregularity and the subsurface soil conditions can be handled separately, as suggested by Ashford et al (1997), or they have to be modelled simultaneously to obtain accurate estimates of the amplification levels.

2.6 Parameters Affecting Topographic Effects

2.6.1 General

Based on the findings of the numerical studies reviewed, the following factors which can affect the amplitude and extent of topographic effects on seismic ground motion are

identified:

(a) characteristics of incident wave (e.g. wave type, angle of incidence, frequency content, duration);

(b) topographic geometry (e.g. slope height, slope inclination, three-dimensional shape);

(c) subsurface soil layering; and

(d) soil parameters.

2.6.2 Type of Incident Waves

The incidence of SH waves has been studied more frequently, as reflection and diffraction of SH waves does not generate other wave types, in contrast to incident P or SV waves. For incident S waves, it has been shown that the amplification of SV waves is usually higher than that of the SH waves. According to Ashford et al (1997), a vertical cliff subjected to vertically propagating SH waves resulted in a maximum amplification at the surface in the order of 1.25 (with respect to the free-field), whereas for the same configuration, a maximum amplification in the order of 1.5 was observed for vertically propagating SV waves (Figure 2.9). Qualitatively, the pattern of distribution of soil amplification and de-amplification of seismic motion as a function of the distance from the cliff is similar for SH and SV waves.

2.6.3 Angle of Incidence

The majority of the numerical studies reviewed considered vertically propagating waves. This is a reasonable assumption in earthquake engineering because seismic waves are refracted towards the vertical as they travel upwards from materials of higher density to materials of lower density. However, this assumption may not be fully valid for ridges or mountains in homogenous rock extending to great depth and subject to relatively shallow earthquakes.

Ashford & Sitar (1997) performed a parametric study to study the effect of the incident angle on topographic effects for a vertical slope (Figure 2.11). Their study was limited to angles smaller than the critical angle. When the angle of incidence of the propagating S waves coincides with the critical angle, a transformation takes place, and a single P wave arises and propagates along the slope. They observed that the horizontal motion at the slope crest is amplified for waves travelling into the slope and attenuated for waves travelling away from the slope, as compared to the motion in the free field behind the slope crest. This amplification can be as much as twice that due to vertically propagating waves. In contrast, the vertical response due to SV waves appeared to be independent of the direction of wave propagation. The authors suggested that the amplification of inclined SV waves travelling into the slope may partially explain field observations of failures on slopes facing in a particular direction, while slopes in the same material, but of different orientation, showed no distress.

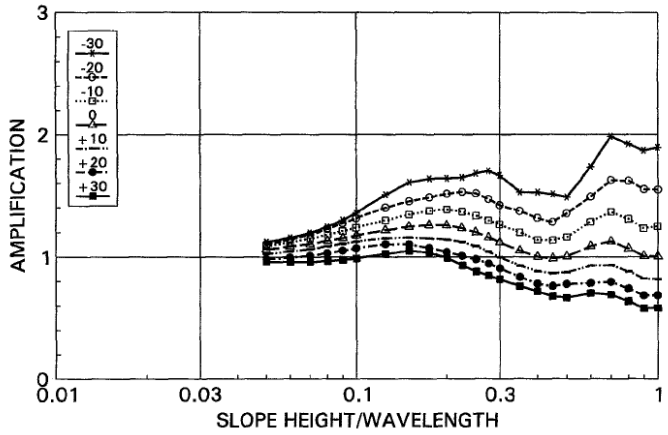

(a) Horizontal amplification for an inclined SH wave

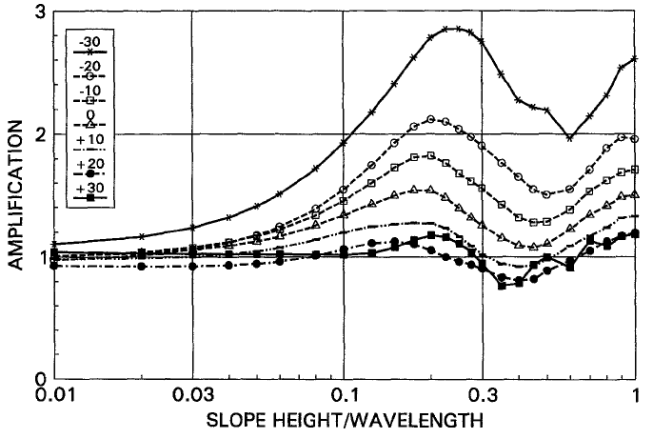

(b) Horizontal amplification for an inclined SV wave

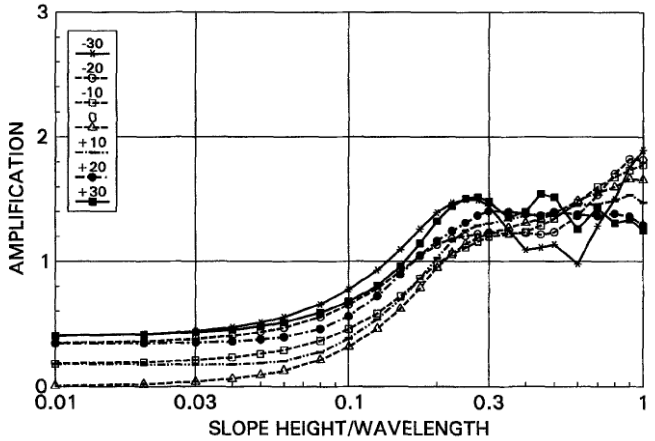

(c) Vertical amplification for an inclined SV wave

Figure 2.11 Amplification at the Crest of a Vertical Slope in a Homogeneous Half-space for Inclined Wave (from Ashford & Sitar, 1997)

2.6.4 Frequency Content of Incident Motion

Topography effects are very significant for wavelengths comparable to the geometric characteristics of the irregularity, whereas they are negligible for very low frequencies, i.e. very long wavelengths (Ohtsuki & Harumi, 1983; Geli et al, 1988; Ashford et al, 1997; Bouckovalas & Papadimitriou, 2005).

For slope type topographies, it has been observed that the surface response is primarily controlled by diffraction of incident waves at the slope surface, the effect of which depends on the ratio of the dimensionless frequency (H/λ). According to Ashford et al (1997) and Bouckovalas & Papadimitriou (2005) (Figures 2.9 and 2.10), who studied topographical effects on the seismic response of steep slopes in a homogeneous half-space, horizontal amplification at slope crest peaks at $H/\lambda = 0.2$ and 0.7 for vertically incident SH waves and peaks at $H/\lambda = 0.2$ and 1.0 for vertically incident SV waves. For the vertical component, there is a monotonic increase of the vertical amplification with the dimensionless frequency of the vertical incident SV waves, and the vertical component is almost zero for very low frequencies ($H/\lambda < 0.05$).

2.6.5 Duration and Type of Time-history Excitations

The majority of the parametric studies reviewed used a single type of time-history excitations, most commonly harmonic motions. Bouckovalas & Papadimitriou (2005) is the only study that considered different types of time-history excitations and evaluated the effects of their duration on seismic response.

Bouckovalas & Papadimitriou (2005) studied the seismic response of steep slope in a homogenous half-space under vertically propagating SV waves. In their study, most of the parametric analyses were performed either with a harmonic excitation of 20 to 40 uniform cycles, or with a Chang's signal excitation aimed to simulate the limited duration as well as the gradual rise and decrease of shaking amplitude. Their results show that the number of significant excitation cycles N has a relatively minor overall effect on the amplifications of peak accelerations (Figure 2.12).

Bouckovalas & Papadimitriou (2005) also performed analyses on the same geometry of a step-like slope using two actual earthquake records and a Chang's signal excitation with similar characteristics of predominant period and number of significant cycles and scaled to the same peak ground acceleration. They observed that all three analyses provide compatible results, with the Chang's signal excitation leading to rather conservative estimates of the topographic amplification of the peak ground accelerations. A possible explanation for this observation is that the much wider frequency content of actual earthquake excitations may prevent the topography from generating large amplification at a particular frequency as the different frequency components of real earthquake excitations can develop different patterns of amplifications and de-amplifications and have different magnitudes of amplification/de-amplification during earthquakes.

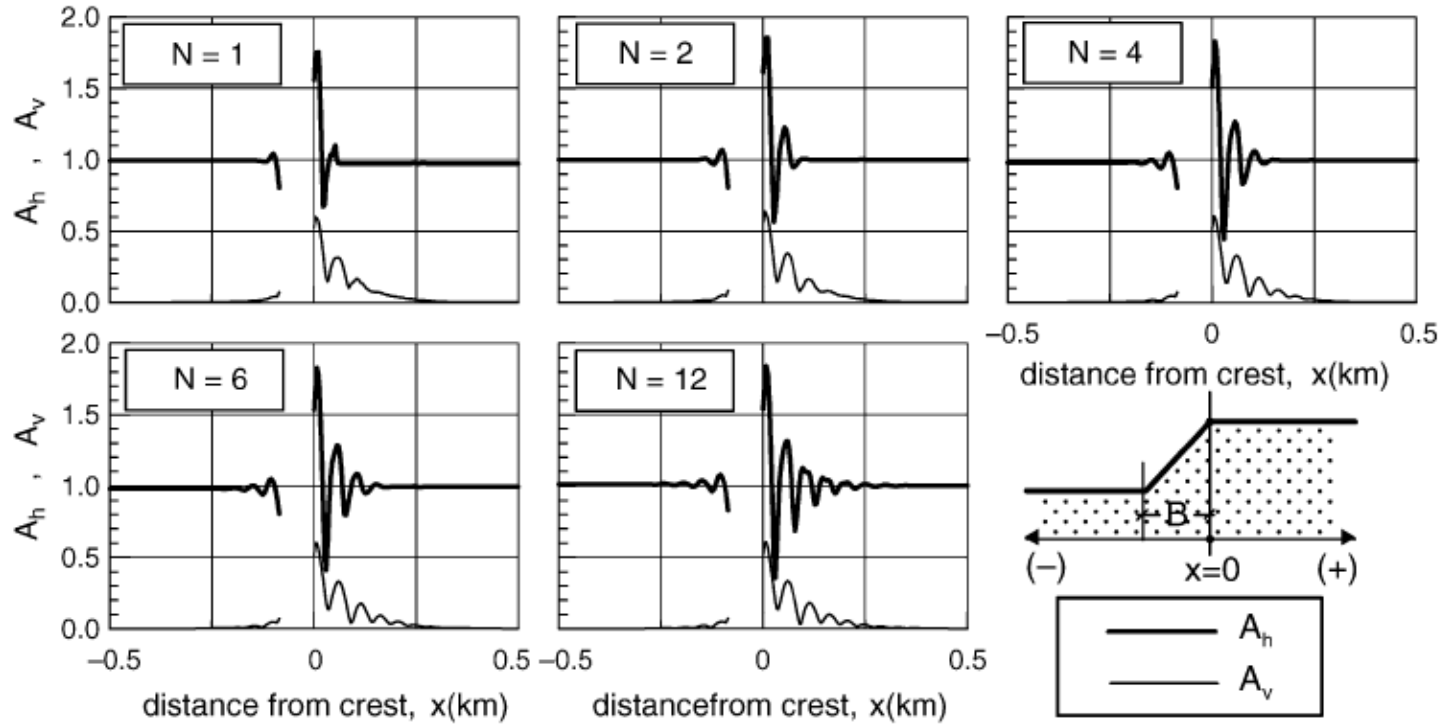

Figure 2.12 Effect of the Number of Significant Cycles *N* on the Horizontal and Vertical Amplification Factors (A_h and A_v), as a Function of Horizontal Distance *x* from the Slope Crest ($H/\lambda = 2$, $i = 30°$, $\beta = 5\%$) (from Bouckovalas & Papadimitriou, 2005)

2.6.6 Slope Inclination

Ashford & Sitar (1997) and Bouckovalas & Papadimitriou (2005) studied the effect of inclination of cliff slope on the response at the crest to vertically propagating SV and SH waves (Figures 2.9 and 2.10). They observed that as the slope becomes less steep from vertical to 30°, the magnitude of horizontal amplification (relative to free-field) at the first peak occurring at H/λ = 0.2 decreases from 25% to about 15% for SH waves and from 55% to 15% for SV waves.

2.6.7 Three-dimensional Topography Shape

Bouchon et al (1996) investigated the effects of three-dimensional shape of a hill on amplification of seismic ground motion and its frequency dependency by considering a hill in an elliptical shape on plan, subject to vertical shear waves polarised along the minor axis and along the direction of elongation of the hill respectively. They found that for incident shear waves polarized along the short minor axis, the amplification at the top of the hill was stronger and the maximum amplification was about two when the wavelength of input excitation is equal to the height of the hill, while for incident shear waves polarized along the direction of elongation of the hill, the maximum amplification was about 1.75 and occurred when the wavelength is equal to four times the height of the hill (the longest of the four wavelengths considered in the study). Bouchon & Barker (1996) also obtained the same finding in their three-dimensional modelling specifically for the case of Tarzana Hill using the same numerical methods.

Apart from numerical modelling, the effects of three-dimensional topography shape on topographic amplification can also be observed in instrumental studies. For example, Nechtschein et al (1995) observed that for ridges having a marked elongation, the amplification effects at ridge top were the largest along the horizontal direction perpendicular to the ridge axis.

2.6.8 Soil Layering

The majority of the literature reviewed considered topographic features in a homogenous half-space, and therefore they did not consider additional amplification due to soil layer effects. As mentioned in Section 2.5.1, some researchers (e.g. Geli et al, 1988) suggested that the discrepancy between observed and theoretical amplifications could be attributed to the presence of subsurface layering that had not been considered in the model, and some work have been done to study how the presence of soil layer overlying homogeneous half-space can influence the topographic effects on seismic ground motions (e.g. Sitar & Clough, 1983; Geli et al, 1988; Ashford et al, 1997; Graizer 2009). In general, these studies were able to predict higher amplification ratios than those considering homogeneous half-space only.

Strong soil amplification is expected when the incoming wavefield is rich in frequencies close to the natural frequency of the soil column behind the slope crest. Sitar & Clough (1983) and Ashford et al (1997) obtained large amplification of horizontal motion at slope crest

(relative to input motion) when the frequency of the input motion was equal to the natural frequency of the soil layer behind the crest. Their results show that the natural frequency of the site behind the crest dominates the surface response and the topographic amplification at the slope crest was small compared to the soil layer amplification in the free field. Therefore, the role of soil layering on the surface response of topographic features can be very important.

However, as mentioned before, the interaction between topographic effects and soil layer effects on amplification of seismic ground motion behind slope crest is still an unsettled issue. Ashford et al (1997) suggested that the topographic effects can be handled separately from amplification due to the natural frequency of the layer behind the crest of the slope whereas some (e.g. Geli et al, 1988) considered that the topographic effects are difficult to isolate from subsurface layering and the amplification of ground motion cannot be predicted by a priori estimations based solely on topography.

2.6.9 Soil Damping

In the parametric study by Ashford et al (1997), the values of critical damping ratios (ξ) used in the analyses varied from 1% to 20%. They found that increased damping significantly reduces the response of both the free field and of the slope, particularly at higher frequencies, but damping has very little effect on the amplification of the motion at the crest as compared to the free field behind the crest (Figure 2.13).

Bouckovalas & Papadimitriou (2005), in their parametric study, also obtained similar results. The damping ratio of soil (ξ) has insignificant effect on the amplification of the motion at slope crest (Figure 2.14). They also observed that material damping can affect the extent of the area where the response is governed by the topographic irregularity, which becomes more confined in the vicinity of the slope as material damping increases.

2.6.10 Discussion

From the literature review, a range of parameters affecting the topographic effects on seismic ground motions have been identified. However, it is noted that the majority of the numerical and parametric studies examined topographic features in a homogenous half-space, and therefore they were unable to investigate the interaction between topographic effects and soil layer effects.

Although a few numerical studies have considered the presence of subsurface soil layer, they were not performed based on sufficient parameters so that a general overall idea of the interaction between topographic effects and soil layer effects can be obtained. Therefore, from a quantitative point of view, it remains uncertain about how the presence of a soil layer overlying bedrock would influence the amplitude of topographic amplification at slope crest, especially when the topography is subjected to incident seismic waves having the same period as the site periods of the one-dimensional soil column at free-field behind the slope crest which results in soil layer amplification of the incident seismic waves.

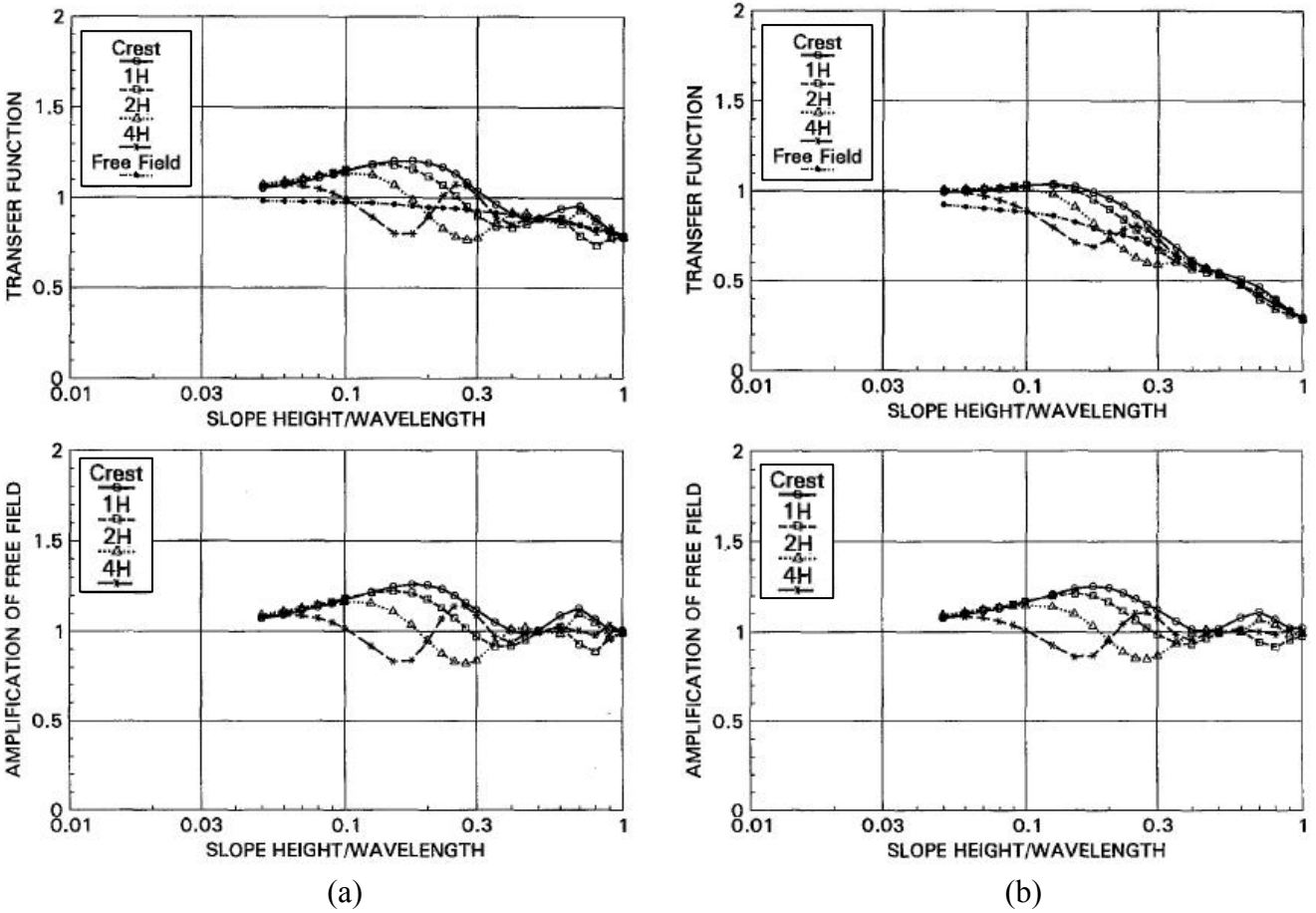

Figure 2.13 Horizontal Amplifications for Vertically Incident SH Wave in a Slope in a Homogeneous Half-space for Various Distances Behind the Crest, (a) β = 1% and (b) β = 5% (from Ashford et al, 1997)

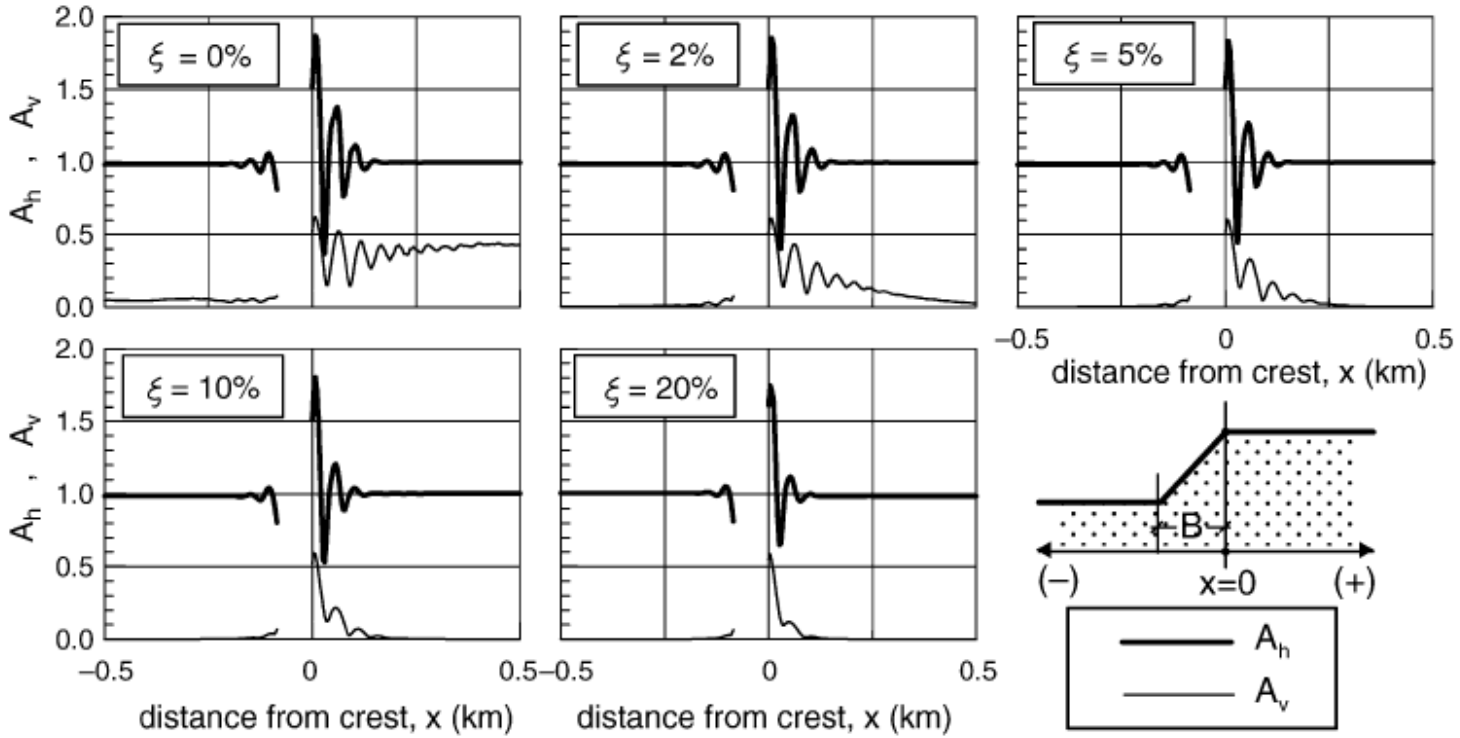

Figure 2.14 Effect of Soil Damping ξ on the Horizontal and Vertical Amplification Factors (A_h and A_v), as a Function of Horizontal Distance x from the Slope Crest ($H/\lambda = 2$, $i = 30°$, $N = 4$) (from Bouckovalas & Papadimitriou, 2005)

2.7 Provisions of Topographic Effects in Seismic Codes

Based on the review of seismic codes carried out by Bouckovalas & Papadimitriou (2005 & 2006) and Tripe (2009), it was found that only the Eurocode 8 (EC-8) (British Standards Institution, 2004) and the French seismic code PS-92 (AFNOR, 1995) have provisions for considering topographic effects of seismic ground motion, particularly for two-dimensional topographic irregularities.

The EC-8 specifies that for important structures on or near slopes, topographic amplification effects should be taken into account. According to the (Informative) Annex A of EC-8 Part 5, the topographic amplification factor, S_T, considered to be independent of the fundamental period of vibration, is multiplied as a constant scaling factor to the ordinates of the elastic response spectrum. The code gives the following recommendations for topographic amplification factor S_T for two-dimensional topographic irregularities:

- S_T is applied as a constant scalar factor at all frequencies.
- S_T is applied for slopes with height greater than 30 m and average slope angle greater than 15°.
- For isolated cliffs and slopes, a value S_T is ≥ 1.2 should be used for sites near the top edge.
- For ridges with crest width significantly less than the base width, a value $S_T \geq 1.4$ should be used near the top of the slopes for average slope angles greater than 30°, and a value $S_T \geq 1.2$ should be used for smaller slope angles.
- In the presence of a loose surface layer, the value of S_T should be increased by at least 20%.
- The value of S_T may be assumed to decrease as a linear function of the height above the base of the cliff or ridge, and to be unity at the base.

It is noteworthy that the EC-8 only specifies the minimum values of topographic amplification factor S_T for different cases, however it does not provide any clear guideline on how to determine the value of S_T.

As the topographic amplification factor is multiplied as a constant scaling factor with the ordinates of the elastic design response spectrum, topographic amplification is considered frequency-independent and applied separately to soil layer effects in the EC-8. It is also noted that the EC-8 prescribes that topographic amplification is applied "near the top edge" or "near the top of the slopes" and hence, the distance to the free field is relatively small but not clearly defined.

The PS-92 code specifies that "except if the effect of the topography on the seismic motion is directly taken into account using a dynamic calculation based on a proper idealization of the relief, a multiplying coefficient τ called site response factor or topography

factor will be used". The PS-92 code provides an empirical method to determine the magnitude of the topographic factor, based on the gradients of the ground at upslope and downslope sides of the topographic convex point, with a maximum value of 1.4. The PS-92 code also prescribes an empirical method to estimate the distances to the free field where topographic effect can be neglected, according to which these distances rarely exceed the height of the slope. Like the EC-8, the PS-92 code prescribes conditions for the geometric dimensions of the slope, below which topographic effect of seismic ground motion should be ignored. The provisions contained in the PS-92 code for topographic effects are summarized in Figure 2.15.

3 Methodology and Parameters Adopted for This Study

3.1 Methodology

A time-domain two-dimensional finite element parametric study using the Imperial College Finite Element Program (ICFEP) (Potts & Zdravkovic, 1999) has been carried out to evaluate the topographic effects at the crest of a soil slope overlying rigid bedrock, for different bedrock depths (and hence site frequencies) and different slope inclinations, under vertically propagating SV waves.

The parametric study has included incident waves with frequencies equal to the fundamental and first harmonic frequencies of the one-dimensional soil column at free-field behind the slope crest so that the topographic and soil layer effects can occur behind the slope crest simultaneously and their interaction can be investigated.

In this study, the values of dimensionless frequency (H/λ) were varied by using input motions of different predominant periods and the variation of topographic amplifications with H/λ for different slope inclinations and bedrock depths were obtained. This allows a direct comparison of the results obtained from this study with those from Ashford et al (1997) and Bouckovalas & Papadimitriou (2005).

3.2 Geometry of the Model

The geometry of the two-dimensional finite element model is presented in Figure 3.1. A soil slope of 50 m in height (H = 50) was considered, and the width of the mesh was set at 1000 m (i.e. 20H) whereas the height of the mesh was varied and equal to the thickness of the soil layer above the rigid bedrock (Z). In this analysis, three different thicknesses of the soil layer were modelled, i.e. Z = 125 m, 250 m and 500 m.

The domain reduction method (DRM) developed by Bielak et al (2003) in conjunction with the standard viscous boundaries of Lysmer & Kuhlemeyer (1969) were used as the boundary conditions in this study. This approach can approximate free-field conditions at the lateral boundaries of the mesh.

The slope height, soil parameters and frequencies of the input motions were selected to cover a sufficiently wide range of the normalised height of the slope (H/λ). Following Ashford et al (1997) and Bouckovalas & Papadimitriou (2005), a range of H/λ = 0.01 to 1.0

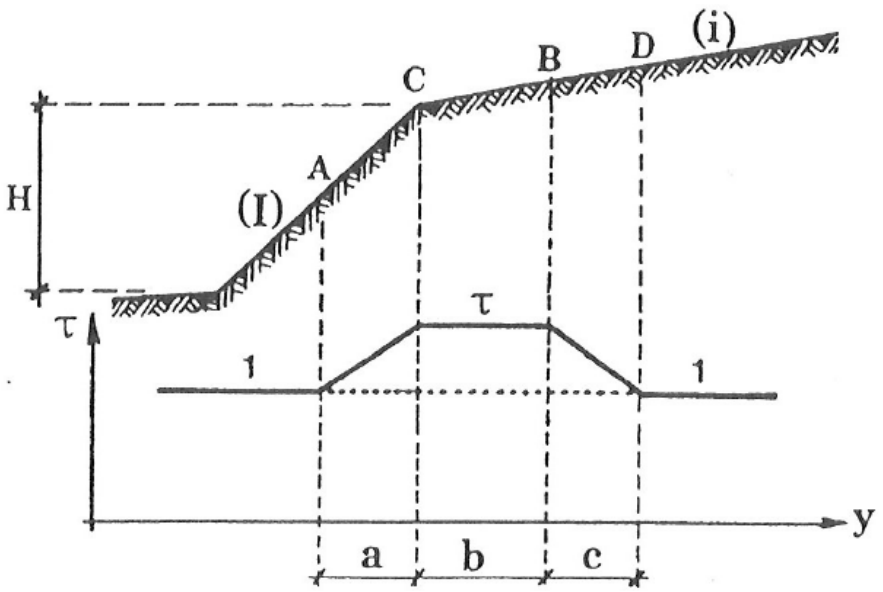

Topography factor τ is required when $H \geq 10$ m and $i \leq I/3$:

$$\begin{cases} \tau = 1 & \text{for } I - i \leq 0.40 \\ \tau = 1 + 0.8\,(I - i - 0.4) & \text{for } 0.40 \leq I - i \leq 0.90 \\ \tau = 1.40 & \text{for } I - i \geq 0.90 \end{cases}$$

$b = 20I$ or $(H + 10)/4$, whichever is the smaller

a = $H/3$
c = $H/4$

Note: i = tangent of upslope angle
I = tangent of downslope angle

Figure 2.15 Provisions for Topographic Effects in the French Seismic Code PS-92

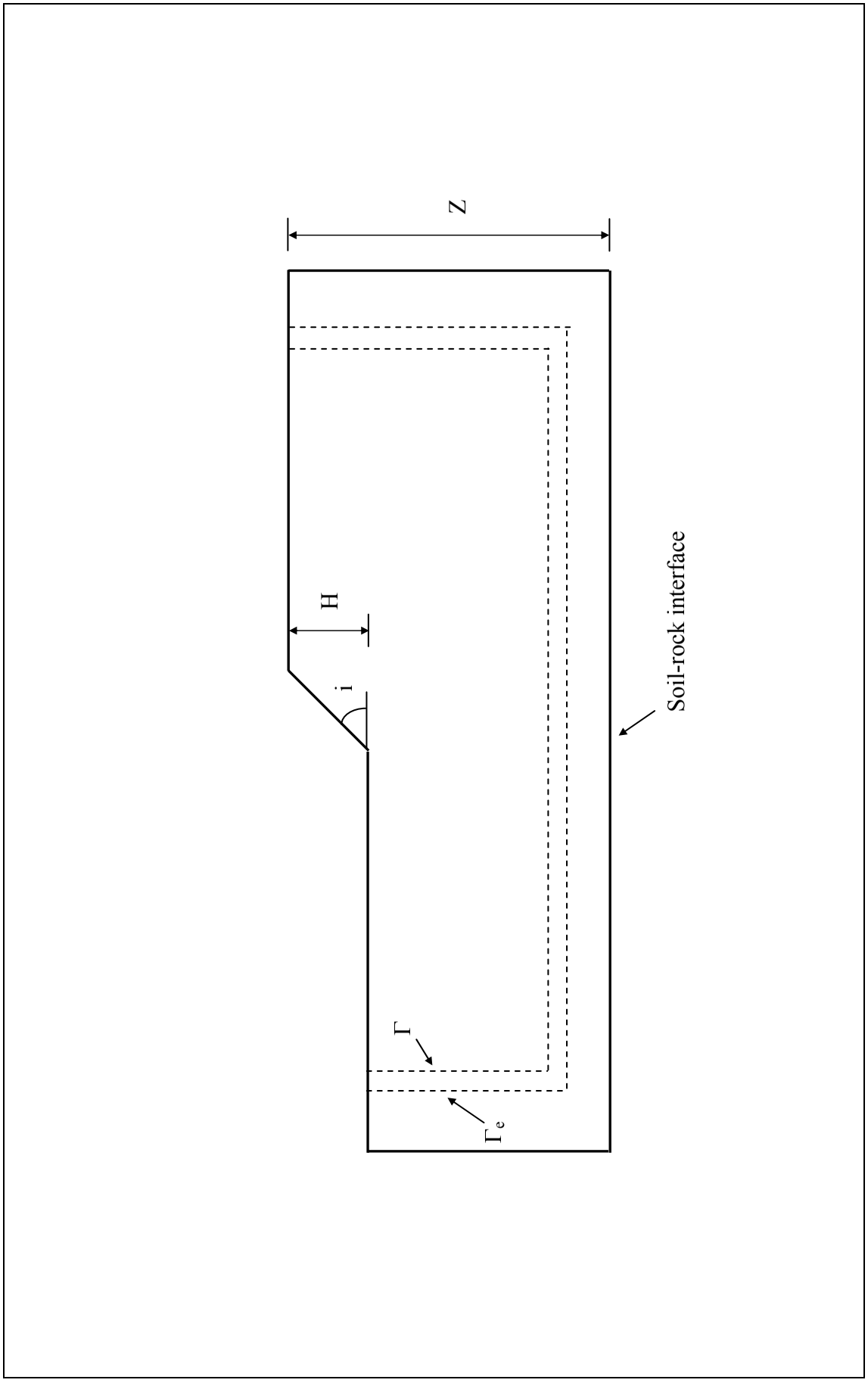

Figure 3.1 Geometry of the Two-dimensional Finite Element Model and Domain Reduction Boundaries

was studied. The values of H/λ were varied by using input motions of different predominant periods, rather than changing the slope height or shear wave velocity, so that the same geometry could be used and the same site periods of the soil layer could be maintained for different analyses. In addition, the predominant period (Tp) of the input motions were specified within the range from 0.1 to 10 s, which practically covers the large majority of possible earthquake events.

Apart from vertical slope, analyses were also performed for slopes with inclinations i = 45°, 30° and 10°, to study the effects of the slope inclination on the topographic amplifications.

3.3 Parameters

In this parametric study, the soil was modelled as a linear elastic material, and thus shear modulus remained constant. The material damping is of the Rayleigh type and therefore it is frequency-dependent. In order to have the same level of soil damping for all frequencies of the input motions, the Rayleigh damping coefficients had to be specified according to the input frequencies of the motions. A damping ratio (ξ) of 5% was adopted in this analysis.

The soil properties adopted in this parametric study are the same as those used in Bouckovalas & Papadimitriou (2005): shear-wave velocity, v_s = 500 m/s, Poisson's ratios ν = 1/3 and mass density ρ = 2000 kg/m^3.

3.4 Time History Excitations

As the ICFEP analyses use the time-domain method, the input excitations have to be discretised to give a time history of acceleration to be introduced at the base of the mesh. Obviously a too large time step will result in an inaccurate solution. In this study, a time-step equal to 1/40 of the predominant period of the input motions was adopted in discretisation of the input acceleration-time history to ensure that an accurate solution can be obtained.

In order to investigate the effects of the frequency of input motions on topographic amplifications, artificial input motions with single predominant frequency have to be used, rather than actual seismic excitations which have very wide frequency spectra. In this analysis, wavelets of Chang's motion, presented in Equation 3.1 below, were used with the aim of simulating the limited duration and the gradual rise and decrease of shaking amplitude of actual earthquakes.

$$a(t) = \sqrt{\beta e^{-\alpha t}\, t^{\gamma}}\, \sin\left(\frac{2\pi t}{T_p}\right) \quad \text{..... (3.1)}$$

where α, β and γ are constants controlling the shape of the envelope of the acceleration-time history and Tp is the predominant period of the motions.

In this parametric study, the adopted predominant period of the Chang's motion (*Tp*) ranges from 0.1 to 10 s, a range practically covering the large majority of possible earthquake events. This range of *Tp* produced the range of H/λ = 0.01 to 1.0 (Table 3.1), as all analyses were performed for a slope of height H = 50 m and uniform shear wave velocity v_s = 500 m/s.

There are two possible approaches of specifying the duration of the input motions. The first one is to maintain the same number of cycles and hence to have different durations for motion records of different predominant period. The other is to maintain the same duration but vary the number of cycles for different motion records. In this investigation, the first approach was adopted because it reflects better the nature of real earthquake records, which show shorter durations when the motions have high frequency contents, i.e. shorter periods.

By varying the values of α, β and γ in Equation 3.1, all the input motions in this investigation were adjusted to have a maximum amplitude of unity and 12 number of excitation cycles. An example of the acceleration-time histories of Chang's motion used in this study is shown in Figure 3.2.

The raw acceleration-time histories, given by Equation 3.1, had to be first corrected using the program SeismoSignal v4.0 (SeismoSoft, 2010) developed by Seismosoft, and these baselined acceleration-time histories were then introduced as the base excitations in the ICFEP analyses.

Table 3.2 presents a summary of the different slope geometries and acceleration-time history cases that have been analysed in this study.

3.5 Finite Element Methodology

3.5.1 General

The parametric study was carried out with the Imperial College Finite Element Program (ICFEP) using two-dimensional dynamic time domain analysis in plane strain. The time-integration was performed with the generalised-α method (Chung & Hulbert, 1993).

Mesh elements have to be small enough to give a sufficiently fine mesh so that the motion of seismic waves, especially those with short wavelength, can be modelled with sufficient accuracy. In this analysis, a maximum element dimension equal to $\lambda/10$ was adopted, in line with the values discussed by Kontoe (2006). Therefore, input motion with the shortest wavelength (i.e. largest frequency or shortest period) is the most critical to determination of element dimension. As the shortest wavelength considered in this investigation is 50 m, the maximum dimension of mesh elements in this analysis should be limited to 5 m. However, outside the middle half of the mesh, i.e. beyond 250 m (5*H*) from the mid-point of the slope, the maximum horizontal dimension of mesh element was increased to $\lambda/5$ (10 m) to reduce the total number of elements and hence computational time. This is considered acceptable because very accurate modelling is relatively not important in this region where the topographic irregularity is far away and in which topographic effects are expected to be very small.

Table 3.1 Predominant Periods of Input Motion Selected for Analysis and the Corresponding Dimensionless Frequency Values

Predominant period, *Tp* (s)	10	4	2	1.333	1	0.667	0.5	0.333	0.2	0.1
Frequency, *f* (Hz)	0.1	0.25	0.5	0.75	1	1.5	2	3	5	10
Wavelength, λ (m)	5000	2000	1000	666.7	500	333.3	250	166.7	100	50
Dimensionless frequency, H/λ	0.01	0.025	0.05	0.075	0.1	0.15	0.2	0.3	0.5	1

Note: v_s = Shear-wave velocity = 500 m/s
H = Height of slope = 50 m

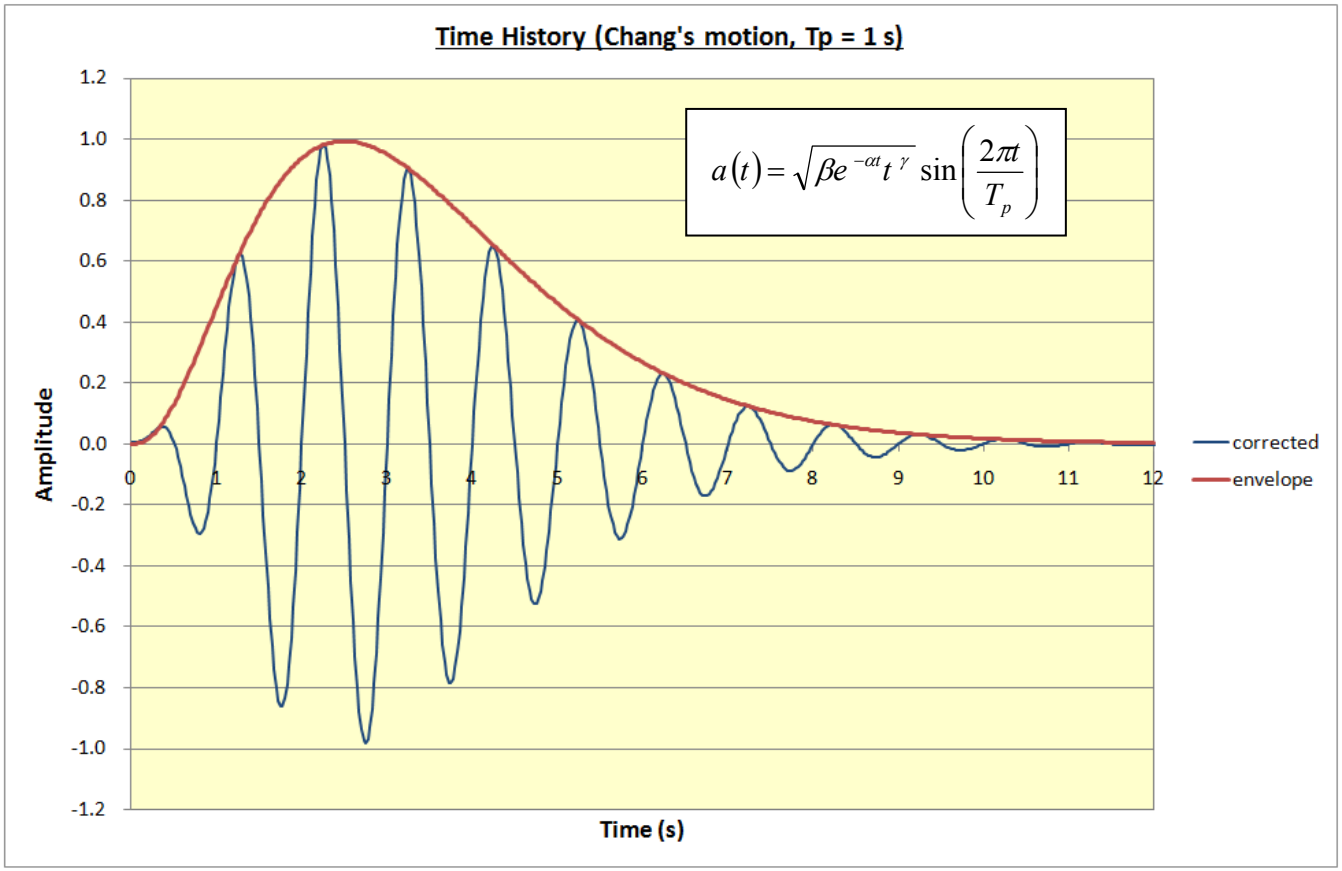

Predominant Period (Tp) = 1 s
Parameters Used: $\alpha = 2$, $\beta = 1.5$, $\gamma = 5$

Figure 3.2 An Example of the Acceleration-time Histories of Chang's Motion Used as Input Excitation in This Study

Table 3.2 Summary of Analyses Performed in the Present Study and Selected Analyses from Tripe (2009) for Review in the Present Study

Bedrock depth, *Z* (m)	Slope inclination, *i* (degrees)	Predominant period of input motion, *Tp* (s)									
		10	4	2	1.333	1	0.667	0.5	0.333	0.2	0.1
		Dimensionless frequency, H/λ									
		0.01	0.025	0.05	0.075	0.1	0.15	0.2	0.3	0.5	1
125	90	✓	×	✓	×	✓	×	✓	✓	✓	✓
	45	o	×	o	×	o	×	o	o	o	o
	30	o	×	o	×	o	×	o	o	o	o
	10	o	×	o	×	o	×	o	o	o	o
250	90	✓	✓	✓	✓	✓	✓	✓	✓	✓	✓
	45	✓	✓	✓	✓	✓	✓	✓	✓	✓	✓
	30	✓	✓	✓	✓	✓	✓	✓	✓	✓	✓
	10	✓	✓	✓	✓	✓	✓	✓	✓	✓	✓
500	90	✓	✓	✓	✓	✓	✓	✓	✓	✓	✓

Legends :

✓ Analysis performed in the present study

× No analysis performed in the present study

o Analysis performed in Tripe (2009) and the results reviewed in the present study

▭ Analysis corresponding to the fundamental and second site periods of the soil column behind the slope crest

3.5.2 Domain Reduction Method

The domain reduction method is a two-step procedure. A detailed description of the implementation and benefits of the domain reduction method is given in Kontoe et al (2009).

In this investigation, the first step of the DRM considered a one-dimensional finite element model corresponding to the soil column extending to the bedrock behind the slope crest (slope topography was not considered). A time history of horizontal acceleration was applied along the bottom mesh boundary as the seismic excitation. Due to the finite element node constraints imposed, no absorbing boundary condition can be specified at the bottom boundary together with the excitation. Vertical displacements were restricted along the bottom and lateral boundaries whereas horizontal displacements were restricted along the bottom boundary after the end of the base excitation. During the step I analyses, the incremental displacements were calculated at various depths of the one-dimensional model. These were then used in the step II analyses to calculate the corresponding equivalent forces.

The second step was performed on a two-dimensional model incorporating the slope topography. The seismic excitation was directly introduced into the computational domain in the form of equivalent forces calculated in the first step. These forces were applied to the corresponding nodes of the step II model located within the boundaries Γ_e and Γ, which are schematically indicated on Figure 3.1. As the excitation is in the form of forces in the step II analyses, absorbing boundary conditions can be applied at the bottom of the mesh together with the excitation. In the two dimensional model, normal and tangential dashpots were applied along the lateral boundaries, whereas vertical and horizontal displacements were restricted along the bottom boundary of the mesh which represents the surface of rigid bedrock. The dashpots and the domain reduction are combined to prevent reflections from the lateral boundaries, by approximating free-field conditions at the lateral sides of the mesh.

However, the above approach of using the DRM in the dynamic finite element analysis results in a major limitation to the investigation of this study. As the one-dimensional finite element analysis of the soil column extending to the bedrock behind the slope crest was used in the DRM to calculate the equivalent forces which were introduced in the subsequent two-dimensional analysis, the ground motions in front of the slope crest could not be modelled accurately in the two-dimensional analysis and therefore they are not considered in this study.

3.6 Procedures

In summary, the procedures of the parametric analysis in this investigation consist of two stages, and are summarised as follow:

Stage 1 – One-dimensional Modelling

The first stage of the analysis consists of the following steps:

(a) Generation, discretisation and baseline processing of the acceleration-time history.

(b) One-dimensional ICFEP dynamic analysis of the soil column behind the slope crest (step I of the DRM).

- The analysis results were used in the step II of the DRM to calculate the equivalent forces to be applied in the step II analyses.
- The one-dimensional analyses also gave the free-field response of the ground, which is free from any topographic effect.
- The results of the two-dimensional ICFEP dynamic analyses would be normalised against this free-field response for determination of the topographic amplification factors.

(c) Equivalent-linear site response analysis of the one-dimensional soil column behind the slope crest, using the EERA program and a soil damping ratio (ξ) of 5%.

- The EERA program version 2000 was developed by the University of Southern California (USC, 2000).
- The results of EERA analysis were compared with the results of the ICFEP one-dimensional dynamic analysis to confirm that the Rayleigh coefficients used in the ICFEP analysis gave the correct level of damping (5%).

The above procedures were repeated for different selected parameters of slope inclination (i), predominant period of input motion (Tp) and bedrock depth (Z).

Stage 2 – Two-dimensional Modelling

The second stage of the analysis consists of the following steps:

(a) Two-dimensional ICFEP static analysis to model removal of soil material in front of the slope in a single excavation stage.

(b) Two-dimensional ICFEP dynamic analysis (step II of the DRM).

- The equivalent forces calculated in the one-dimensional ICFEP dynamic analysis (step I of the DRM) were introduced in the two-dimensional dynamic analysis as the seismic excitation.
- The two-dimensional analyses gave the response (acceleration-time history) at different locations (nodes)

on ground surface behind the slope crest. The peak acceleration values were normalised against the corresponding free-field response obtained from the one-dimensional analyses for determination of the topographic amplification factors.

4 Parametric Study

4.1 Topographic Amplification Factors

In this parametric study, the topographic amplification factors at a particular point of ground surface behind the slope crest were determined by the acceleration values at that point normalised against the free-field horizontal acceleration of the ground behind the slope crest, which is free from any topographic effects. The free-field response was obtained from the one-dimensional ICFEP dynamic analysis of the soil column behind the crest.

It is important to note that in this study, comparison is made between the acceleration value at the point of interest and the free-field horizontal acceleration of the ground behind the slope crest. This approach is the same as that adopted in Bouckovalas & Papadimitriou (2005). If comparison is made directly with the magnitude of acceleration of the input excitation, it would not be able to determine the topographic amplification factors because the ground motion has been modified by both topographic and soil layer effects (i.e. topographic and soil layer effects are coupled).

The topographic amplification factors, A_h and A_v for horizontal and vertical motions respectively, were calculated using the following simple equations:

$$A_h = \frac{a_h}{a_{h,ff}} \quad \text{and} \quad A_v = \frac{a_v}{a_{h,ff}} \qquad \text{..... (4.1)}$$

where a_h and a_v are the peak horizontal and peak vertical accelerations at the point of interest; $a_{h,ff}$ is the peak free-field horizontal acceleration.

It should be noted that $a_{h,ff}$ is used for normalisation of both a_h and a_v, because the free-field vertical acceleration, $a_{v,ff}$, is zero for a vertically propagating SV wave.

From Equation 4.1, it is important to note that topographic de-amplification ($A_h < 1$) means that the horizontal acceleration value at the point of interest is smaller than that of the free-field motion behind the slope crest. It does not necessarily mean that the horizontal acceleration value is smaller than that of the input excitation at rock level.

Similarly, the one-dimensional soil layer amplification factor, A_{1D}, was determined by the following equation:

$$A_{1D} = \frac{a_{h,ff}}{a_{h,in}} \qquad \text{..... (4.2)}$$

where $a_{h,in}$ is the peak acceleration of the input motion.

When the topographic amplification factors, A_h and A_v, are plotted against the distance along the ground surface behind the slope crest, the following trends of topographic effects on seismic ground motion can be indentified:

(a) The horizontal ground motion behind the slope crest is modified by topographic effects and becomes different from the free-field response.

(b) Parasitic vertical motion is generated at the ground surface behind the slope crest, even though the input motion, a vertically propagating SV wave, has no vertical component. This vertical component of seismic motion may become comparable to the horizontal free-field motion in some cases.

(c) In some cases, the magnitudes of topographic effects on horizontal and vertical motions fluctuate with distance away from the slope crest, resulting in zones of alternating amplification and de-amplification of the horizontal motion along the ground surface behind the slope crest (Figure 4.1).

(d) The magnitudes of topographic effects generally decrease with distance away from the slope crest (Figure 4.1).

(e) When the wavelength of the input motion is very large compared with the height of the slope (very small H/λ), the topographic effects on the ground motion response are insignificant (Figure 4.2).

(f) By comparing the results obtained from the same dimensionless frequency but different slope inclination and bedrock depth, it can be seen that the pattern of topographic effects depends primarily on the dimensionless frequency of the input motion (H/λ) whereas the problem geometry (slope inclination and bedrock depth) can only affect the magnitudes of the topographic effects. One exception is that the bedrock depth can also control the site periods of the soil column behind the slope crest, leading to soil layer amplification which can significantly influences the pattern of topographic effects.

(g) When the predominant frequency of input motion is equal to the site periods of the soil column behind the slope crest, soil amplification of the input motion occurs, and this results in a large horizontal free-field motion. In this case, the magnitude of horizontal ground motion at the slope crest becomes smaller than the horizontal free-field motion. In other words, topographic de-amplification occurs. However, the magnitude of horizontal ground motion at the slope crest could still be larger than that of the input excitation. More details of this finding will be given in the following sections.

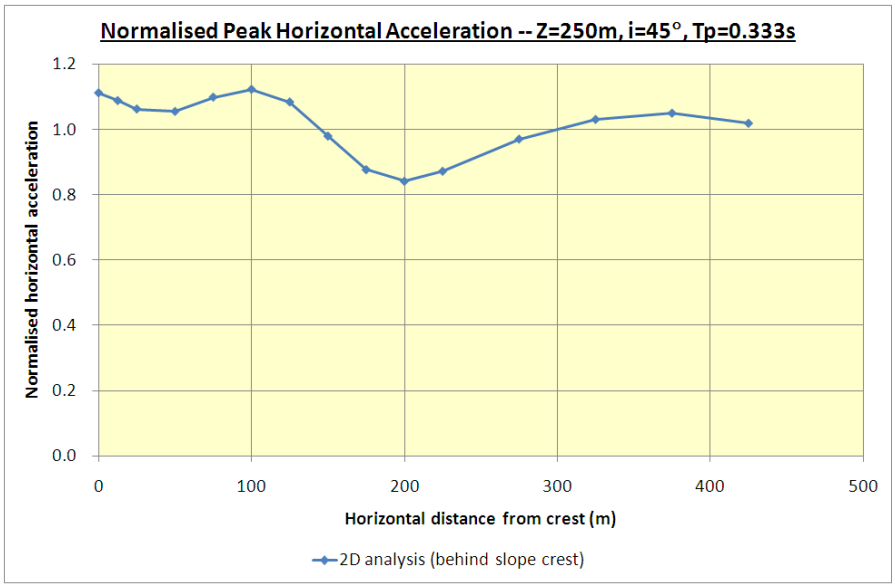

(a) Horizontal Amplification

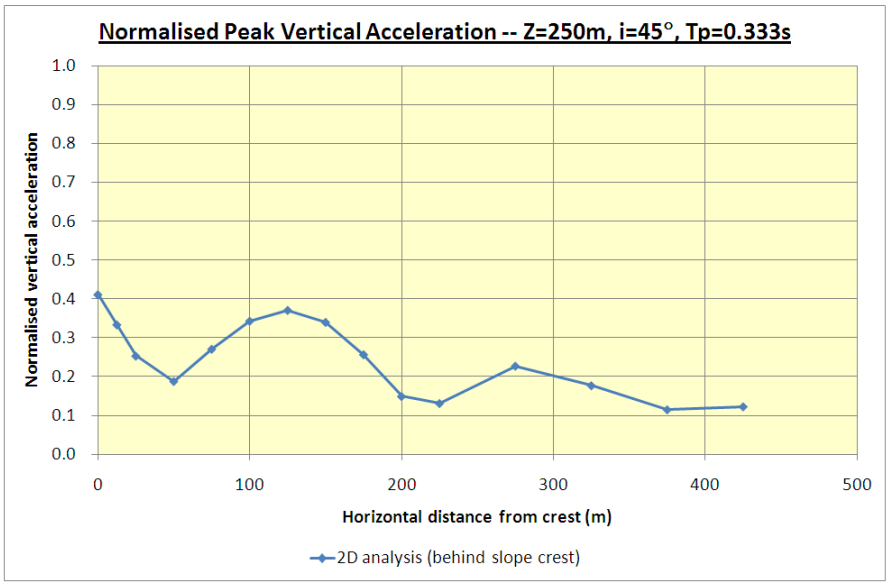

(b) Vertical Amplification

Figure 4.1 Topographic Amplifications (A_h and A_v) as a Function of Horizontal Distance from Slope Crest (Z = 250 m, i = 45°, Tp = 0.333 s, H/λ = 0.3)

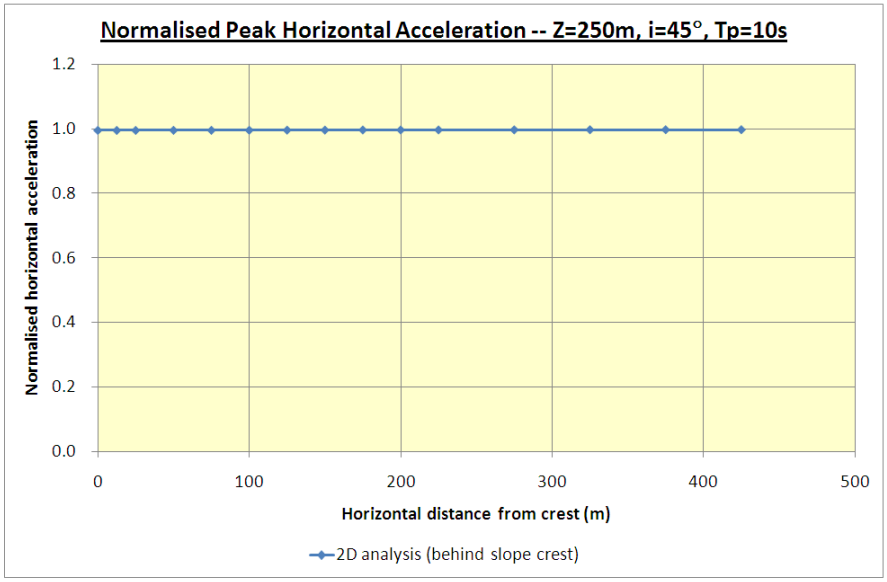

(a) Horizontal Amplification

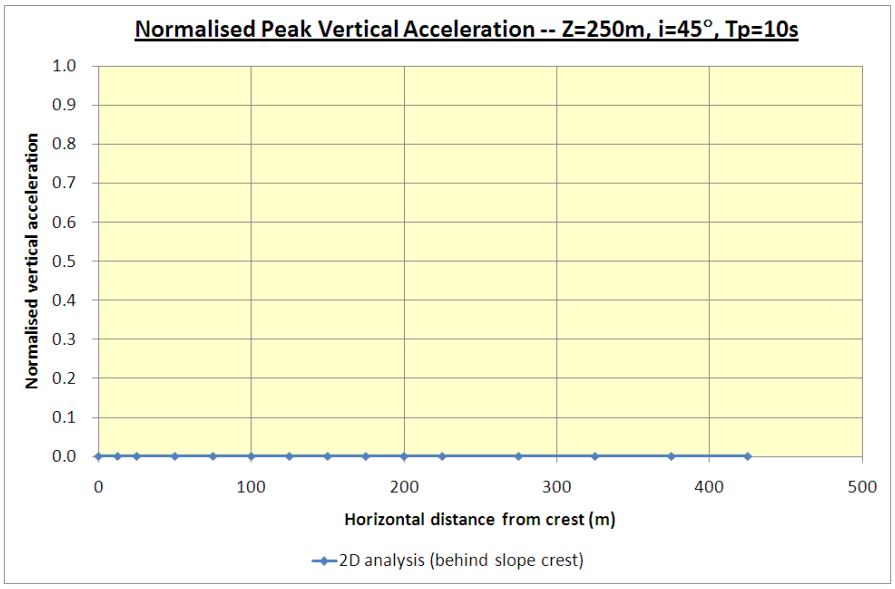

(b) Vertical Amplification

Figure 4.2 Topographic Amplifications (A_h and A_v) as a Function of Horizontal Distance from Slope Crest (Z = 250 m, i = 45°, Tp = 10 s, H/λ = 0.01)

The values of the peak horizontal acceleration (a_h) and peak vertical acceleration (a_v) at the slope crest obtained from the numerical analysis in this parametric study are presented in Table 4.1. The values of the peak accelerations of the input motion ($a_{h,in}$) and the peak free-field horizontal accelerations ($a_{h,ff}$) are also presented in the same table. From these values, the one-dimensional soil layer amplification factor (A_{1D}) and the topographic amplification factors for horizontal and vertical motions (A_h and A_v) can be determined using Equations 4.1 and 4.2. Table 4.1 can illustrate the effects of dimensionless frequency (H/λ), slope inclination (i) and bedrock depth (Z) on the topographic effects of seismic ground motion and also the interaction between soil layer effects and topographic effects. These will be discussed in detail in the coming sections.

4.2 Effects of Varying Dimensionless Frequency (H/λ)

4.2.1 General

In order to allow a direct comparison of the results obtained from this investigation with those from previous studies carried out by Ashford et al (1997) and Bouckovalas & Papadimitriou (2005), the results of the analyses of this study are presented as a function of the dimensionless frequency (H/λ).

The dimensionless frequency (H/λ) can be expressed in terms of the period of input motion (T), slope height (H) and shear-wave velocity of soil (v_s) as follow:

$$\frac{H}{\lambda} = \frac{fH}{v_s} = \frac{1}{T} \times \frac{H}{v_s} \quad \text{..... (4.3)}$$

According to Equation 2.6, the natural site periods of the soil layer with thickness Z is given by:

$$T_n = \frac{4Z}{(2n+1)v_s} \qquad , n = 0, 1, 2, \ldots\infty$$

Equation 4.3 becomes:

$$\frac{H}{\lambda} = \frac{(2n+1)v_s}{4Z} \times \frac{H}{v_s} = \frac{(2n+1)H}{4Z} \qquad , n = 0, 1, 2, \ldots\infty \quad \text{..... (4.4)}$$

As a result, the values of H/λ corresponding to the fundamental (n = 0) and second (n = 1) site periods of the soil layer can be determined.

The one-dimensional soil layer amplification factor, A_{1D}, was determined for different bedrock depths, and its variation with the dimensionless frequency is presented in Figure 4.3. It can be seen that in all cases, a sharp amplification peak occurs at the dimensionless frequency corresponding to the fundamental site period of the soil column behind the slope crest and also another peak of smaller magnitude occurs at the dimensionless frequency corresponding to the second site period.

Table 4.1 Summary of the Results of the Numerical Analysis Performed in This Study (Sheet 1 of 5)

H/λ		0.01	0.025	0.05	0.075	0.1	0.15	0.2	0.3	0.5	1
Tp (s)		10	4	2	1.333	1	0.667	0.5	0.333	0.2	0.1
$Z = 125$ $i = 90°$	$a_{h,in}$	1.005	-	0.999	-	0.982	-	1.002	1.003	1.005	1.005
	$a_{h,ff}$	1.017	-	1.435	-	7.105	-	1.146	2.426	1.527	0.922
	$a_{h,crest}$	1.018	-	1.428	-	6.443*	-	3.019	1.580	1.847	1.347
	$a_{v,crest}$	0.004	-	0.065	-	1.199	-	3.328	2.285	2.129	1.490
	$a_{h,crest}/a_{h,in}$	1.013	-	1.429	-	6.560	-	3.012	1.576	1.839	1.341
	A_{1D}	1.013	-	1.436	-	7.235	-	1.143	2.419	1.520	0.918
	A_h	1.000	-	0.995	-	0.907	-	2.634	0.651	1.210	1.461
	A_v	0.004	-	0.045	-	0.169	-	2.904	0.942	1.395	1.616
$Z = 125$ $i = 45°$	$a_{h,in}$	1.005	-	0.999	-	0.982	-	1.002	1.003	1.005	1.005
	$a_{h,ff}$	1.017	-	1.435	-	7.105	-	1.146	2.426	1.527	0.922
	$a_{h,crest}$	-	-	1.366	-	5.082*	-	2.183	1.663	1.682	0.670
	$a_{v,crest}$	-	-	0.004	-	0.175	-	1.865	1.407	0.583	0.395
	$a_{h,crest}/a_{h,in}$	-	-	1.368	-	5.175	-	2.178	1.658	1.675	0.667
	A_{1D}	1.013	-	1.436	-	7.235	-	1.143	2.419	1.520	0.918
	A_h	-	-	0.952	-	0.715	-	1.905	0.685	1.102	0.727
	A_v	-	-	0.003	-	0.025	-	1.627	0.580	0.382	0.429

Table 4.1 Summary of the Results of the Numerical Analysis Performed in This Study (Sheet 2 of 5)

H/λ		0.01	0.025	0.05	0.075	0.1	0.15	0.2	0.3	0.5	1
Tp (s)		10	4	2	1.333	1	0.667	0.5	0.333	0.2	0.1
$Z = 125$ $i = 30°$	$a_{h,in}$	1.005	-	0.999	-	0.982	-	1.002	1.003	1.005	1.005
	$a_{h,ff}$	1.017	-	1.435	-	7.105	-	1.146	2.426	1.527	0.922
	$a_{h,crest}$	-	-	1.355	-	4.824*	-	2.127	1.545	1.892	1.273
	$a_{v,crest}$	-	-	0.012	-	0.332	-	1.849	1.053	0.763	0.295
	$a_{h,crest}/a_{h,in}$	-	-	1.356	-	4.912	-	2.122	1.541	1.883	1.267
	A_{1D}	1.013	-	1.436	-	7.235	-	1.143	2.419	1.520	0.918
	A_h	-	-	0.944	-	0.679	-	1.856	0.637	1.239	1.381
	A_v	-	-	0.008	-	0.047	-	1.613	0.434	0.500	0.320
$Z = 125$ $i = 10°$	$a_{h,in}$	1.005	-	0.999	-	0.982	-	1.002	1.003	1.005	1.005
	$a_{h,ff}$	1.017	-	1.435	-	7.105	-	1.146	2.426	1.527	0.922
	$a_{h,crest}$	-	-	1.368	-	5.028*	-	1.732	1.582	1.728	1.020
	$a_{v,crest}$	-	-	0.010	-	0.381	-	1.581	0.605	0.632	0.123
	$a_{h,crest}/a_{h,in}$	-	-	1.369	-	5.120	-	1.728	1.578	1.720	1.015
	A_{1D}	1.013	-	1.436	-	7.235	-	1.143	2.419	1.520	0.918
	A_h	-	-	0.953	-	0.708	-	1.511	0.652	1.132	1.106
	A_v	-	-	0.007	-	0.054	-	1.380	0.249	0.414	0.134

Table of Contents
Table of Contents
Table of Contents
Table of Contents

Table 4.1 Summary of the Results of the Numerical Analysis Performed in This Study (Sheet 3 of 5)

H/λ		0.01	0.025	0.05	0.075	0.1	0.15	0.2	0.3	0.5	1
Tp (s)		10	4	2	1.333	1	0.667	0.5	0.333	0.2	0.1
$Z = 250$ $i = 90°$	$a_{h,in}$	1.005	1.005	0.999	1.004	0.982	1.001	1.002	1.003	1.005	1.005
	$a_{h,ff}$	1.057	1.424	7.227	1.845	1.123	2.494	1.433	1.256	0.921	0.433
	$a_{h,crest}$	1.054	1.395	6.552*	2.655	1.849	2.069	2.374	1.592	1.036	0.642
	$a_{v,crest}$	0.003	0.023	0.483	0.474	1.274	0.923	0.836	1.755	1.233	0.665
	$a_{h,crest}/a_{h,in}$	1.049	1.389	6.559	2.643	1.882	2.068	2.368	1.588	1.032	0.639
	A_{1D}	1.052	1.417	7.235	1.837	1.144	2.492	1.430	1.252	0.917	0.431
	A_h	0.997	0.980	0.907	1.439	1.646	0.830	1.656	1.268	1.125	1.481
	A_v	0.002	0.016	0.067	0.257	1.135	0.370	0.583	1.398	1.339	1.535
$Z = 250$ $i = 45°$	$a_{h,in}$	1.005	1.005	0.999	1.004	0.982	1.001	1.002	1.003	1.005	1.005
	$a_{h,ff}$	1.057	1.424	7.227	1.845	1.123	2.494	1.433	1.256	0.921	0.433
	$a_{h,crest}$	1.052	1.379	6.192*	2.410	1.584	1.783	1.701	1.396	0.947	0.320
	$a_{v,crest}$	0.001	0.001	0.080	0.215	0.775	0.708	0.697	0.517	0.250	0.199
	$a_{h,crest}/a_{h,in}$	1.047	1.372	6.199	2.399	1.613	1.782	1.697	1.392	0.943	0.318
	A_{1D}	1.052	1.417	7.235	1.837	1.144	2.492	1.430	1.252	0.917	0.431
	A_h	0.995	0.968	0.857	1.306	1.411	0.715	1.187	1.112	1.029	0.738
	A_v	0.001	0.001	0.011	0.116	0.691	0.284	0.486	0.412	0.271	0.458

Table 4.1 Summary of the Results of the Numerical Analysis Performed in This Study (Sheet 4 of 5)

H/λ		0.01	0.025	0.05	0.075	0.1	0.15	0.2	0.3	0.5	1
Tp (s)		10	4	2	1.333	1	0.667	0.5	0.333	0.2	0.1
$Z = 250$ $i = 30°$	$a_{h,in}$	1.005	1.005	0.999	1.004	0.982	1.001	1.002	1.003	1.005	1.005
	$a_{h,ff}$	1.057	1.424	7.227	1.845	1.123	2.494	1.433	1.256	0.921	0.433
	$a_{h,crest}$	1.051	1.375	6.123*	2.365	1.536	1.743	1.651	1.415	1.044	0.605
	$a_{v,crest}$	0.001	0.004	0.144	0.241	0.705	0.688	0.800	0.311	0.276	0.154
	$a_{h,crest}/a_{h,in}$	1.046	1.368	6.130	2.355	1.564	1.741	1.647	1.412	1.039	0.603
	A_{1D}	1.052	1.417	7.235	1.837	1.144	2.492	1.430	1.252	0.917	0.431
	A_h	0.995	0.966	0.847	1.282	1.367	0.699	1.152	1.127	1.133	1.397
	A_v	0.001	0.003	0.020	0.130	0.628	0.276	0.558	0.248	0.300	0.355
$Z = 250$ $i = 10°$	$a_{h,in}$	1.005	1.005	0.999	1.004	0.982	1.001	1.002	1.003	1.005	1.005
	$a_{h,ff}$	1.057	1.424	7.227	1.845	1.123	2.494	1.433	1.256	0.921	0.433
	$a_{h,crest}$	1.052	1.380	6.307*	2.397	1.502	1.754	1.718	1.396	1.007	0.477
	$a_{v,crest}$	0.001	0.006	0.236	0.309	0.580	0.568	0.615	0.296	0.112	0.019
	$a_{h,crest}/a_{h,in}$	1.047	1.374	6.314	2.386	1.529	1.753	1.714	1.392	1.003	0.475
	A_{1D}	1.052	1.417	7.235	1.837	1.144	2.492	1.430	1.252	0.917	0.431
	A_h	0.995	0.970	0.873	1.299	1.337	0.703	1.199	1.112	1.094	1.101
	A_v	0.001	0.004	0.033	0.168	0.517	0.228	0.429	0.236	0.121	0.044

Table of Contents Table of Contents Table of Contents Table of Contents

Table 4.1 Summary of the Results of the Numerical Analysis Performed in This Study (Sheet 5 of 5)

H/λ		0.01	0.025	0.05	0.075	0.1	0.15	0.2	0.3	0.5	1
Tp (s)		10	4	2	1.333	1	0.667	0.5	0.333	0.2	0.1
$Z = 500$ $i = 90°$	$a_{h,in}$	1.005	1.005	0.999	1.004	0.982	1.001	1.002	1.003	1.005	1.005
	$a_{h,ff}$	1.246	7.492	1.142	2.465	1.404	1.253	1.071	0.788	0.433	0.104
	$a_{h,crest}$	1.235	7.455*	1.278	2.920	1.893	1.833	1.520	1.023	0.481	0.156
	$a_{v,crest}$	0.005	0.224	0.256	0.298	0.293	0.865	0.867	0.912	0.584	0.157
	$a_{h,crest}/a_{h,in}$	1.229	7.419	1.280	2.907	1.928	1.831	1.516	1.020	0.479	0.155
	A_{1D}	1.240	7.456	1.144	2.454	1.430	1.252	1.068	0.786	0.431	0.103
	A_h	0.991	0.995	1.119	1.185	1.348	1.463	1.420	1.298	1.111	1.496
	A_v	0.004	0.030	0.224	0.121	0.208	0.691	0.810	1.157	1.349	1.514

H = Height of slope = 50 m
λ = Wavelength of input motion
Tp = Predominant period of input motion
Z = Bedrock depth
i = Slope inclination

$a_{h,in}$ = Peak acceleration of input motion
$a_{h,ff}$ = Peak free-field horizontal acceleration
$a_{h,crest}$ = Peak horizontal acceleration at slope crest
$a_{v,crest}$ = Peak vertical acceleration at slope crest
A_{1D} = One-dimensional soil layer amplification factor
A_h & A_v = Topographic amplification factors for horizontal and vertical motions

Legend:

▭ Analysis corresponding to the fundamental and second site periods of the soil column behind the slope crest

Notes: (1) Results of the analysis performed for (Z = 125 m, i = 45°), (Z = 125 m, i = 30°) and (Z = 125 m, i = 10°) are extracted from Tripe (2009).
(2) Results shown with * refer to the largest peak horizontal acceleration at slope crest.

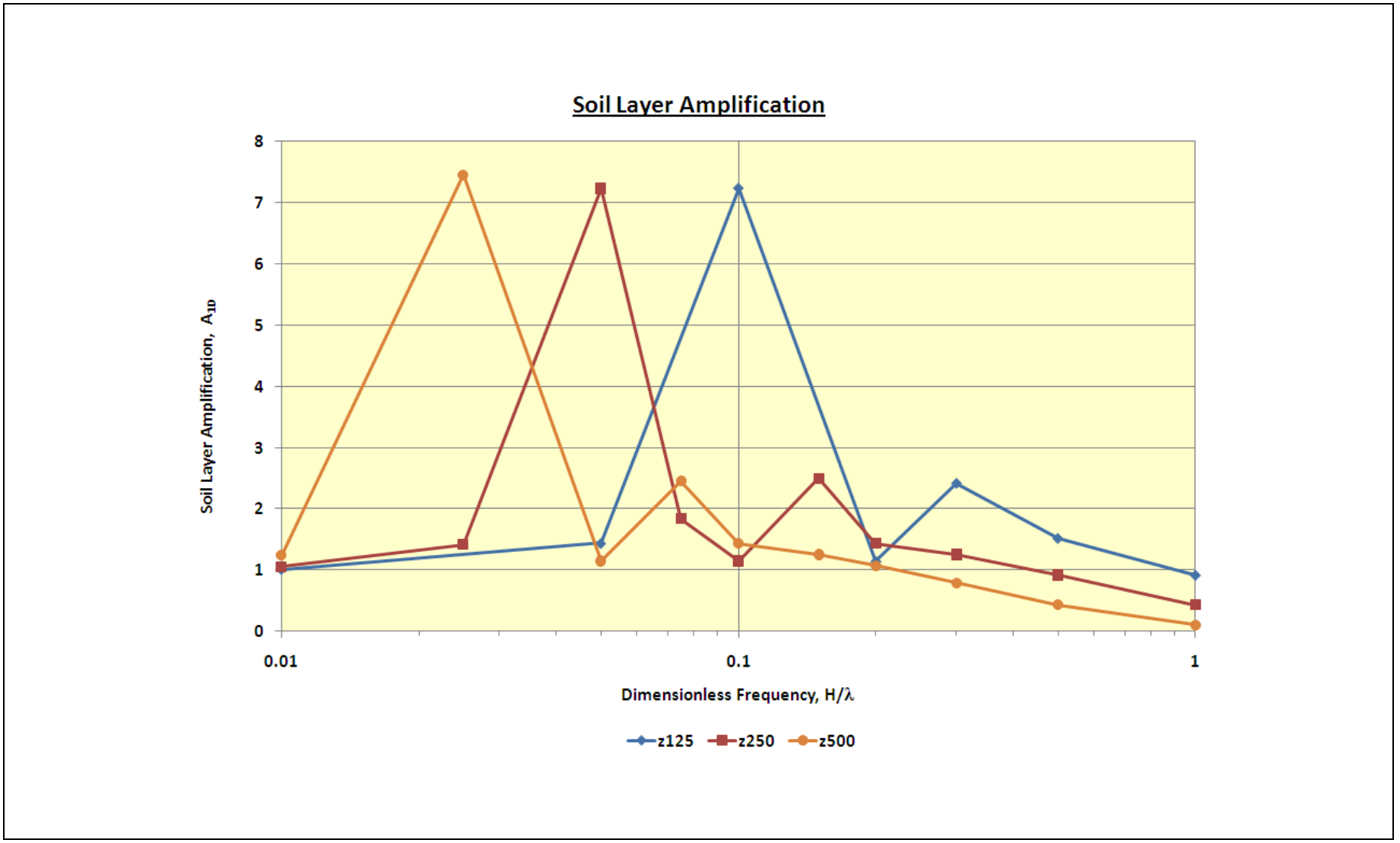

Figure 4.3 Plots of Soil Layer Amplification Factor with Dimensionless Frequency, for Bedrock Depths of 125 m, 250 m and 500 m

It has been shown that topographic amplification factors for both horizontal and vertical motions vary with the dimensionless frequency (H/λ). However, such relationship is not the same for the three different bedrock depths analysed in this study.

4.2.2 Bedrock Depth Z = 250 m

The results of the horizontal response for the bedrock depth Z = 250 m are presented in Figure 4.4. It is clear that the trend of topographic effects for the bedrock depth Z = 250 m are quite different from those given in Ashford et al (1997) and Bouckovalas & Papadimitriou (2005). The following main differences amongst the various studies are observed:

(a) For all slope inclinations, topographic de-amplification ($A_h < 1$) occurs at the slope crest at H/λ = 0.05 and 0.15. It should be noted that this de-amplification is relative to the free-field response behind the slope crest and the horizontal acceleration value at the slope crest is still larger than that of the input excitation (i.e. the ratio of $a_{h,crest}/a_{h,in}$ is still larger than unity, see Table 4.1). On the other hand, both Ashford et al (1997) and Bouckovalas & Papadimitriou (2005) obtained topographic amplification at these two H/λ values. It is interesting to note that these H/λ ratios correspond to the fundamental and second site periods of the 250 m thick soil column behind the slope crest.

(b) For all slope inclinations, the peak horizontal amplifications occurs at H/λ = 0.1. This is different from Ashford et al (1997) and Bouckovalas & Papadimitriou (2005) who reported that peak amplification occurs at H/λ = 0.2 in all analysed cases. It is interesting to note that the peak horizontal amplifications occur at an H/λ ratio in-between those corresponding to the fundamental and second site periods of the 250 m thick soil layer.

(c) The magnitudes of the amplification peaks at H/λ = 0.1 obtained in this study are much higher than those at H/λ = 0.2 obtained from Ashford et al (1997) and Bouckovalas & Papadimitriou (2005). For example, an amplification factor of around 40% was obtained for 45° slope in this study but the corresponding value at H/λ = 0.2 given in Ashford et al (1997) was only about 15%.

The above discrepancies occur within the range of H/λ ratios between 0.05 and 0.15, which are the fundamental and second site periods of the 250 m thick soil layer. Outside this range, the results of this study have similar trend and magnitudes of horizontal topographic amplification compared with Ashford at al (1997) and Bouckovalas & Papadimitriou (2005).

The results of the vertical response for the bedrock depth Z = 250 m are presented in Figure 4.5. Again, the results from Ashford et al (1997) for slopes in a homogeneous

half-space are superimposed as background for comparison. Figure 4.5 shows that, for all slope inclinations, the vertical topographic amplifications at the slope crest at the fundamental and second site periods of the 250 m thick soil column (H/λ = 0.05 and 0.15) are much smaller, compared with Ashford et al (1997) and Bouckovalas & Papadimitriou (2005). De-amplification for vertical motion ($A_v < 0$) is not possible according to its definition (see Equation 4.1). In addition, there exist a sharp peak of the vertical topographic amplification, for all slope inclinations, at H/λ = 0.1, which is in-between those corresponding to the fundamental and second site periods of the 250 m thick soil layer.

In summary, the trend and magnitudes of both horizontal and vertical topographic effects at the crest of a soil slope overlying rigid bedrock are different from those for a slope in a homogeneous half-space. It is reasonable to postulate that the differences are due to the soil layer effects that have significantly affected the magnitude of the horizontal ground response of the soil column, which is taken as the free-field response for evaluation of the two-dimensional topographic effects.

4.2.3 Bedrock Depth Z = 125 m

For bedrock depth Z = 125 m, only one analysis (vertical slope) was performed. The analysis results are presented in Figures 4.6 and 4.7 for the horizontal and vertical response at the slope crest respectively.

The horizontal response shows de-amplification ($A_h < 1$) when the predominant period of the input motions is equal to the fundamental and second site periods of the soil column behind the slope crest (H/λ = 0.1 and 0.3 in this case). Again, this de-amplification is relative to the free-field response behind the slope crest and the horizontal acceleration value at the slope crest is still larger than that of the input excitation (i.e. the ratio of $a_{h,crest}/a_{h,in}$ is still larger than unity, see Table 4.1). Although the peak amplification for the bedrock depth Z = 125 m occurs at H/λ = 0.2 which is in agreement with Ashford et al (1997) and Bouckovalas & Papadimitriou (2005), this result should be treated with caution. In fact, this agreement is just a coincidence because H/λ = 0.2 is in-between the values corresponding to the fundamental and second site periods of the 125 m thick soil layer.

In addition, the vertical topographic amplifications at the slope crest at the fundamental and second site periods of the 125 m thick soil column are much smaller than the values reported in Ashford et al (1997) and Bouckovalas & Papadimitriou (2005). A sharp peak of the vertical topographic amplification also exists at H/λ = 0.2, which is again in-between those corresponding to the fundamental and second site periods of the 125 m thick soil layer.

A comparison between the results for the bedrock depths Z = 250 m and Z = 125 m shows that they have the same pattern in the variations between the horizontal and vertical topographic amplifications and the dimensionless frequency (H/λ), taking into account the natural and second site periods of the soil column behind the slope crest. However, the bedrock depth Z = 125 m has much larger magnitudes of both the horizontal and vertical topographic amplification factors than the bedrock depth Z = 250 m.

4.2.4 Bedrock Depth Z = 500 m

Analysis for a vertical slope was also carried out for a much deeper bedrock depth Z = 500 m. Figures 4.8 and 4.9 show the analysis results for the horizontal and vertical response at the slope crest respectively.

It is interesting to note that for bedrock depth Z = 500 m, the analysis results of both the horizontal and vertical topographic amplifications obtained from this study are very similar to those given in Ashford et al (1997) and Bouckovalas & Papadimitriou (2005). The aforementioned differences due to the presence of soil/rock interface observed for bedrock depths Z = 125 m and Z = 250 m are insignificant in this case. Therefore, it is reasonable to conclude that with a bedrock depth Z = 500 m (or a ratio of the soil layer thickness to the slope height (Z/H) equal to 10), the soil/bedrock interface has little influence on the topographic effects on ground motion at the slope crest. In other words, the model behaves like a homogeneous half-space even with an impedance contrast.

There is one point concerning Figure 4.8 worth mentioning. Originally, the horizontal amplification factor at H/λ = 0.2 obtained in this study by using Chang's signal excitation is lower than the value expected from Ashford et al (1997). Considering that the computational model adopted by Ashford et al in their study was based on steady-state condition, another analysis for H/λ = 0.2 was conducted using harmonic motion with the same peak amplitude, predominant period and duration as the previously adopted Chang's signal excitation. The purpose of this additional analysis is to model the steady-state behaviour. Interestingly, the results of this additional analysis using harmonic input motion fit very well with the value given in Ashford et al (1997). With this additional analysis included, the horizontal topographic amplification factor for bedrock depth Z = 500 m reaches maximum at H/λ = 0.2, and the peak value is around 1.5.

The good match between the analysis results obtained in this study for bedrock Z = 500 m and those obtained from Ashford et al (1997) and Bouckovalas & Papadimitriou (2005) for a slope in homogeneous half-space shows that although three different methodologies of analyses are used (finite element, finite difference and generalised consistent transmitting boundary methods respectively), they produce practically identical results. This helps to verify the computational model adopted in this study.

4.3 Effects of Varying Slope Inclination (i)

It can be seen that with decreasing slope inclination, the magnitudes of both the horizontal topographic amplification at the first peak and of the vertical topographic amplification at the slope crest decrease.

This is in agreement with the findings from Ashford et al (1997) and Bouckovalas & Papadimitriou (2005).

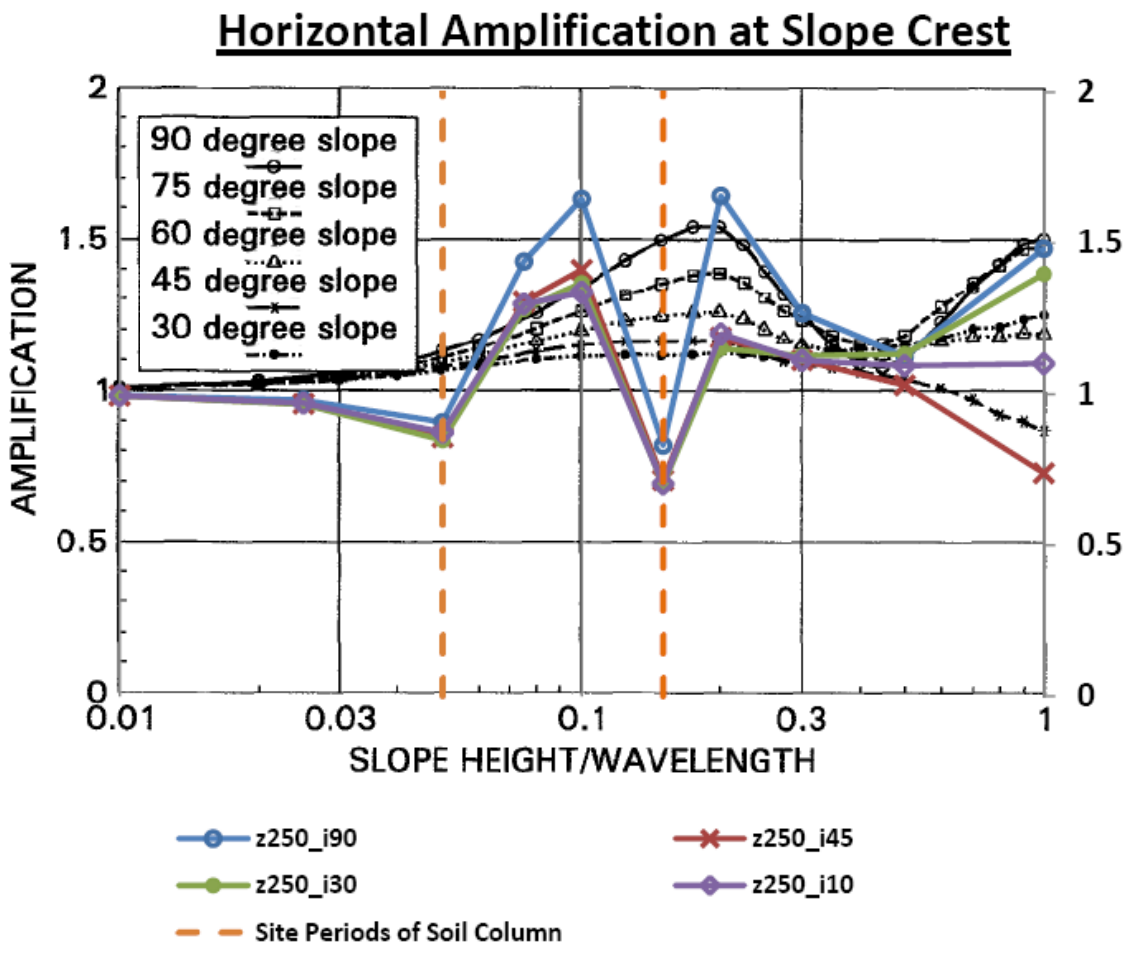

Notes:

(1) The horizontal topographic amplification factor is determined by normalising the horizontal acceleration value at that point against the free-field horizontal acceleration (i.e. not against the acceleration of the input excitation).

(2) Background curves coloured black are extracted from Ashford et al (1997) which are applicable to slopes in a homogeneous half-space.

Figure 4.4 Horizontal Amplification at Slope Crest for a Vertically Incident SV Wave on a Slope with a Bedrock Depth of 250 m

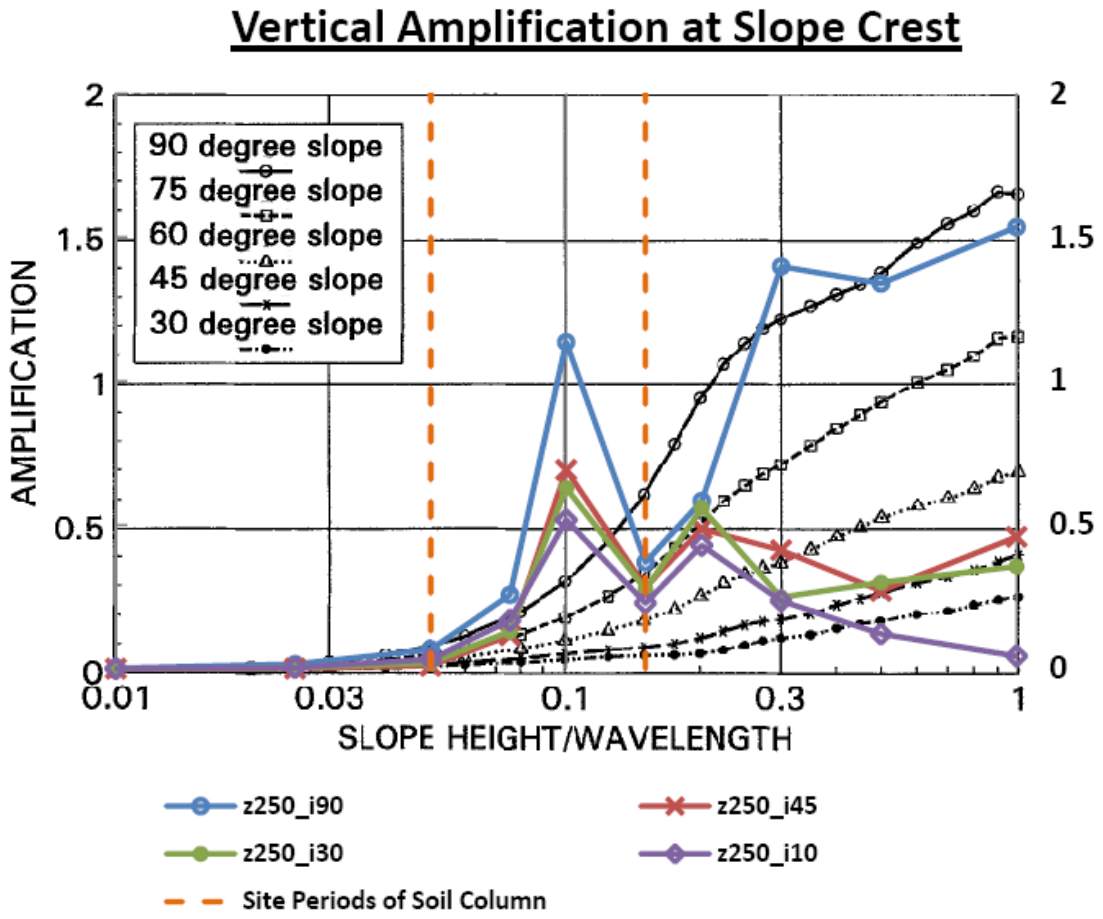

Notes:

(1) The vertical topographic amplification factor is determined by normalising the vertical acceleration value at that point against the free-field horizontal acceleration (i.e. not against the acceleration of the input excitation).

(2) Background curves coloured black are extracted from Ashford et al (1997) which are applicable to slopes in a homogeneous half-space.

Figure 4.5 Vertical Amplification at Slope Crest for a Vertically Incident SV Wave on a Slope with a Bedrock Depth of 250 m

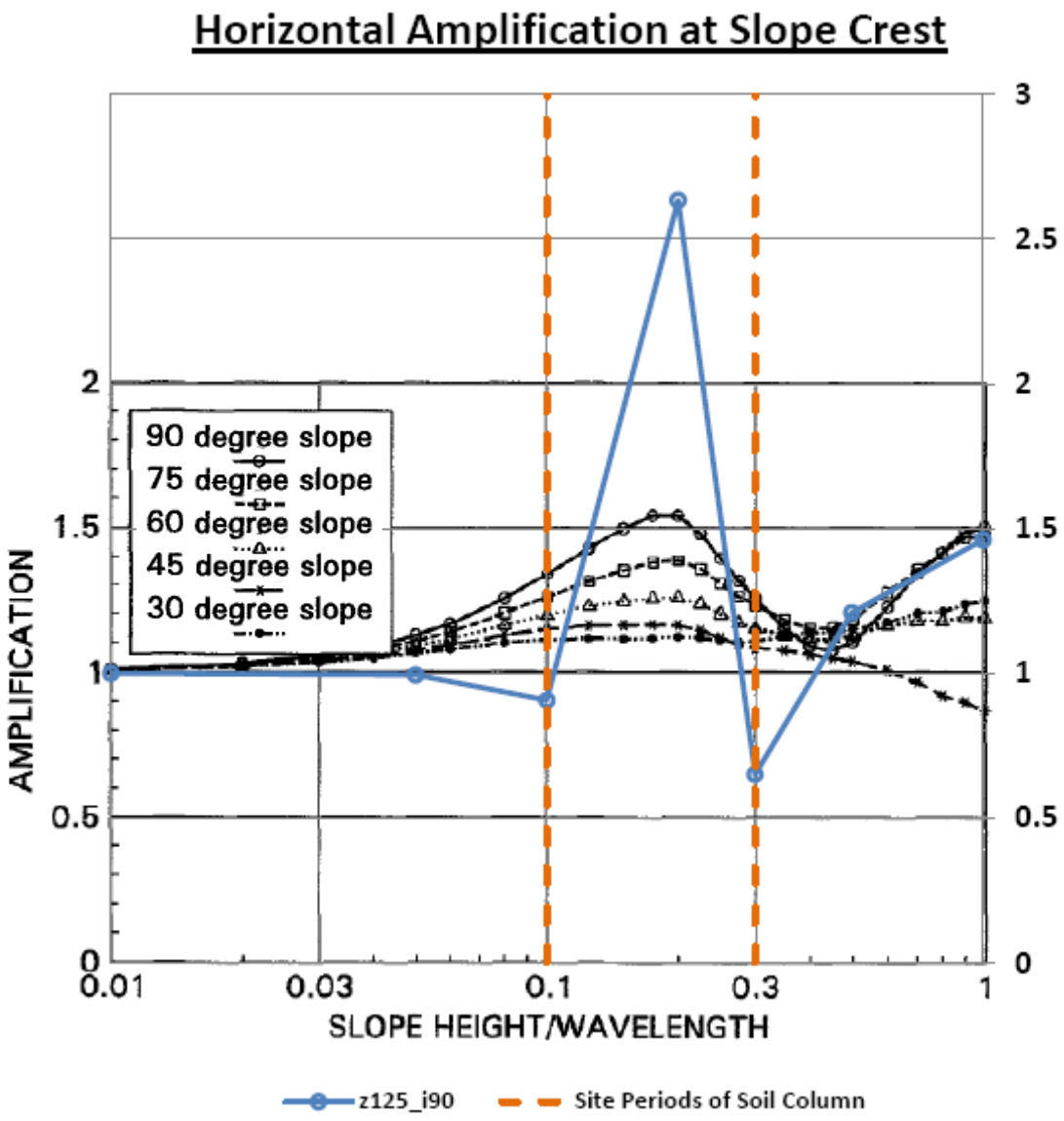

Notes:

(1) The horizontal topographic amplification factor is determined by normalising the horizontal acceleration value at that point against the free-field horizontal acceleration (i.e. not against the acceleration of the input excitation).

(2) Background curves coloured black are extracted from Ashford et al (1997) which are applicable to slopes in a homogeneous half-space .

Figure 4.6 Horizontal Amplification at Slope Crest for a Vertically Incident SV Wave on a Slope with a Bedrock Depth of 125 m

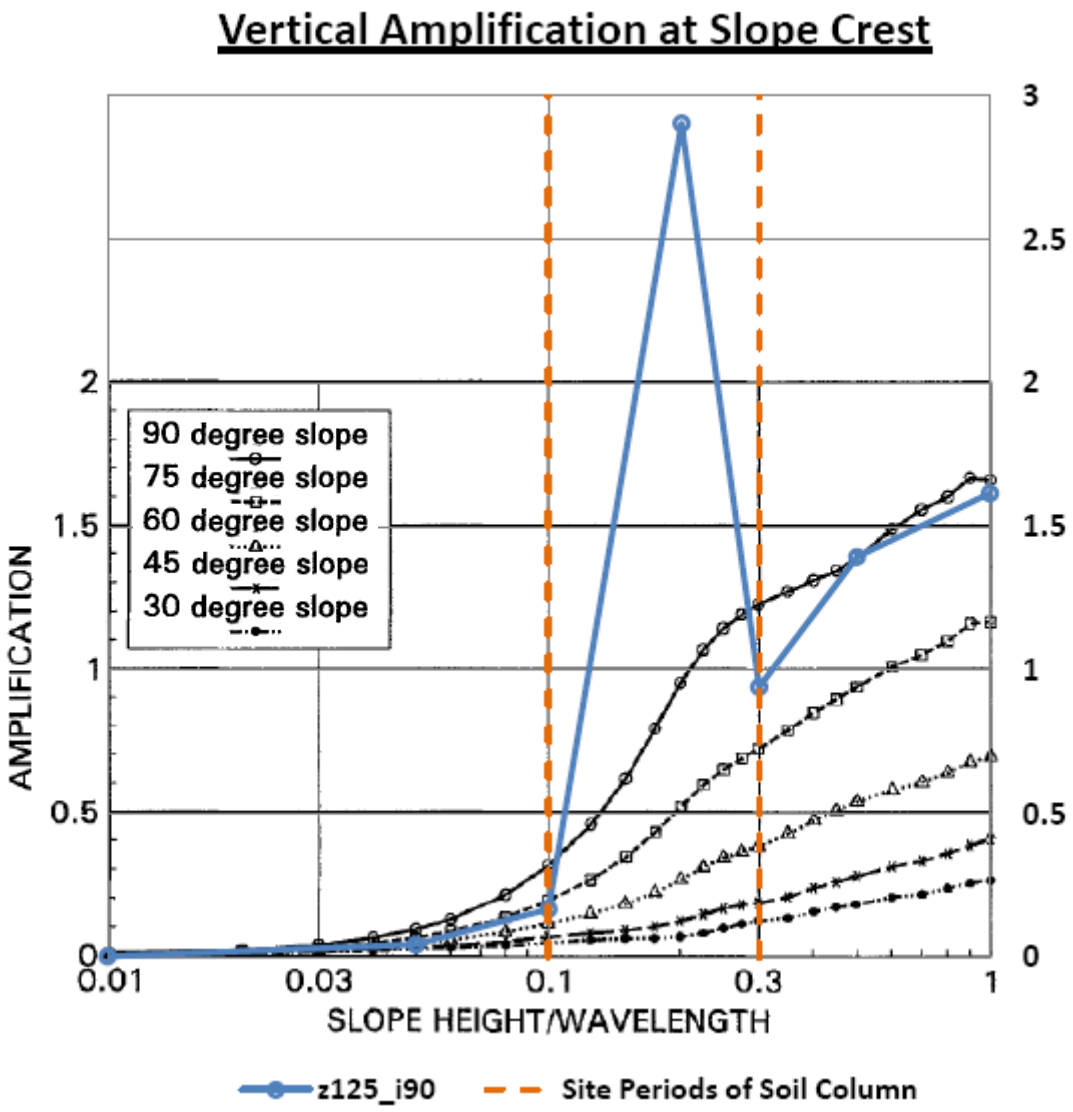

Notes:

(1) The vertical topographic amplification factor is determined by normalising the vertical acceleration value at that point against the free-field horizontal acceleration (i.e. not against the acceleration of the input excitation).

(2) Background curves coloured black are extracted from Ashford et al (1997) which are applicable to slopes in a homogeneous half-space.

Figure 4.7 Vertical Amplification at Slope Crest for a Vertically Incident SV Wave on a Slope with a Bedrock Depth of 125 m

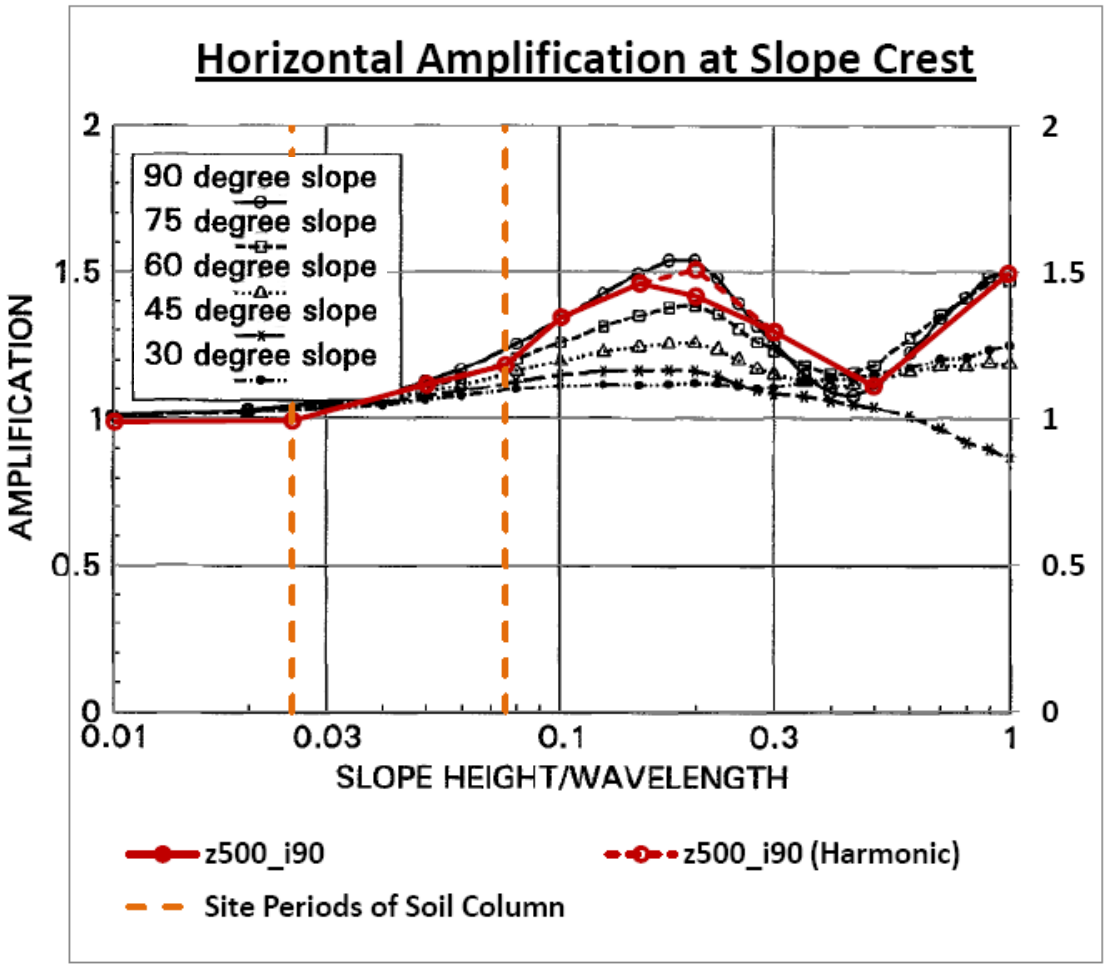

Notes:

(1) The horizontal topographic amplification factor is determined by normalising the horizontal acceleration value at that point against the free-field horizontal acceleration (i.e. not against the acceleration of the input excitation).

(2) Background curves coloured black are extracted from Ashford et al (1997) which are applicable to slopes in a homogeneous half-space.

Figure 4.8 Horizontal Amplification at Slope Crest for a Vertically Incident SV Wave on a Slope with a Bedrock Depth of 500 m

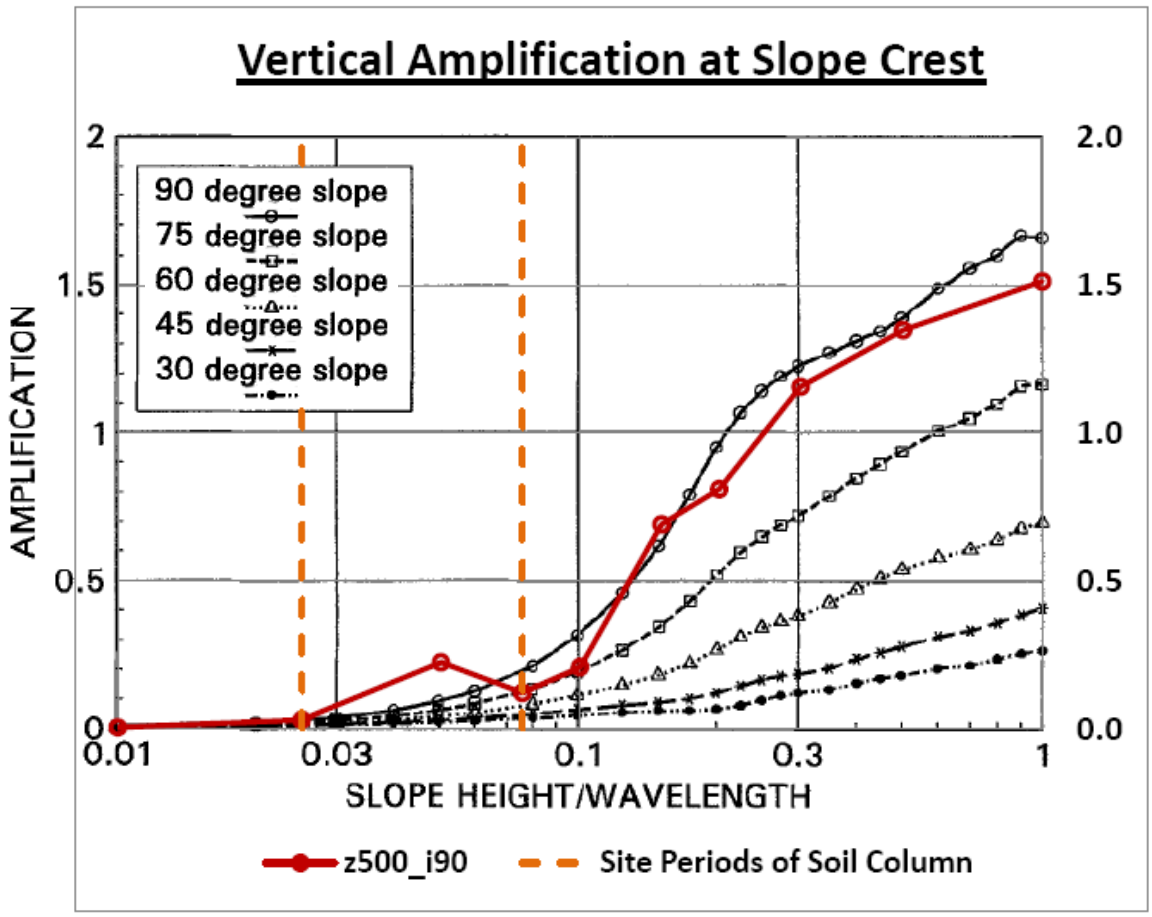

Notes:

(1) The vertical topographic amplification factor is determined by normalising the vertical acceleration value at that point against the free-field horizontal acceleration (i.e. not against the acceleration of the input excitation).

(2) Background curves coloured black are extracted from Ashford et al (1997) which are applicable to slopes in a homogeneous half-space.

Figure 4.9 Vertical Amplification at Slope Crest for a Vertically Incident SV Wave on a Slope with a Bedrock Depth of 500 m

4.4 Effects of Varying Bedrock Depth (Z)

Previous parametric studies, including Ashford et al (1997) and Bouckovalas & Papadimitriou (2005), considered slopes in a homogeneous half-space and thus they did not consider the influence of bedrock depth on topographic effects.

From Table 4.1 and by comparing among Figures 4.4 to 4.9, it can be seen that the bedrock depth has the following effects on the topographic effects on ground motion at slope crest:

(a) The presence of a soil/rock interface results in soil layer effects, and the bedrock depth controls the site periods of the soil column behind the slope crest. Therefore, the bedrock depth determines the dimensionless frequencies at which amplification of the input motion due to soil layer effects occurs. This in turn affects the magnitudes of the topographic amplification factors and also their variation patterns with dimensionless frequency, because the horizontal motion at the ground surface of the soil column, which is subject to soil layer effects, is taken as the free-field response for evaluation of the topographic amplification.

(b) From (a) above, it is expected that when the predominant period of the input motion is equal or close to the site periods of the soil column behind the slope crest, very large horizontal response at the ground surface of the soil column is obtained. This large free-field response results in a horizontal topographic de-amplification ($A_h < 1$) and a small vertical topographic amplification (A_v) of the ground motion at the slope crest. It should be noted that this horizontal topographic de-amplification is relative to the free-field response behind the slope crest and the horizontal acceleration value at the slope crest is still larger than that of the input excitation (i.e. the ratio of $a_{h,crest}/a_{h,in}$ is still larger than unity, see Table 4.1).

(c) Similarly, the bedrock depth also controls the dimensionless frequency at which the peak horizontal and vertical topographic amplifications occur. It is observed that these peak topographic amplifications occur at an H/λ ratio in-between those corresponding to the fundamental and second site periods of the soil column behind the slope crest.

(d) With a very deep bedrock (Z = 500 m), the influence of the soil/rock interface on the topographic effects becomes insignificant.

(e) The magnitudes of horizontal and vertical topographic

amplifications increase with decreasing bedrock depths, and much larger amplification factors are obtained in this study compared with the ones given in Ashford et al (1997) and Bouckovalas & Papadimitriou (2005) who studied slopes in a homogeneous half-space.

4.5 Interaction between Soil Layer Effects and Topographic Effects

It has been demonstrated that with the presence of a soil/rock interface, soil layer effects and topographic effects can occur simultaneously, unless the bedrock is very deep (for example, 10 times the slope height).

From Table 4.1 and Figures 4.3, 4.4 and 4.6, the following observations concerning the interaction between topographic effects and soil layer effects can be made:

(a) Even though the topographic amplification factors are determined by normalising the two-dimensional analysis results against the free field response, the soil layer effects still influence the magnitudes of topographic amplifications as well as the variation patterns of the topographic amplifications with dimensionless frequency.

(b) The magnitude of peak amplification due to soil layer effects is larger than that of peak horizontal topographic amplification. For example, for bedrock depth $Z = 250$ m, the maximum soil layer amplification factor is 7.2 (at $H/\lambda = 0.05$) while the maximum horizontal topographic amplification factor is 1.65 (at $H/\lambda = 0.1$ for vertical slope).

(c) The peak soil layer amplification and the peak horizontal topographic amplification do not occur at the same dimensionless frequency. In fact, when large amplification (relative to the input excitation) due to soil layer effects occurs, the predominant period of the input motion is equal to the site periods of the soil column behind the slope crest and topographic de-amplification of horizontal motion (relative to the free-field response) (i.e. $A_h < 1$) occurs.

(d) Where there is little or no amplification due to soil layer effects, the horizontal topographic amplification is larger for the case of a soil slope overlying bedrock, than the case of a slope in a homogeneous half-space. The maximum horizontal and vertical topographic amplification factors increase with decreasing bedrock depth.

(e) Because the peak soil layer amplification and the peak horizontal topographic amplification do not occur simultaneously and the magnitude of peak amplification due

to soil layer effects is larger than that of peak horizontal topographic amplification, it follows that the actual magnitude of maximum horizontal ground acceleration at the slope crest is dominated by soil layer effects (i.e. when the predominant period of input motion is equal to the fundamental site period of the soil column behind the slope crest), rather than topographic effects. This refers to the analysis results shown with * in Table 4.1.

(f) On the other hand, as vertical ground motion is generated by topographic effects only, the actual magnitude of the maximum vertical ground acceleration at the slope crest is independent of soil layer effects and the site periods of the soil column behind the slope crest.

Based on the above, it can be concluded that the presence of a soil/rock interface underneath slope toe has complicated the topographic effects compared to the simple case of a slope in a homogeneous half space that has been studied by many researchers such as Ashford et al (1997) and Bouckovalas & Papadimitriou (2005). This complex interaction between topographic effects and soil layer effects suggests that these effects should be considered simultaneously. It is noteworthy that this is in contrast to the conclusion made by Ashford et al (1997).

5 Discussion

5.1 Comparison with Seismic Code Provisions

EC-8 recommends that the topographic amplification factor S_T should be applied as a constant scalar factor to the elastic response spectrum, which implies that topographic effects are considered separately to soil layer effects. This study has demonstrated, in principle, that topographic effects and soil layer effects are not independent, and hence they should be considered simultaneously due to their complex interaction.

This study has also shown that at an H/λ value in between those corresponding to the fundamental and second site periods of the soil column behind the slope crest, very large horizontal topographic amplification would occur, particularly when the bedrock is shallow. In these circumstances, the topographic amplification factors recommended by the EC-8 may be too low. However, it could be argued that as the peak soil layer amplification and the peak horizontal topographic amplification do not occur simultaneously (in other words, these two effects amplify different frequency ranges of the seismic motion), it may not be reasonable to take into account the soil layer effect by adopting an elastic response spectrum that corresponds to a particular ground type as recommended by EC-8 and at the same time, to using a large amplification factor to account for topographic effect.

It is of interest to note that if only the simple cases of slopes in a homogeneous half-space or slopes with a very deep bedrock are considered, then the magnitudes of peak horizontal topographic amplification obtained from previous numerical analyses (see Section 2.5) and the current study are quite similar in order with the factors recommended by

the seismic codes reviewed in this study (i.e. EC-8 and PS-92).

It should be noted that this study has investigated the topographic effect on ground surface accelerations and did not consider the acceleration response spectra. Therefore, the direct comparison of the results from this study with the EC-8's recommendations which apply to the ordinates of elastic response spectra should be taken as approximate only.

As mentioned in Section 2.7, the EC-8 does not give clear guidance on the extent of the area over which topographic effect should be considered, while the empirical relation given in the PS-92 would generally result in a distance to the free field being less than the height of the slope. However, according to the results of this study, both of these seismic codes have apparently underestimated the distance from the slope crest to the free field where topographic effect could be ignored.

6 Conclusions

An extensive parametric study has been conducted to investigate the topographic effects on seismic ground motion for a soil slope overlying rigid bedrock, by carrying out time-domain finite element analyses using the Imperial College Finite Element Program (ICFEP).

The parametric study has shown that the topographic effects for the simulated soil slope overlying rigid bedrock are very similar in certain aspects with those reported in previous studies for slopes in a homogeneous half-space (e.g. Ashford et al, 1997; Bouckovalas & Papadimitriou, 2005). These similarities include:

(a) The horizontal ground motion behind the slope crest is modified by topographic effects and becomes different from the free-field response.

(b) Parasitic vertical motion is generated at the ground surface behind the slope crest, even with an input motion with no vertical excitation. This vertical component of seismic motion may become comparable to the horizontal free-field motion in some cases.

(c) In some cases, zones of alternating amplification and de-amplification of the horizontal motion along the ground surface behind the slope crest are observed.

(d) The magnitudes of topographic effects generally decrease with distance away from the slope crest.

(e) In cases where the wavelength of the input motion is very large compared with the height of the slope (the dimensionless frequency H/λ is very small), the topographic effects on ground motion is insignificant.

(f) With decreasing slope inclination, the magnitudes of both the horizontal topographic amplification at the first peak and of the vertical topographic amplification decrease.

On the other hand, the soil/rock interface included in the model of this study has complicated the topographic effects by introducing additional soil layer amplification. This study has shown that compared with the topographic effects for slopes in a homogeneous half-space obtained in Ashford et al (1997) and Bouckovalas & Papadimitriou (2005), the inclusion of soil/rock interface has resulted in the following differences:

(a) Horizontal topographic de-amplification occurs at the slope crest at dimensionless frequencies (H/λ) corresponding to the fundamental and second site periods of the soil column behind the slope crest, and therefore this pattern is dependent on the bedrock depth. It must be re-iterated that this de-amplification is relative to the free-field response behind the slope crest and the horizontal acceleration value at the slope crest is still larger than that of the input excitation. It is noted that at these H/λ values, amplification of the input motion occurs due to soil layer effects, and this results in a large horizontal free-field motion and the horizontal ground motion is de-amplified at the slope crest. The physical phenomenon explaining occurrence of this horizontal topographic de-amplification at the slope crest is not examined in this study. However, it is logical to consider that the one-dimensional soil layer amplification is a pure resonance at the free field, which is interfered with at the crest because of the more complex geometry there. On the other hand, both Ashford et al (1997) and Bouckovalas & Papadimitriou (2005) did not obtain horizontal topographic de-amplification at any H/λ values.

(b) Peak horizontal amplifications occurs at an H/λ value in between those corresponding to the fundamental and second site periods of the soil column behind the slope crest. On the other hand, both Ashford et al (1997) and Bouckovalas & Papadimitriou (2005) reported that the peak horizontal amplification occurs at $H/\lambda = 0.2$ in all analysed cases.

(c) Similar to points (a) and (b) above, the vertical topographic amplifications at the slope crest at dimensionless frequencies (H/λ) corresponding to the fundamental and second site periods of the soil column behind the slope crest are much smaller than the values reported in Ashford et al (1997) and Bouckovalas & Papadimitriou (2005). In addition, a sharp peak of the vertical topographic amplification also exists at an H/λ value in between those corresponding to the fundamental and second site periods of

the soil column behind the slope crest.

(d) For all slope inclinations, the maximum horizontal and vertical amplification factors obtained in this study increase with decreasing bedrock depths, and they are much larger than those obtained from Ashford et al (1997) and Bouckovalas & Papadimitriou (2005), who studied slopes in a homogeneous half-space.

In addition, this study has the following findings concerning the interaction between topographic effects and soil layer effects:

(a) The occurrence of soil layer effects can significantly influence the magnitudes of the topographic amplifications and the variation patterns of the topographic amplifications with the dimensionless frequency.

(b) The factor of peak amplification due to soil layer effects is larger than that of peak horizontal topographic amplification.

(c) Peak soil layer amplification and peak horizontal topographic amplification do not occur at the same dimensionless frequency.

(d) Maximum horizontal ground acceleration at the slope crest appears when the peak soil layer amplification occurs, rather than the peak horizontal topographic amplification. This suggests that the actual magnitude of the maximum horizontal ground acceleration at the slope crest is dominated by soil layer effects.

(e) As vertical ground motion can be generated from vertically propagating SV wave by topographic effects only, the actual magnitude of the maximum vertical ground acceleration at the slope crest is controlled by topographic effects and not affected by soil layer effects.

This study has shown that the presence of a soil/rock interface underneath the slope toe has complicated the topographic amplification response compared to the simple case of slopes in a homogeneous half space that have been studied by many researchers such as Ashford et al (1997) and Bouckovalas & Papadimitriou (2005). The presence of a soil/rock interface has resulted in larger topographic amplification factors. In addition, topographic irregularities and soil layering amplify different frequency components of seismic excitation. The complex interaction between topographic effects and soil layer effects suggests that they should not be handled separately for prediction of the overall site amplification factors. This is in contrast to the conclusion made by Ashford et al (1997).

It should be noted that this parametric study considered a simplified model only.

Some other parameters (e.g. type and direction of incident wave and three-dimensional topography shape) that can influence topographic effects on seismic ground motion were not considered in this study. These factors can make actual topographic effects more complicated than the ones predicted in this study.

7 References

AFNOR (1995). *Règles de Construction Parasismique - Règles PS Applicables Aux Bâtiments, Dites Règles PS 92*. Normes NF P 016-013, Norme Francaise.

Ashford, S.A. & Sitar, N. (1997). Analysis of topographic amplification of inclined shear waves in a steep coastal bluff. *Bulletin of the Seismological Society of America*, 87 (3), pp 692-700.

Ashford, S.A., Sitar, N., Lysmer, J. & Deng, N. (1997). Topographic effects on the seismic response of steep slopes. *Bulletin of the Seismological Society of America*, 87 (3), pp 701-709.

Bard, P.Y. & Riepl-Thomas, J. (2000). Wave propagation in complex geological structures and their effect on strong ground motion. In: Kausel E. and Manolis G. D. (eds.) *Wave Motion in Earthquake Engineering*. Southampton, WIT Press, pp 37-95.

Bard, P.Y. & Tucker, B.E. (1985). Underground and ridge site effects: a comparison of observation and theory. *Bulletin of the Seismological Society of America*, 75 (4), pp 905-922.

Bielak, J., Loukakis, K., Hisada, Y. & Yoshimura, C. (2003). Domain reduction method for three-dimensional earthquake modelling in localized regions, part I: theory. *Bulletin of the Seismological Society of America*, 93 (2), pp 817-824.

Boore, D.M. (1972). A note on the effect of simple topography on seismic SH waves. *Bulletin of the Seismological Society of America*, 62 (1), pp 275-284.

Boore, D.M., Harmsen, S.C. & Harding, S.T. (1981). Wave scattering from a step change in surface topography. *Bulletin of the Seismological Society of America*, 71 (1), pp 117-125.

Bouchon, M. & Barker, J.S. (1996). Seismic response of a hill: the example of Tarzana, California. *Bulletin of the Seismological Society of America*, 86 (1A), pp 66-72.

Bouchon, M., Schultz, C.A. & Toksoz, M.N. (1996). Effect of three-dimensional topography on seismic motion. *Journal of Geophysical Research*, 101 (B3), pp 5835-5846.

Bouckovalas, G.D., Gazetas, G. & Papadimitriou, A.G. (1999). Geotechnical aspects of the 1995 Aegion, Greece, earthquake. In: *Proceedings of the Second International Conference on Geotechnical Earthquake Engineering, June 1999, Lisbon*. Rotterdam, Balkema, volume 2, pp 739-748.

Bouckovalas, G.D. & Papadimitriou, A.G. (2005). Numerical evaluation of slope topography effects on seismic ground motion. *Soil Dynamics and Earthquake Engineering*, 25, pp 547-558.

Bouckovalas, G.D. & Papadimitriou, A.G. (2006). Aggravation of Seismic Ground Motion due to Slope Topograhy. In: *Proceedings of the First European Conference on Earthquake Engineering and Seismology, 3-8 September 2006, Geneva Switzerland.*

British Standards Institution (2004). *Eurocode 8: Design of Structures for Earthquake Resistance. Part 5: Foundations, Retaining Structures and Geotechnical Aspects. BS EN 1998-5:2004.* London, British Standards Institution.

Celebi, M. (1987). Topographical and geological amplifications determined from strong-motion and aftershock records of the 3 March 1985 Chile earthquake. *Bulletin of the Seismological Society of America*, 77 (4), pp 1147-1167.

Celebi, M. (1991). Topographical and geological amplification: case studies and engineering implications. *Structural Safety*, 10, pp 199-217.

Celebi, M. (1995). Northridge (California) earthquake: Unique ground motions and resulting spectral and site effects. In: *Proceedings of the Fifth International Conference on Seismic Zonation, 17-19 October, 1995, Nice.*

Chavez-Garcia, F.J., Sanchez, L.R. & Hatzfeld, D. (1996). Topographic site effects and HVSR. A comparison between observations and theory. *Bulletin of the Seismological Society of America*, 86 (5), pp 1559-1573.

Chung, J. & Hulbert, G.M. (1993). A time integration algorithm for structural dynamics with improved numerical dissipation: the generalized-α method. *Journal of Applied Mechanics*, 60, pp 371-375.

Davis, L.L. & West, L.R. (1973). Observed effects of topography on ground motion. *Bulletin of the Seismological Society of America*, 63 (1), pp 283-298.

Gazetas, G., Kallou, P.V. & Psarropoulos P.N. (2002). Topography and soil effects in the Ms 5.9 Parnitha (Athens) earthquake: the case of Adames. *Natural Hazards*, 27, pp 133-169.

Geli, L., Bard, P.Y. & Jullien, B. (1988). The effect of topography on earthquake ground motion: a review and new results. *Bulletin of the Seismological Society of America*, 78 (1), pp 42-63.

Graizer, V. (2009). Low-velocity zone and topography as a source of site amplification effect on Tarzana hill, California. *Soil Dynamics and Earthquake Engineering*, 29, pp 324-332.

Griffiths, D.W. & Bollinger, G.A. (1979). The effect of Appalachian Mountain topography on seismic waves. *Bulletin of the Seismological Society of America*, 69 (4), pp 1081-1105.

Hartzell, S.H., Carver, D.L. & King, K.W. (1994). Initial investigation of site and topographic effects at Robinwood Ridge, California. *Bulletin of the Seismological Society of America*, 84 (5), pp 1336-1349.

Idriss, I.M. (1968). Finite element analysis for the seismic response of earth banks. *Journal of the Soil Mechanics and Foundations Division, ASCE*, 94 (SM3), pp 617-636.

Idriss, I.M. & Seed, H.B. (1967). Response of earth banks during earthquakes. *Journal of the Soil Mechanics and Foundations Division, ASCE*, 93 (SM3), pp 61-82.

Kawase, H. & Aki, K. (1990). Topography effect at the critical SV-wave incidence: possible explanation of damage pattern by the Whittier Narrows, California, earthquake of 1 October 1987. *Bulletin of the Seismological Society of America*, 80 (1), pp 1-22.

Kontoe, S. (2006). *Development of Time Integration Schemes and Advanced Boundary Conditions for Dynamic Geotechnical Analysis.* Ph.D. Thesis, Imperial College, London.

Kontoe, S., Zdravkovic, L. & Potts, D.M. (2009). An assessment of the domain reduction method as an advanced boundary condition and some pitfalls in the use of conventional adsorbing boundaries. *International Journal for Numerical and Analytical Methods in Geomechanics*, 33, pp 309-330.

Kovacs, W.D., Seed, H.B. & Idriss, I.M. (1971). Studies of seismic response of clay banks. *Journal of the Soil Mechanics and Foundations Division, ASCE*. 97 (SM2), pp 441-455.

Kramer, S.L. (1996). *Geotechnical Earthquake Engineering*. New Jersey, Prentice-Hall.

LeBrun, B., Hatzfeld, D. Bard, P.Y. & Bouchon M. (1999). Experimental study of the ground motion on a large scale topography hill at Kitherion (Greece). *Journal of Seismology*, 3, pp 1-15.

Levret, A., Loup, C. & Goula, X. (1986). The Provence earthquake of June 11th, 1909 (France): A new assessment of near-field effects. In: *Proceedings of the Eighth European Conference on Earthquake Engineering, Lisbon, September 1986*, volume 2, pp 4.2/79-4.2/86.

Lysmer, J. & Kuhlemeyer, R.L. (1969). Finite dynamic model for infinite media. *Journal of the Engineering Mechanics, ASCE*, 95 (EM4), pp 859-877.

Nechtschein, S., Bard, P.Y., Gariel, J.C., Meneroud, J.P., Dervin, P., Cushing, M., Gaubert, C., Vidal, S. & Duval, A.M. (1995). A Topographic Effect Study in the Nice Region. In: *Proceedings of the Fifth International Conference on Seismic Zonation, October 1995, Nice France*. Ouest Editions Presses Academiques, pp 1067-1074.

Ohtsuki, A. & Harumi, K. (1983). Effect of topography and subsurface inhomogeneities on seismic SV waves. *Earthquake Engineering and Structural Dynamics*, 11, pp 441-462.

Table of Contents
Table of Contents
Table of Contents
Table of Contents

Pedersen, H.A., Sanchez-Sesma, F.J. & Campillo, M. (1994a). Three-dimensional scattering by two-dimensional topographies. *Bulletin of the Seismological Society of America*, 84 (4), pp 1169-1183.

Pedersen, H., LeBrun, B., Hatzfield, D., Campillo, M. & Bard, P.Y. (1994b). Ground-motion amplitude across ridges. *Bulletin of the Seismological Society of America*, 84 (6), pp 1786-1800.

Potts, D.M. & Zdravkovic, L. (1999). *Finite Element Analysis in Geotechnical Engineering: Theory*. London, Thomas Telford.

Restrepo, J.I. & Cowan, H.A. (2000). The 'Eje Cafetero' earthquake, Colombia of January 25 1999. *Bulletin of the New Zealand Society for Earthquake Engineering*, 33 (1), pp 1-29.

Rogers, A.M., Katz, L.J. & Bennett, T.J. (1974). Topographic effects on ground motion for incident P waves: a model study. *Bulletin of the Seismological Society of America*, 64 (2), pp 437-456.

Sanchez-Sesma, F.J. (1990). Elementary solutions for response of a wedge-shaped medium to incident SH and SV waves. *Bulletin of the Seismological Society of America*, 80 (3), pp 737-724.

SeismoSoft (2010). SeismoSignal v4.0. [Online] Available from URL: http://seismosoft.com. [Accessed 25 June 2010].

Sitar, N. & Clough, G.W. (1983). Seismic response of steep slopes in cemented soils. *Journal of Geotechnical Engineering, ASCE*, 109 (2), pp 210-227.

Sitar, N., Nova-Roessig, L., Ashford, S.A. & Stewart, J.P. (1997). Seismic response of steep natural slopes, structural fills and reinforced soil slopes and walls. In: Seco e Pinto (ed.) *Proceedings of the 14th International Conference on Soil Mechanics and Foundation Engineering, 6-12 September 1997, Hamburg*. Rotterdam, Balkema.

Spudich, P., Hellweg, M. & Lee, W.H.K. (1996). Directional topographic site response at Tarzana observed in aftershocks of the 1994 Northridge, California, earthquake: implications for mainshock motions. *Bulletin of the Seismological Society of America*, 86 (1B), S193-S208.

Tripe, R. (2009). *Topographic Effects on Seismic Motion*. M.Sc. Dissertation, Imperial College, London.

Tucker, B.E., King, J.L., Hatzfeld, D. & Nersesov, I.L. (1984). Observations of hard-rock site effects. *Bulletin of the Seismological Society of America*, 74 (1), pp 121-136.

University of Southern California (2000). Equivalent-linear Earthquake site Response Analysis (EERA) version 2000. [Online] Available from URL: http://gees.usc.edu/GEES/. [Accessed 25 June 2010].

Table of Contents
Table of Contents
Table of Contents
Table of Contents

GEO PUBLICATIONS AND ORDERING INFORMATION
土力工程處刊物及訂購資料

A selected list of major GEO publications is given in the next page. An up-to-date full list of GEO publications can be found at the CEDD Website http://www.cedd.gov.hk on the Internet under "Publications". Abstracts for the documents can also be found at the same website. Technical Guidance Notes are published on the CEDD Website from time to time to provide updates to GEO publications prior to their next revision.

部份土力工程處的主要刊物目錄刊載於下頁。而詳盡及最新的土力工程處刊物目錄，則登載於土木工程拓展署的互聯網網頁 http://www.cedd.gov.hk 的"刊物"版面之內。刊物的摘要及更新刊物內容的工程技術指引，亦可在這個網址找到。

Copies of GEO publications (except geological maps and other publications which are free of charge) can be purchased either by:

Writing to
Publications Sales Unit,
Information Services Department,
Room 626, 6th Floor,
North Point Government Offices,
333 Java Road, North Point, Hong Kong.

or

- Calling the Publications Sales Section of Information Services Department (ISD) at (852) 2537 1910
- Visiting the online Government Bookstore at http:// www.bookstore.gov.hk
- Downloading the order form from the ISD website at http://www.isd.gov.hk and submitting the order online or by fax to (852) 2523 7195
- Placing order with ISD by e-mail at puborder@isd.gov.hk

讀者可採用以下方法購買土力工程處刊物(地質圖及免費刊物除外):

書面訂購
香港北角渣華道333號
北角政府合署6樓626室
政府新聞處
刊物銷售組

或

- 致電政府新聞處刊物銷售小組訂購 (電話：(852) 2537 1910)
- 進入網上「政府書店」選購，網址爲 http://www.bookstore.gov.hk
- 透過政府新聞處的網站 (http://www.isd.gov.hk) 於網上遞交訂購表格，或將表格傳真至刊物銷售小組 (傳真：(852) 2523 7195)
- 以電郵方式訂購 (電郵地址：puborder@isd.gov.hk)

1:100 000, 1:20 000 and 1:5 000 geological maps can be purchased from:

Map Publications Centre/HK,
Survey & Mapping Office, Lands Department,
23th Floor, North Point Government Offices,
333 Java Road, North Point, Hong Kong.
Tel: (852) 2231 3187
Fax: (852) 2116 0774

讀者可於下列地點購買1:100 000、1:20 000及1:5 000地質圖：

香港北角渣華道333號
北角政府合署23樓
地政總署測繪處
電話: (852) 2231 3187
傳真: (852) 2116 0774

Requests for copies of Geological Survey Sheet Reports and other publications which are free of charge should be directed to:

For Geological Survey Sheet Reports which are free of charge:
Chief Geotechnical Engineer/Planning,
(Attn: Hong Kong Geological Survey Section)
Geotechnical Engineering Office,
Civil Engineering and Development Department,
Civil Engineering and Development Building,
101 Princess Margaret Road,
Homantin, Kowloon, Hong Kong.
Tel: (852) 2762 5380
Fax: (852) 2714 0247
E-mail: jsewell@cedd.gov.hk

For other publications which are free of charge:
Chief Geotechnical Engineer/Standards and Testing,
Geotechnical Engineering Office,
Civil Engineering and Development Department,
Civil Engineering and Development Building,
101 Princess Margaret Road,
Homantin, Kowloon, Hong Kong.
Tel: (852) 2762 5346
Fax: (852) 2714 0275
E-mail: florenceko@cedd.gov.hk

如欲索取地質調查報告及其他免費刊物，請致函：

免費地質調查報告:
香港九龍何文田公主道101號
土木工程拓展署大樓
土木工程拓展署
土力工程處
規劃部總土力工程師
(請交:香港地質調查組)
電話: (852) 2762 5380
傳真: (852) 2714 0247
電子郵件: jsewell@cedd.gov.hk

其他免費刊物:
香港九龍何文田公主道101號
土木工程拓展署大樓
土木工程拓展署
土力工程處
標準及測試部總土力工程師
電話: (852) 2762 5346
傳真: (852) 2714 0275
電子郵件: florenceko@cedd.gov.hk

Table of Contents
Table of Contents
Table of Contents

MAJOR GEOTECHNICAL ENGINEERING OFFICE PUBLICATIONS
土力工程處之主要刊物

GEOTECHNICAL MANUALS

Geotechnical Manual for Slopes, 2nd Edition (1984), 302 p. (English Version), (Reprinted, 2011).

斜坡岩土工程手冊(1998)，308頁(1984年英文版的中文譯本)。

Highway Slope Manual (2000), 114 p.

GEOGUIDES

Geoguide 1	Guide to Retaining Wall Design, 2nd Edition (1993), 258 p. (Reprinted, 2007).
Geoguide 2	Guide to Site Investigation (1987), 359 p. (Reprinted, 2000).
Geoguide 3	Guide to Rock and Soil Descriptions (1988), 186 p. (Reprinted, 2000).
Geoguide 4	Guide to Cavern Engineering (1992), 148 p. (Reprinted, 1998).
Geoguide 5	Guide to Slope Maintenance, 3rd Edition (2003), 132 p. (English Version).
岩土指南第五冊	斜坡維修指南，第三版(2003)，120頁(中文版)。
Geoguide 6	Guide to Reinforced Fill Structure and Slope Design (2002), 236 p.
Geoguide 7	Guide to Soil Nail Design and Construction (2008), 97 p.

GEOSPECS

Geospec 1	Model Specification for Prestressed Ground Anchors, 2nd Edition (1989), 164 p. (Reprinted, 1997).
Geospec 3	Model Specification for Soil Testing (2001), 340 p.

GEO PUBLICATIONS

GCO Publication No. 1/90	Review of Design Methods for Excavations (1990), 187 p. (Reprinted, 2002).
GEO Publication No. 1/93	Review of Granular and Geotextile Filters (1993), 141 p.
GEO Publication No. 1/2006	Foundation Design and Construction (2006), 376 p.
GEO Publication No. 1/2007	Engineering Geological Practice in Hong Kong (2007), 278 p.
GEO Publication No. 1/2009	Prescriptive Measures for Man-Made Slopes and Retaining Walls (2009), 76 p.
GEO Publication No. 1/2011	Technical Guidelines on Landscape Treatment for Slopes (2011), 217 p.

GEOLOGICAL PUBLICATIONS

The Quaternary Geology of Hong Kong, by J.A. Fyfe, R. Shaw, S.D.G. Campbell, K.W. Lai & P.A. Kirk (2000), 210 p. plus 6 maps.

The Pre-Quaternary Geology of Hong Kong, by R.J. Sewell, S.D.G. Campbell, C.J.N. Fletcher, K.W. Lai & P.A. Kirk (2000), 181 p. plus 4 maps.

TECHNICAL GUIDANCE NOTES

TGN 1	Technical Guidance Documents